Mohamed Khider University - Biskra

Faculty of Science and Technology

Department: Civil and Hydraulic Engineering

Ref: …………………………………..

جـــامعة محمد خيضر بــسكرة

كـلية الـعلــوم و التكــنولوجـيا

قـسـم : الهندسـة المدنيـة و الـري

المـرجع: ....

A dissertation submitted for the degree of doctor in civil engineering

Field: Numerical Modelling in Civil Engineering

Improvement stability of retaining walls in the presence of flow

Presented by :

Ilyes OUZAID

Publicly supported on: 30 Mai 2021

In front of the jury composed of:

Mr. Ahmed OUAMANE	**Professor**	**President**	**University of Biskra**
Mme. Naima BENMEBAREK	**Professor**	**Supervisor**	**University of Biskra**
Mr. Rafik DEMAGH	**Professor**	**Examiner**	**University of Batna**
Mr. Abdelhamid MESSAMEH	**Senior lecturer**	**Examiner**	**University of Biskra**

DECLARATION

I hereby declare that, except where reference is made to the work of others, the contents of this dissertation are a result of my own work and include nothing which is the outcome of work done in collaboration.

This dissertation has not been submitted in whole or part for consideration for any other degree, diploma or other qualification to this University or any other institution, except where cited specifically.

This dissertation contains no more than 35,000 words, inclusive of appendices, references, footnotes, tables and equations, and taking in consideration some original figures.

Name: Ilyes OUZAID

Registration number: 15/PG/D/LMD/GC/15

Date: *30 Mai 2021*

Signature:

To my dear parents

And

to all my family...

ACKNOWLEDGEMENTS

CONTENTS

First part: Bibliographical summary on the retaining of excavations

Chapter 1: Generality on the supported excavation with flow of water in soil

Chapter 2 : Methods for evaluating the stability of excavation bottoms with respect to hydraulic failure: literature review

Second part : Numerical modelling of excavation basal stability

Chapter 3 : Presentation of numerical modelling tool

Chapter 4 : Numerical analysis of the excavations stability in the presence of flow

List of Figures

List of Tables

LIST OF ABBREVIATIONS

C_u Uniformity coefficient

Δh Head difference

h Head

i Hydraulic Gradient

k Permeability Coefficient

PSD Particle size distribution

N_d Number of equipotential drops

N_f Number of flow channels

q Flow per unit length

Q Discharge

R_n Reynolds Number

s.i Système International

u pore water pressure

v Velocity

Y_w Unit weight of water

Σ Sum of

σ Stress

ρ density of a fluid

μ coefficient of viscosity

∂ partial derivative

w The deflection

θ The quantity

n The number of nodes

ε Strain vector

F Applied loads

S The relative flow force

GB' The stabilizing weight under buoyancy

GA' The load filter under buoyancy

d_A The thickness of the load filter

n A soil of porosity

A A soil section area

A_V Section area of voids

v_s The seepage velocity

J The seepage force

i_c The critical hydraulic gradient

i_e The exit hydraulic gradient

u Pressure

g Acceleration due to gravity

L Distance

D_{30} Diameter of particle size at 30% passing, m

T The time interval

σ'_h The horizontal effective stress

σ'_V The vertical effective stress

K The earth pressure coefficient

E Young's modulus

E_0 Young's modulus at the surface

E_u Undrained Young's modulus

$I\rho$ Influence factor for vertical movement

Improvement stability of retaining walls in the presence of flow

Abstract

With the existence of high groundwater level, the head difference between the inside and outside of the excavation may lead to the loss stability of the excavation's surface. In some cases, the failure mechanism cannot be predicted exactly because of its mechanical complexity as well as a major lack of protection systems and not adopting effective countermeasures against this phenomenon. Several methods of calculating the basal stability with respect to hydraulic failure have been proposed in the literature, sometimes leading to crucial differences in the values of the hydraulic head loss causing the failure. In this thesis, the objective of this study is to analyse the stability of excavation in the presence of water flow around the retaining wall. This, through numerical analysis using the Plaxis 2D finite element code, This work took a real case located in the Ruhr area, Germany to establish the model and analyse the instability of the excavation base surface caused by the groundwater flow and to present the effectivity of an adopted drainage system inside the excavation pit. By using the finite element method (*FEM*) analysis, the failure mechanism was investigated before applying any countermeasures, and the total length of the adopted countermeasure system was minimised. Also, various position tests were performed on the adopted drainage system to confirm the optimised position. The results of this numerical study allowed the deduction of the importance of the used drainage system by achieving *44%* more in the excavating process and they can be provided as reference for the optimised position of the sand columns where they must be applied right by the wall and limited by a critical distance, *D/2*, half of the embedded depth of the wall. By using the technic of cavity expansion for stone columns installation provide an extra excavation deep, also the reinforced soil surrounding the retaining wall keep stable in which insure the safety of the wall against failure

Keywords: circular deep excavation; hydraulic failure of soil; failure of support system, diaphragm walls; lateral land pressure; pore pressures; drainage system; stability analysis, factor of safety, permeability.

Amélioration la stabilité des murs de soutènement en présence d'infiltration d'eau

Résumé

Avec l'existence d'un niveau élevé de la nappe phréatique, la différence de hauteur entre l'intérieur et l'extérieur d'une excavation peut entraîner une perte de stabilité de la surface de l'excavation. Dans certains cas, le mécanisme de défaillance ne peut pas être prédit exactement en raison de sa complexité mécanique ainsi que d'un manque majeur de systèmes de protection et de la non-adoption de contre-mesures efficaces contre ce phénomène. Plusieurs méthodes de calcul de la stabilité à la rupture hydraulique ont été proposées dans la littérature, conduisant parfois à des différences cruciales dans les valeurs de la perte de charge hydraulique à l'origine de la rupture. Dans cette thèse, l'objectif est d'analyser la stabilité de l'excavation en présence d'écoulement d'eau autour du mur de soutènement. Ceci, grâce à une analyse numérique utilisant le code d'éléments finis Plaxis 2D. Ce travail a pris un cas réel situé dans la région de la Ruhr, en Allemagne pour établir le modèle et analyser l'instabilité de l'excavation causée par l'écoulement des eaux souterraines et présenter l'efficacité d'un système de drainage adopté à l'intérieur de la fosse d'excavation. En utilisant l'analyse de la méthode des éléments finis (*FEM*), le mécanisme de rupture a été élaboré avant d'appliquer des contre-mesures, et la longueur totale du système de contre-mesures adopté a été minimisée. De plus, divers tests de position ont été effectués sur le système de drainage adopté pour confirmer la position optimisée. Les résultats de cette étude numérique ont permis de déduire l'importance du système de drainage utilisé en réalisant 44% de plus dans le processus d'excavation et ils peuvent être fournis comme référence pour la position optimisée des colonnes de sable où elles doivent être appliquées juste à côté du mur et limité par une distance critique, *D / 2*, la moitié de la profondeur encastrée de la paroi. En utilisant la technique d'expansion de la cavité pour l'installation de colonnes ballastées, fournir une excavation supplémentaire en profondeur, le sol renforcé entourant le mur de soutènement être plus stable, ce qui assure la sécurité du mur contre la défaillance

Mots-clés : excavation circulaire profonde ; rupture hydraulique du sol ; défaillance du système de soutènement, parois moulées ; pression latérale des terres ; pressions interstitielles ; système de drainage ; analyse de stabilité, facteur de sécurité, perméabilité.

تحسين ثبات الجدران الداعمة للحفر العميقة تحت تأثير جريان المياه

الملخص

مع وجود مستوى مرتفع للمياه الجوفية ، قد يؤدي اختلاف مستوى الماء بين داخل وخارج الحفريات إلى فقدان استقرار سطح الحفريات. في بعض الحالات ، لا يمكن التنبؤ بآلية الفشل بالضبط بسبب تعقيدها الميكانيكي وكذلك النقص الكبير في أنظمة الحماية وعدم اعتماد إجراءات مضادة فعالة ضد هذه الظاهرة. تم اقتراح عدة طرق لحساب الثبات فيما يتعلق بالفشل الهيدروليكي في المؤلفات ، مما أدى في بعض الأحيان إلى اختلافات جوهرية في قيم فقدان الرأس الهيدروليكي مما تسبب في الفشل. الهدف من هذه الدراسة هو تحليل ثبات الحفريات في وجود تدفق المياه حول الجدار الاستنادي. هذا ، من خلال التحليل العددي باستخدام رمز العنصر المحدود Plaxis 2D ، أخذ هذا العمل حالة حقيقية تقع في منطقة الرور بألمانيا لإنشاء نموذج وتحليل عدم استقرار سطح قاعدة الحفر الناجم عن تدفق المياه الجوفية وتقديمه فعالية نظام الصرف المعتمد داخل حفرة التنقيب. باستخدام تحليل طريقة العناصر المحدودة *FEM*، تم فحص آلية الفشل قبل تطبيق أي إجراءات مضادة ، وتم تقليل الطول الإجمالي لنظام الإجراءات المضادة المعتمد. أيضًا ، تم إجراء اختبارات موضع مختلفة على نظام الصرف المعتمد لتأكيد الوضع الأمثل. سمحت نتائج هذه الدراسة العددية بخصم أهمية نظام الصرف المستخدم من خلال تحقيق 44٪ أكثر في عملية الحفر ويمكن توفيرها كمرجع للوضع الأمثل لأعمدة الرمل حيث يجب تطبيقها مباشرة من الجدار ومحدودة بمسافة حرجة ، *D / 2* ، نصف عمق الجدار المضمن. باستخدام تقنية توسيع التجويف لتركيب الأعمدة الحجرية ، توفر حفرًا أعمق ، كما أن التربة المقواة المحيطة بالجدار الاستنادي تحافظ على ثباتها مما يضمن سلامة الجدار ضد الفشل.

الكلمات المفتاحية: حفر دائري عميق. الانهيار الهيدروليكي للتربة. فشل نظام الدعم ، جدران الحجاب الحاجز ؛ ضغط الأرض الجانبي، ضغوط المسام نظام الصرف الصحي؛ تحليل الاستقرار ، عامل الأمان ، النفاذية.

General Introduction

1. Backgrounds

The realization of the infrastructure of the various structures often requires the execution of deep excavations in aquiferous soils supported by sheet pile walls or by diaphragm walls. And requires drainage and the temporary or definitive lowering of the water table, which are often essential for the stability of structures. The design of these excavations is generally dominated by the flow of water through the retaining wall from the upstream side to the downstream side. The said flow is generated by the lowering of the water level inside the enclosure of the excavation (drying up of the excavation), and influences the overall stability of the wall and the stability of the bottom of the excavation. Where a lifting of a soil- block in front of the embedding length of the wall, a seepage phenomenon, a liquefaction of the soil, or a mechanical failure by reduction of the passive pressure of the earth can occur produce according to the properties of the soil, the soil / structure interface, the types and conditions of the support structure, and the surrounding aquifer environment.

The critical states of hydraulic failures are the most feared and severe of the critical conditions in the practice of geotechnical engineering. These failure states often occur with little or no warning, and it is extremely difficult to stop these phenomena once start. The upward flow of water causes particles of powdery soils to rise and 'reduction of the passive earth pressure' in front the wall. These phenomena can lead to relatively sudden catastrophic failures of support structures, causing enormous material damage and sometimes even regrettable loss of life. Hence the need to take into account the effects of water flow in the calculation and in the analysis of the behaviour of retaining structures. According to the bibliographical research which has been carried out, and from a practical point of view, one has for the calculation of the pressures and the dimensioning of support a panoply of methods which lack in many cases of theoretical justifications and give scattered results, generally difficult to interpret and apply. And whose effect of water flow around the wall on stability is very often overlooked. These methods proposed in the literature for the analysis of stability are based on fairly restrictive assumptions. They only take on the role of waterproofing wall where the effect of reducing passive earth pressure is ignored. In

addition, they cannot predict the deformations and failure mechanisms of retaining structures. And the values of the critical hydraulic head loss causing failure also proposed in the literature sometimes show critical differences.

2. Outline of thesis

Faced with this general problematic, the aim of this study is to analyse the overall stability of deep excavation in the presence of high groundwater level and to observe the correspondent failures mechanism, also to present optimal parameters of suitable Countermeasures against the failure of excavation bottom by the hydraulic heave. For that, numerical modelling was carried out using the code plaxis 2D, in finite elements method, for a real project case in Germany. With the aim of providing an aid tool for the design and assured sizing of retaining screens through the understanding of their behaviour and the prediction of their failure mechanisms in the presence of flow.

This thesis begins with a general introduction, and it consists of two parts:

The first part, is consecrated to the bibliographical synthesis of the flow of water in soil and the support systems of the excavations in adequacy with the studied cases, and it is composed of four chapters:

Chapter 1, is dedicated to reminders of a certain number of basic knowledge which will serve as both theoretical and practical supports. We will successively address the flow of water in the soil, the mechanical action of water on the soil and the stresses in the soil;

Followed by some very brief descriptions concerning the role, the different types and methods of deep excavation systems of support, in order to specify the performances, and the field of application of each of them;

Finally, presents the bibliographical concerning the behaviour, the failure mechanisms, and the calculation methods of retaining walls.

Chapter 2, presents a review of previous work published in the literature on the evaluation of the stability with respect to hydraulic failure of cofferdams and deep excavations invaded by the flow of water, and having a direct connection with the cases considered in this thesis. This chapter is punctuated by deductions, discussions and comparisons of the different approaches and methods proposed in literature.

The second part is devoted to the numerical modelling of excavation stability, and it includes two chapters:

Chapter 3, relates to some important elements on numerical modeling in geotechnics, presents the simulation tool (the numerical code Plaxis 2D) as well as its process of resolution, and recalls the models of behaviour most used in the modelling of soils, structure, the soil / structure interface, and the effect of water flow in the soil. Which are necessary for the analysis of the stability of retaining walls and excavations;

Chapter 4, is dedicated to the present numerical modelling of the stability of the excavations in the presence of flow around retaining wall. In this chapter which begins with an introduction of the case study, we present, first, a numerical modelling of the excavation of the real case without application of any countermeasures, we exposes the present numerical analysis carried out by means of the numerical code plaxis 2D (in finite elements) to predict the failure mechanism caused by groundwater flow and to perceive the factor of safety values against the failure of the excavation base.

Furthermore, to underscore the scientific value of this research work, the optimised length of the drainage system and its optimised position from the wall have been analysed with regard to the economic aspect, bearing in mind the safety as the first criterion.

finally, use the stone columns technic to test the column installation effect on the improvement of excavation base stability where the columns installation technics modifies the properties of the surrounding natural soil in which can give a good result of our problematic.

After the description of the used numerical model, the boundary conditions and the simulation and verification procedure for stability in the presence of flow, the present numerical results are presented in the form of charts. We compare the obtained failure mechanism and other results to those presented in literature.

First part

Bibliographical summary on the retaining of excavations

Chapter 1

Generality on the supported excavations with flow of water in soil

Chapter 1: Generality on the supported excavations with flow of water in soil

1.1 Introduction:

Water, as it is part of the constitution of soils, its presence is at the origin of several phenomena characterizing the soil such as capillarity and pore pressure. The latter has an important role in soil deformation. On the other hand, water and its movements have a direct effect on the behaviour of soils. Water is an important and decisive factor in most geotechnical problems such as swelling, freezing, seepage, uplift (buoyance), settlement, overturning, landslide, erosion ... etc.

Statistically, accidents involving the failure of cofferdams, earth dams and embankments, by internal erosion, have caused, in addition to material damage, greater loss of life than any loss caused by other types of breakage of civil engineering structures.

The study of water movements in porous media (soils) is an important problem for the geotechnical engineer, because these movements can modify over time the distribution of the pressures exerted in the mass of soils, both from a mechanical point of view (modification of mass masses and hydrostatic uplift) and hydraulic point of view (evolution of flow forces). The determination of the pore pressure field in the massifs and its evolution over time is therefore a given that must be taken into account in the calculation of the dimensioning of the structures.

Drainage and temporary or definitive lowering of the water table are often essential for the construction of structures, such as retaining walls, and for their stability. Theoretical knowledge of the laws of the flow of water in the soil, like that of the resulting mechanical action, will be necessary for the designer, they will allow him to understand the physical and mechanical principles which are not fundamentally given. involved by the results of the practice, as well as predicting and explaining the particular behaviour of soil massifs. Knowledge of the practice of the work is no less fundamental because it must meet the designer's objective, on a site which is always an exceptional case, and with means which depend on both technological and financial factors.

A background and summary of essential theory are presented in this chapter. The first subchapter delivers an overview of water flow through soil, in order to provide the reader a background of water flow mechanics in soils and the factors that influence it. Followed by the retaining system used to fix excavations and their methods of analysis.

1.2.   Definition of a porous medium:

A porous medium is a skeleton or "porous matrix", inside which flows one (or more) fluid (s) (gas or liquid) in one (or more) phase (s). In the case of an application to soil and rock mechanics, the porous medium studied is a mass of natural soil (diffusion of pollutants, infiltration, flow and lowering of the water table), a mass around a structure (foundation, tunnel, sheet pile wall, diaphragm wall, etc.), or additional soil (earth embankments and dams, etc.).

1.3.   Analysis of groundwater problems

1.3.1. Flow of water in soils

The water stays in or circulates in the interstices (pores or cracks) of the masses of soil or rock. Water has essentially two forms of interaction with a porous medium: it moves through the pores and it exerts pressure on the solid phase (matrix) and deforms it.

In soil hydraulics, we are most often dealing with permanent regimes, i.e stabilized flows for which the speed of the water at any point in the massif is independent of time. Fluid particles therefore follow trajectories (or liquid streams), called streamlines, invariable over time. Unlike the transient regime which is unstable and variable over time.

Along a liquid stream, the pressure and speed of the water vary according to certain laws.

1.3.2. Flow velocity and flow pressure

Seepage is generally given as a term for the movement of water through a soil mass. On a microscopic scale, the water when flowing follows a snaky path through the voids in the soil. From a practical point of view, however, it is supposed to follow a straight-line path. In Darcy's equation, the velocity v is interpreted as the apparent or superficial velocity, i.e. the velocity of flow relative to a soil section area A. The velocity through pores will be sizeable, and this is called the *seepage velocity* (v_s).

Consider a soil of porosity: $n = A_V/A$

For a given flow rate: $q = Av = A_V v_s$

where A= section area of soil (perpendicular to flow direction)

A_V= section area of voids

$$\upsilon_s = \upsilon \frac{A}{A_V} = \frac{\upsilon}{n} = \frac{ki}{n}$$

[1.1]

The task made by water during seepage results in a seepage force (J) being applied on the particles. With regard to the column of soil shown in Figure 1.1. When the valve at level A-A is large open, flow takes place under the influence of a head of h_s, thus an upward-acting seepage force is pursued on the soil particles between C-C and B-B.

The water level will rise until it reaches O-O by closing the valve at level A-A where it will remain stationary. At this point there will be no seepage. It may be concluded, subsequently, that the seepage force has now been equiponderant by the additional weight of water between A-A and O-O .

Then seepage force, $(J) = \gamma_w h_s A$ [1.2]
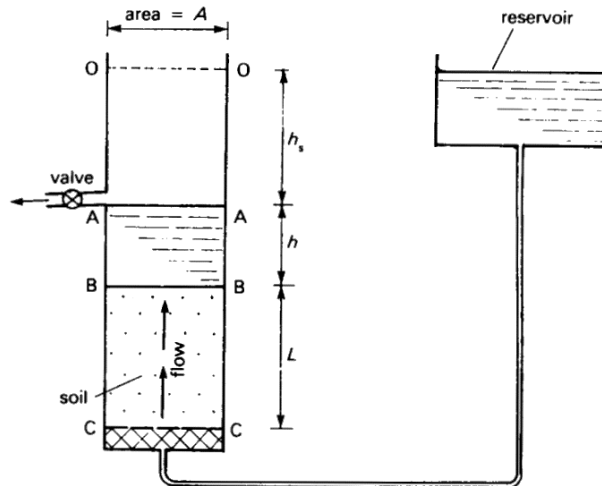
Figure 1.1 Seepage pressure.

But since the flow velocity is constant the seepage force acting on the soil will also be constant between C-C and B-B.

$$j = \frac{\gamma_w h_s A}{LA}$$

[1.3]

So that seepage force per unit volume,

And as $\dfrac{h_s}{L} =$ hydraulic gradient i

Then
$$j = i\gamma_w \qquad\qquad [1.4]$$

The seepage force per unit volume (j) is usually generally to as the seepage pressure.

1.3.3. Quick condition and critical hydraulic gradient

The effect of water flowing upwards in a soil mass in creating a seepage pressure on the soil particles is to reduce the inter-granular or effective stress. If a sufficiently high flow rate is achieved, the seepage pressure can completely cancel out effective stress causing a quick condition. This is basically a condition in which the soil has no shear strength, since the inter-granular stress has been reduced to zero.

At the quick condition (the situation in Figure 1.1.), the flow will cause a seepage force at C-C which will be equal and opposite to the effective stress due to the weight of soil.

Then equating forces at C-C:

$$\gamma_w(L + h + h_s)A = (\gamma_{sat}L + \gamma_w h)A \qquad\qquad [1.5]$$

Giving
$$\gamma_w h_s = (\gamma_{sat} - \gamma_w)L \qquad\qquad [1.6]$$

Or
$$\gamma_w i_c = \gamma' \qquad\qquad [1.7]$$

In which i_c is named the critical hydraulic gradient, i.e. the hydraulic gradient where rapidly condition occurs. A numerical value may be obtained for i_c therefore:

$$i_c = \frac{\gamma'}{\gamma_w} = \frac{\gamma_{sat} - \gamma_w}{\gamma_w} \qquad\qquad [1.8]$$

$$= \frac{(G_s + e)\gamma_w / (1 + e) - \gamma_w}{\gamma_w} \qquad\qquad [1.9]$$

$$= \frac{G_s + 1}{1 + e} \qquad\qquad [1.10]$$

1.4. Bernoulli's Equation

According to Bernoulli's equation based on fluid mechanics, we know that, the total height at a point in moving water can be given by the sum of the pressure, velocity and elevation loads, or

$$h = \frac{u}{\gamma_w} + \frac{\upsilon}{2g} + z \qquad [1.11]$$

Where

h= total head

u= pressure

v= velocity

g= acceleration due to gravity

γ_w= unit weight of water

Which the elevation head, Z, is the vertical distance of a given point above or below a datum plane. The pressure head is the water pressure, u, at that point divided by the unit weight of water, γ_w.

On the flow of water through a porous soil medium, the term containing the velocity head can be neglected if Bernoulli's equation is applied, because the seepage velocity is small, and the total head at any point can be adequately represented by

$$h = \frac{u}{\gamma_w} + z \qquad [1.12]$$

1.5. Darcy's Law

Water below the water table may be either static or infiltrating into the ground in response to a hydraulic gradient (by Terzaghi, et al., 1996). Bernoulli's theorem applies to pore water, as seepage velocities in soils are normally so small the velocity head can be neglected (Das, 2007), as result head can be calculated as follows:

$$h = \frac{u}{\gamma_w} + z \qquad [1.13]$$

13

Where
h= total head
u= pressure
γ_w= unit weight of water
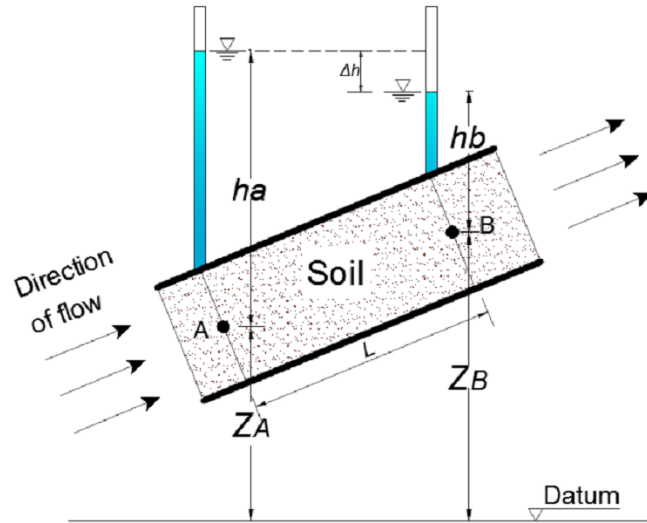
Figure 1.2 Development of Darcy's Law

In normal conditions, water will not flow in saturated soil where an impermeable boundary below the soil resists vertical flow, but when there is a difference in pressure heads (Δh) water will flow in the direction of the reduced head. The head loss between A and B as shown in Figure 1.2 is calculated as follows:

$$\Delta h = (Z_A + h_A) - (Z_B + h_B) \qquad [1.14]$$

The hydraulic gradient (i) over a distance (L) is calculated as follows:

$$i = \frac{\Delta h}{L} \qquad [1.15]$$

Darcy (1856) established an empirical relationship through observing the rate of water flow through granular soil, this became known as Darcy's Law, which states the discharge velocity, v is proportionate to the hydraulic gradient i. From these observations he derived the following equation:

$$\frac{q}{A} = v = ki \qquad [1.16]$$

Where:

q = flow

k = coefficient of permeability

A = Cross section area of a soil sample

As the hydraulic gradient is the force that causes the water to flow, the rate of seepage, q with the S.I unit's m³/s can be calculated from the above equation as follows:

$$q = Aki \qquad [1.17]$$

Darcy's law is said to be true for laminar flow, this occurs when q is directly proportional to h (Powers, et al., 2007). Muskat (1938) carried out a study to investigate the range for which Darcy's law is valid. Muskat established that the range could be provided with the Reynolds number. The ratio of inertial forces to viscous forces is defined as the Reynolds number, with laminar flow occurring when viscosity is dominant. In soils the Reynolds number (R_n) is calculated as follows:

$$R_n = \frac{vD_{30}\rho}{\mu} \qquad [1.18]$$

Where

v = discharge velocity, m/s

D_{30} = diameter of particle size at 30% passing, m

ρ = density of the fluid, kg/m³

μ = coefficient of viscosity, kg/m-s

1.6.   Permeability of soils

Soil samples consist of solid particles of various sizes with interconnected void spaces, consequently all soils can be stated to be permeable in nature. These continuous voids in a soil sample permit the flow of fluids from a point of high energy to a point of low energy.

Primary permeability refers to flow through the voids of a soil or rock, while secondary permeability refers to flow through fractures or fissures in soils, for the purpose of this dissertation only primary permeability will be considered. Permeability is a vital parameter when calculating seepage as the velocity at which water travels through soil is greatly influenced by it.

1.6.1. Coefficient of Permeability (k Value)

The coefficient of permeability is measured in *m/s*. As the coefficient of permeability is also a measure of the ease at which water passes through soils the viscosity of the liquid is also important.

1.6.2. Approximation of Coefficient of Permeability (*k*) in the Lab

There are two methods frequently used to measure the value of *k* in the laboratory conditions, the constant head permeability test and the falling head test. The constant head permeability test (BS 1377:1990) is used to determine the permeability of granular soils like sands and gravels containing little or no silt with *k* values between 10^{-2} and 10^{-5} m/s (Criag, 2004), the falling head test is used to measure permeability of silts and clays with *k* values of 10^{-6} m/s and slower.

1.6.2.1. Constant Head permeameter

The constant head permeameter (Figure 1.3) is perhaps the simplest method of measuring permeability.

The test entails the flow of water through a cylindrical soil sample under a constant head of water with a pressure differential generated by two tapings at different levels on the side of the cylinder (Figure 1.3).

The soil sample is placed in a permeameter, with the diameter dependent on the size of grain, Head (1982) proposed that the largest grain size ratio to permeameter diameter should be greater than 1:12 for accurate results.

The testing apparatus is equipped with a constant head reservoir and an outlet at the bottom of the permeameter which facilitates the preservation of a constant head during the test.

Water used for testing is de-aired water at constant temperature and a coarse filter is placed at the bottom of the permeameter to prevent any soil particles escaping (Mc Geever, 2012).

The soil must be fully saturated before the test can begin. During the test, a quantity of water flowing through the permeameter is measured for given time intervals, the difference in head *Δh* between the tapings is also recorded. The parameters as follows are now known:

- The height of the soil sample column L
- The sample cross section area A
- The constant pressure difference Δh
- The volume of passing water Q
- The time interval T

Using Darcy's Law an equation can be used to calculate k as follows:

$$k = \frac{Q \times L}{A \times \Delta h \times T}$$
[1.19]

The constant head test uses disturbed soil samples so this test can only give an estimation to actual in-situ conditions.
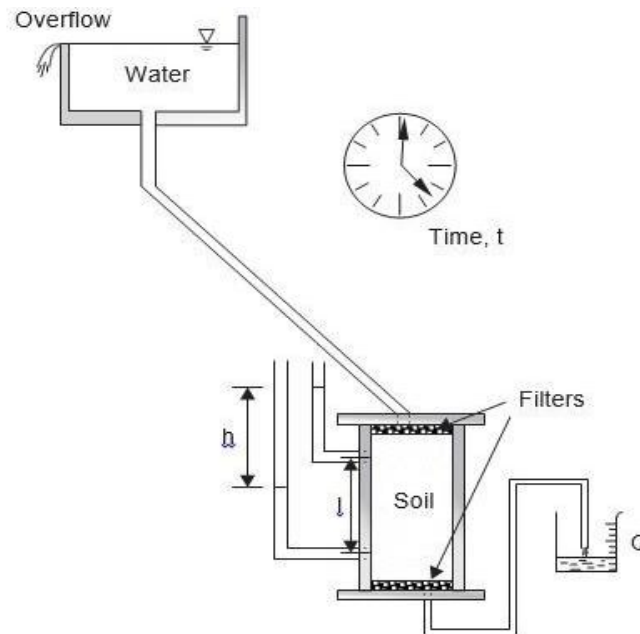
Figure 1.3 Constant head permeameter.

1.6.2.2. Falling head permeameter

The constant head permeameter is not suitable for investigating the permeability of fine-grained (with low permeability) soils where the flow rates are so small that evaporation from the measuring cylinder could lead to significant error. For fine soils, a falling head permeameter is used (Figure 1.4). Water flows from a small-bore tube of cross-sectional area A_2, through the soil specimen that is contained within a larger tube of cross-sectional area A_1.

At the start of the test (time t =0), the water level in the upper (small-bore) tube is at a height h_1 above the outlet of the permeameter. The water level in the upper tube then falls as water flows through the soil sample. At the end of the test (time $t = T$), the water level in the upper tube has fallen to a height h_2 above the outlet.

At a general time t $(0 < t < T)$, the water level is at a general height h $(h_1 > h > h_2)$. Applying Darcy's Law at a general time t to the soil specimen in the large tube,

$$q = Aki = A_1kh/L \qquad\qquad [1.20]$$

In the small-bore tube, the flow rate is given by the cross-sectional area multiplied by the velocity

$$q = A_2v$$

but the velocity $\qquad\qquad v = -dh/dt$,so

$$q = -A_2dh/dt \qquad\qquad [1.21]$$

(the negative sign is needed because v has been taken as positive downward, while h is measured as positive upward). Equating (1.20) and (1.21)

$$dh/dt = -(A1/A2)(k/L)h \qquad\qquad [1.22]$$
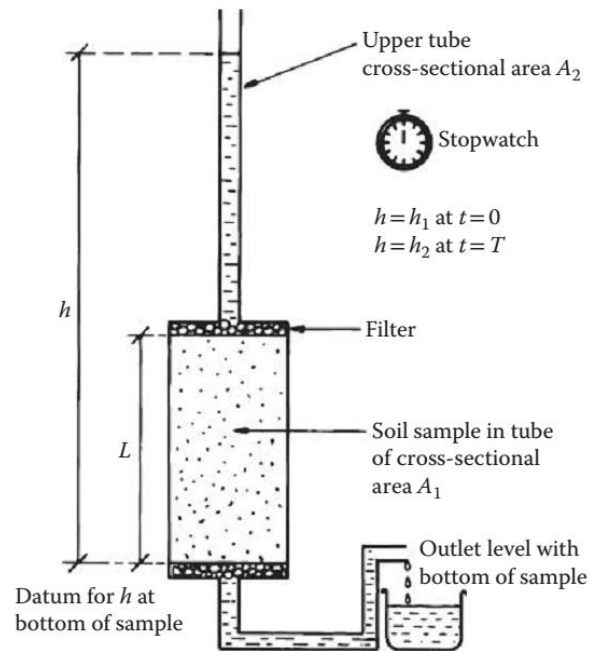
Figure 1.4 Falling head permeameter.

Integrating between limits of $h = h_1$ at $t=0$ and $h=h_2$ at $t=T$:

$$\int_{b1}^{b2} dh / h = -\int_0^T (\frac{A_1}{A_2} \cdot \frac{k}{L})dt \qquad [1.23]$$

Hence,
$$\ln(h_2 / h_1) = -(A_1 / A_2)(k / L)T \qquad [1.24]$$

Or
$$k = (A_2 L / A_1 T) \ln(h_1 / h_2) \qquad [1.25]$$

1.7. Excavation methods and lateral supporting systems

The construction of basements in particular deep excavation includes the construction of retaining walls, the construction of foundations and floor slabs, the installation of struts, and all stuff related to excavations. With the great variety of excavation methods and lateral supporting systems, to come to the most appropriate design, we have to consider, in combination, the environmental conditions, the local geological conditions, the allowable construction period, the available construction equipment, with the budget where make an overall plan accordingly.

1.7.1. Retaining walls types

1.7.1.1 Soldier piles

Types of steel for soldier piles include the rail pile, the steel H-pile (or W section) and the steel I-pile (or S section). The rail pile and the steel H-pile are more commonly used than the
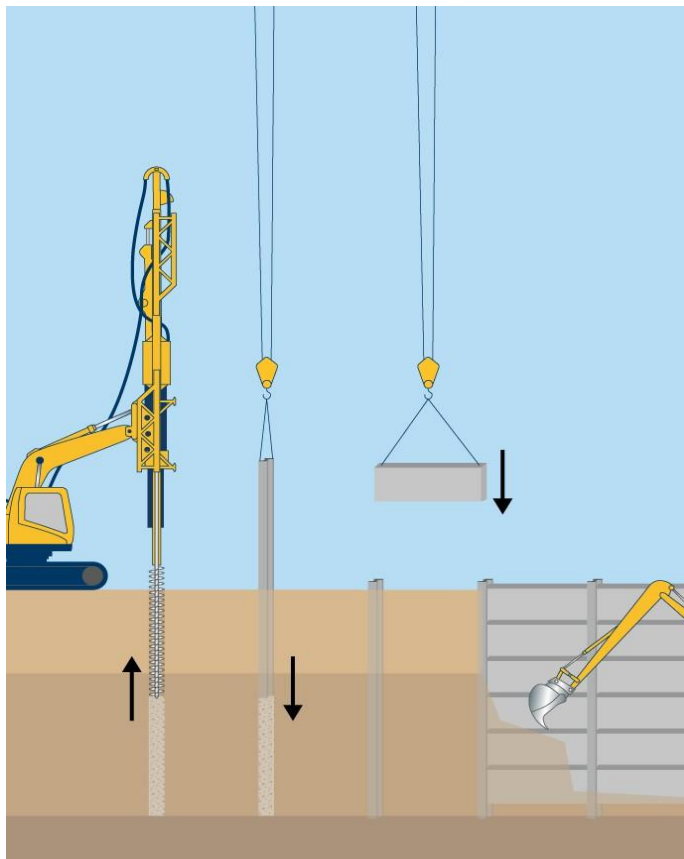
Figure 1.5 Photo of the soldier pile method. Ou, C. Y. (2014). Deep excavation: Theory and practice. Crc Press.

steel I-pile. The section of the rail pile is usually expressed in weight per unit length (kg/m) as commonly used sizes. Figure 1.5 is a picture of the soldier pile method.

1.7.1.2 Sheet piles

Sheet piles can be driven into soil by striking or static vibrating and have them interlocked or connected with one another. Figure 1.6 shows the front view of sheet piles and Figure 1.7 is a photo show in g the sheet pile s in an excavation.
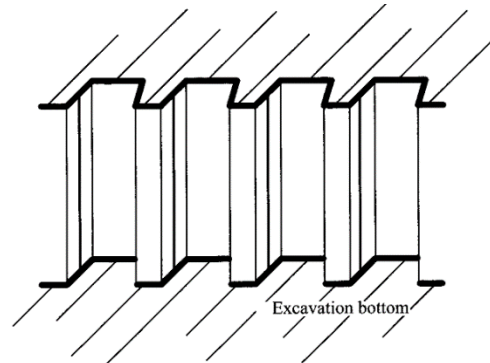
Figure 1.6 Steel sheet pile method. Ou, C. Y. (2014). Deep excavation: Theory and practice. Crc Press.
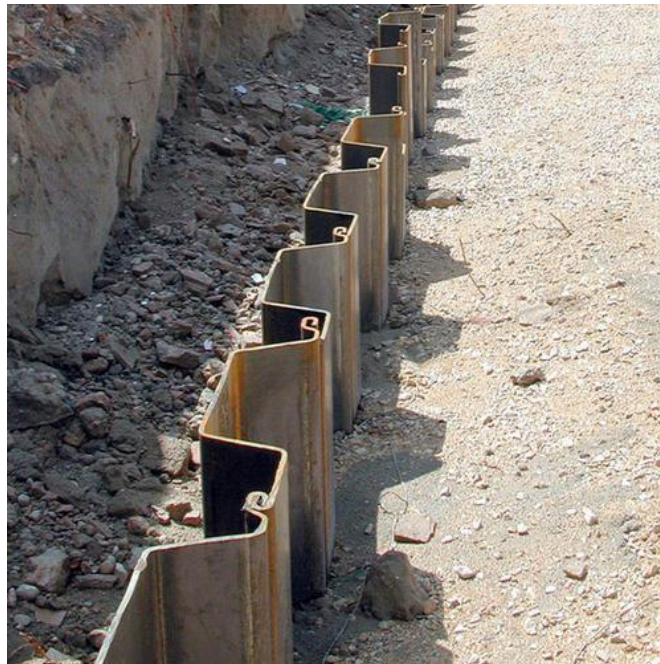
Figure 1.7 Photo of the sheet pile method. Ou, C. Y. (2014). Deep excavation: Theory and practice.

1.7.1.3 Column piles

The column pile method is to introduce rows of concrete piles as retaining walls by either the cast-in situ pile method or the precast pile method. Figure 1.8 shows the column pile wall and according to their construction characteristics, the cast-in situ method can be divided into three subtypes.

1.7.1.3.1. Packed in place piles:

PIP pile method, also called The packed in place pile method, can be described as a dig to the designed depth with a helical drill, while lifting the chopping bit gently, fill in prepacked mortar from the front end to press away from the loosened soil to the ground surface and put steel cages or steel H-piles into the hole after grouting is finished

Figure 1.8 Photo of column piles, https://worldbuilding.stackexchange.com/questions/152572/how-quickly-could-a-country-build-a-tall-concrete-wall-around-a-city/152620
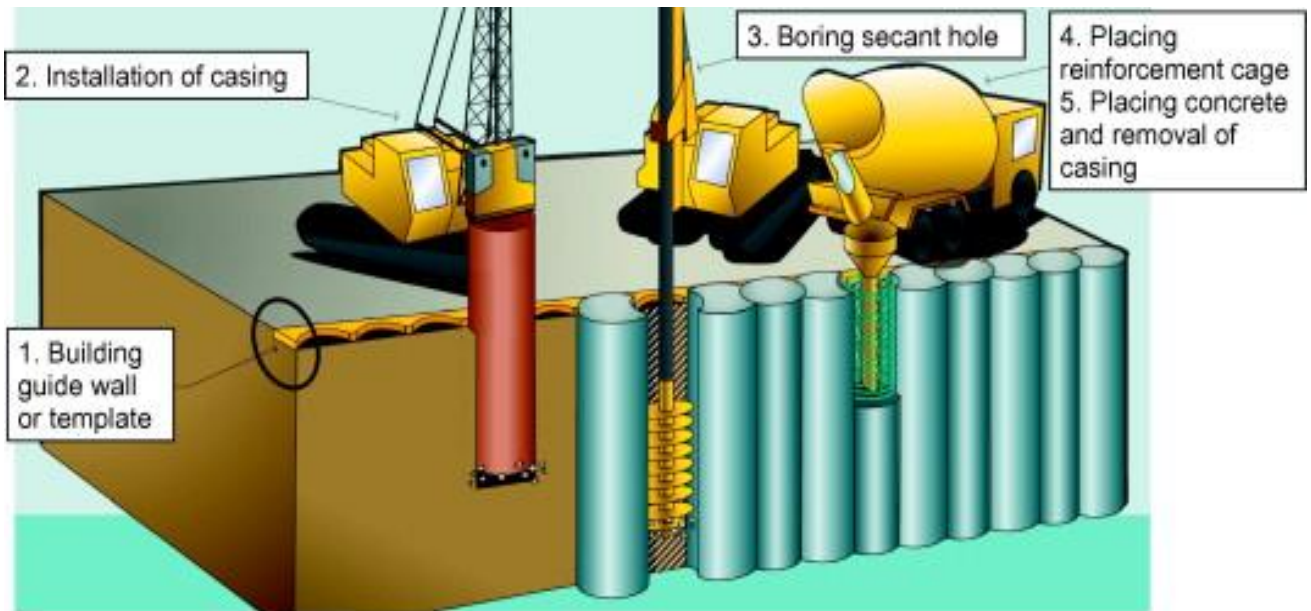
Figure 1.9 Construction procedure of a packed in place (PIP) pile. Ou, C. Y. (2014). Deep excavation: Theory and practice. Crc Press.

The diameter of a PIP pile use d to be around 30 to 60 cm. It often happens that PIP piles cannot be installed completely vertically, so connection voids often cause groundwater leaks and connections are therefore not always airtight. Thus, if the PIP pile is adopted for the retaining wall in sandy soils with high groundwater level, sealing and grouting are often required. Figure 1.9 illustrates the construction method of a PIP pile.

1.7.1.3.2. Concrete piles:

The construction of concrete piles can be described as follows: drill a hole to the designed depth by machine, put the steel cages into it, and fill it with concrete using Tremie tubes.

The reverse circulation drill method (also called the reverse method), which is to employ stabilizing fluid to stabilize the hole wall during drilling, is the most commonly used construction method for concrete piles. It is also feasible to build following the all casing method, which is to drill with simultaneous casing-instalment to protect the hole wall. Since the wall is protected by casings, stabilizing fluid is not required. The cost of the all casing method is rather high. Nevertheless, it can be easily applied to cobble-gravel layers or soils with seepage whereas the reverse method cannot. The diameters of the concrete piles are around 60-200 cm.

1.7.1.3.3. Mixed piles:

Mixed piles are also called MIP piles (mixed in place piles) or SMW (soil mixed wall). The method is to employ a special chopping bit to drill a hole with the concrete mortar sent out from the front of the bit to be mixed with soil. When the designed depth is reached, lift the bit a little, keeping swirling and grouting simultaneously, and let mortar mix with soil thoroughly.

(a)   (b)   (c)   (d)
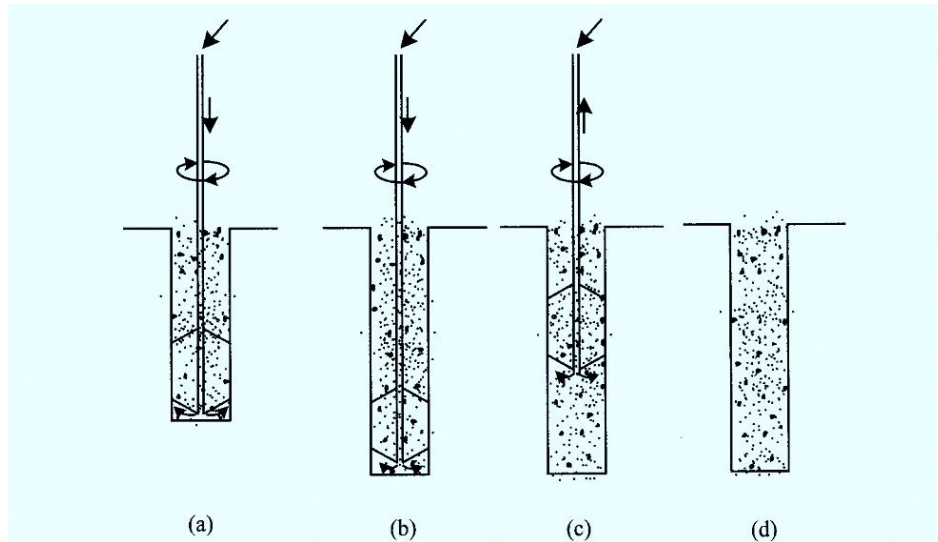
Figure 1.10 Construction procedure of a mixed in place (MIP) pile. Ou, C. Y. (2014). Deep excavation: Theory and practice. Crc Press.

After pulling out the drilling rod, put steel cages or H-piles into the hole if necessary. Figure 1.10 illustrates the construction process for a mixed pile. Figure 1.11 shows MIP piles with H steels.
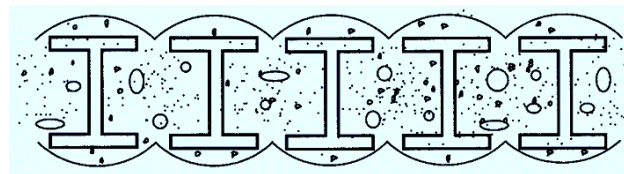
Figure 1.11 Soil mixed wall (SMW). Ou, C. Y. (2014). Deep excavation: Theory and practice. Crc Press.

1.7.1.4. Diaphragm walls

Diaphragm walls are also called slurry walls. Since first adopted in Italy in the 1950s, they have been widely used around the world. With technological advances, more and more new

methods and construction equipment have been developed. The basement wall (BW) method and Impresa Construzioni Opere Specializzate (ICOS) method, designed separately by a Japanese company and an Italian company are commonly used in some Asian countries. The Masago Hydraulic Long bucket (MHL) method, taking advantage of a bailing bucket to excavate the trenches of the diaphragm wall, are also used in many countries. As shown in Figure 1.12, the teeth of the steel bailing bucket can clutch soils and rock s and store them inside the bucket. Then, the full buck et is lifted out of the trench and soil and rocks inside are bailed out.

Figure 1.12 Trench excavation by the MHL method. Ou, C. Y. (2014). Deep excavation: Theory and practice. Crc Press.

Thus, stabilizing fluid need not be pumped out and mud separation equipment is saved. The method is easy in operation. The span of the bailing bucket is about 2.5 - 3.3 m.

1.7.2 Strutting systems

According to the function of a strut, it is classified as an earth berm, a horizontal strut, a raker, an anchor, or as a top-down floor slab, etc. Figure 1.13 shows an earth berm, which is made by removing the soil in the central area while retaining an earth berm with a certain width for the lateral support of retaining walls. The earth berm is usually supplementary to island excavation

methods. With the limitation of the width, the earth berm has accordingly limited lateral resistance and is useful only on grounds with high strength, and is rendered useless on soft ground.

Horizontal struts can be made of wood, RC, or steel, whose merits and drawbacks are as mentioned earlier.
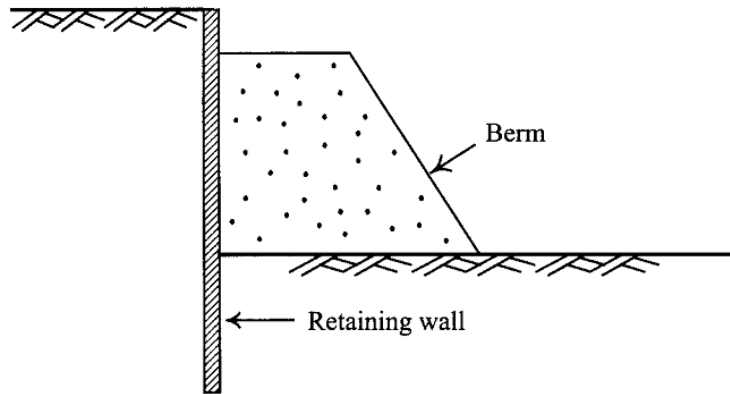
Figure 1.13 Earth bern as lateral support Ou, C. Y. (2014). Deep excavation: Theory and practice. Crc Press.
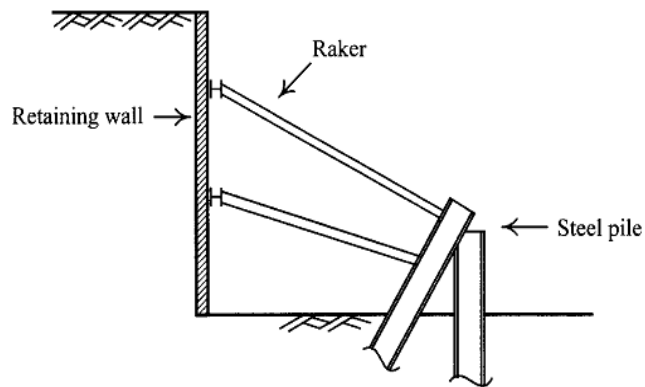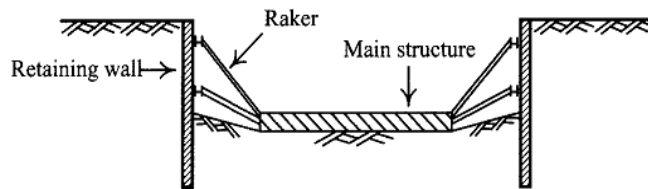
Figure 1.14 Rakers. Ou, C. Y. (2014). Deep excavation: Theory and practice. Crc Press.

A raker is a type of strut and can also be made of wood, RC, or steel. Known from the systematic characteristics of a structure, the lateral support from the raker is smaller than that from the horizontal strut. Rakers are mostly employed in the island excavation method though they can also be used separately as shown in Figure 1.14. Anchors and top-down floor slabs are two other types of struts.

1.8. Behaviour and different calculation methods for excavation supports

Flexible supports are an effective way to support a mass of earth, installing them by driving them into the ground in the form of vertical screens made up of long thin elements (steel, concrete or wood). Where the soil constitutes, at the same time, the support and the load for these works. Of which the transfer of thrust forces is carried out in depth by the length of the lower part (embedding length) commonly designated by the embedment.

Compared to massive gravity retaining walls (concrete or stone masonry), flexible supports are distinguished primarily by the redistributions of earth pressures caused by their deformation and the presence of stabilizing elements (anchoring) such as tie rods or the struts.

Flexible supports are structures, in which bending moments are developed under the effect of lateral soil pressures and water pressures, and they must be designed so that they can withstand the maximum bending moment. This leads to complex operating structures which cannot be apprehended correctly from simple theories such as classical calculations of active or passive thrust of the earth.

For this reason, several methods of analysis, of different levels of complexity, have been developed for these works: theoretical and experimental studies (both on reduced models and on real curtains), and numerical simulations.

The methods of calculating retaining screens in use today are very diverse, methods born at the beginning of the 20th century and methods developed from the 1970s, completely empirical methods and methods based only on theoretical models, methods claiming to account for the in-service behaviour of structures, while being qualified as "failure" methods.

The development, at the beginning of the 20th century, of retaining screens, flexible structures taking support in the ground and presenting a specific deformation, will considerably widen the question of the soil-structure interaction. To the question of the thrust of the earth is now

added the question of the earth-history, given the support opposed by the ground to the sheet part of the structure. To the kinematics of rotation at the foot are added kinematics of rotation at the head.

1.8.1. Wall and ground movements

Because the ground surface geometry is altered during retaining wall construction, there is redistribution of forces, and displacements occur. The following sections examine the causes of wall movements, the basic patterns of movement that occur, and the effect of these on the movement of the surrounding ground.

1.8.2. Wall flexibility

Most walls are not completely rigid, so they undergo both rigid body movement and flexing. Steel sheet piling is particularly flexible, but even bored piles will flex significantly when used to support a deep excavation. A braced, strutted or anchored embedded wall constructed to retain the soil below adjacent buildings will undergo relatively small amounts of lateral translation at the support levels, once the supports are placed, but will flex between them. However, it is inevitable that some horizontal movement of the wall will occur as the construction of the wall is carried out, resulting from

- The reduction in support for the soil when excavating for bored piles or diaphragm walls

- Wall movements as top-down excavation occurs in each stage of excavation, before support can be installed

- Wall flexure

- Movement in the support system as load comes onto it, for example, due to compression of struts and packing between struts and the wall, or extension of ground anchor tendons

Figure 1.15 gives sketches of some basic patterns of movement for different wall types.

(a)
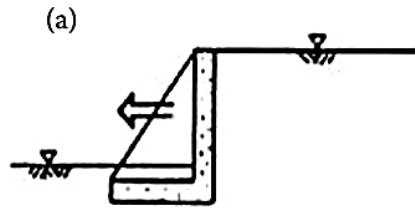
Reinforced concrete buttressed wall: structure does not bend, due to stiffening effect of buttresses. The wall may translate rather than rotate about its base, when loads are applied.

(b)
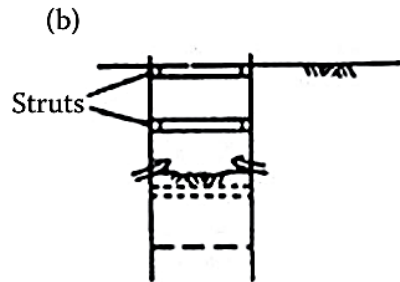
Struts

Strutted steel sheet piling: interlocking steel sheet piling is driven from ground level before excavation starts. Steel wales and struts are placed in position at the bottom of the excavation as it is dug. Between strut levels the sheets tend to deflect inward, effectively giving rotation about ground level.

(c)

Support

(O)
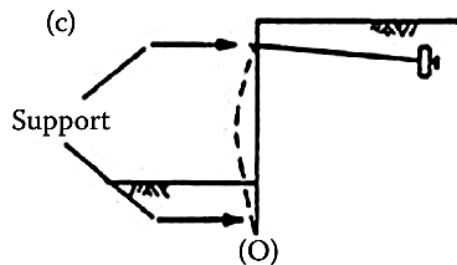
Anchored sheet-pile wall: for pressure calculation is assumed to rigidly rotate about its toe (O). In reality, the sheets deflect as shown by the dotted line, causing a redistribution of pressures.

(d)

Bridge deck — Abutment
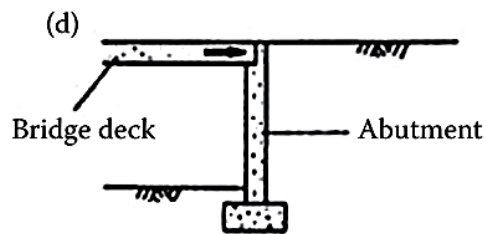
Bridge abutment: thermal expansion of the bridge deck (perhaps after casting *in situ* concrete) forces abutment against soil, and earth pressures rise. This effect also applies to strutted excavations under large ambient temperature changes.

(e)
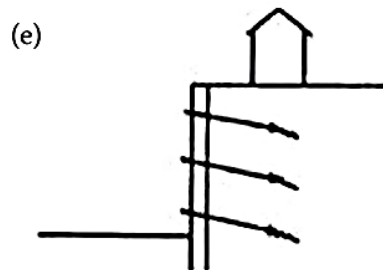
Diaphragm wall: carefully constructed and restrained to restrict settlements beneath adjacent structures. Lateral movements are restricted, and full shear strength is not mobilized. Forces probably lie between 'at rest' (c) and 'active' (a), but rotation is not about bottom of wall.

Figure 1.15 Example of retaining wall movements. Clayton, C. R., Woods, R. I., & Milititsky, J. (2014). Earth pressure and earth-retaining structures. CRC press.

1.8.3. Earth pressure Principles

This section considers the basic principles controlling the earth pressures applied to walls. These provide earth pressure coefficients for some detailed but simple methods of analyses for a range of wall and soil conditions.

1.8.3.1. Earth pressure at rest

Consider a deposit of soil formed by sedimentation in thin layers over a wide area. No lateral yield occurs as a result of the imposition of load upon it by the deposition of successive layers above. The *in situ* horizontal effective earth pressure σ_h' in such a soil is known as the '*earth pressure at rest*'.

Terzaghi used the concept of an earth pressure coefficient, K,

$$k = \sigma_h' / \sigma_V' \qquad [1.26]$$

$\sigma_h' =$ the horizontal effective stress at any depth below the soil surface, and

$\sigma_V' =$ the vertical effective stress at any depth below the soil surface, which for the simple case of a uniform dry soil equals the product of the depth below the soil surface (m) and the bulk unit weight (kN/m^3) of the soil.

The effective horizontal and vertical pressures in the at-rest state are related by K_0.

$$k_0 = \left[\sigma_h' / \sigma_V' \right]_{\text{at rest}} \qquad [1.27]$$

1.8.3.2 Earth pressure coefficients

In the simplest case of a smooth rigid vertical wall retaining horizontal granular backfill, Rankine theory predicts

$$K_a = \frac{(1 - \sin\phi')}{(1 + \sin\phi')}$$

And
$$K_p = \frac{(1 + \sin\phi')}{(1 - \sin\phi')} = 1 / K_a \qquad [1.28]$$

1.8.4. Defining Failure

Retaining structures shall be designed, constructed, and after all maintained in such a way where they are suitable for use throughout their entire working life. In particular, they should fulfill satisfactorily under both extreme and expected conditions

Bearing capacity, sliding, and overall stability failure are examples of situations where failure can occur through the soil (or soil/structure interface) without the undertaking of the structural strength. Examples of overall instability for gravity and anchored retaining walls are presented in figure 1.16, whereas in figure 1.17 can found how these may vary, depending upon how the wall is supported. For a further example, the vertical equilibrium of an embedded retaining wall (that can have a relatively small bearing capacity at its toe) may need to be checked to guarantee that the implied vertical component of anchor forces can be met by the resistance due to the wall/soil friction.

The capacity of the structure to support the overstrained loads by the ground must also be examined. This includes not only the strength of the retaining structure, but also structural elements such as struts, wales, anchorages, and failure of the connection between such elements.
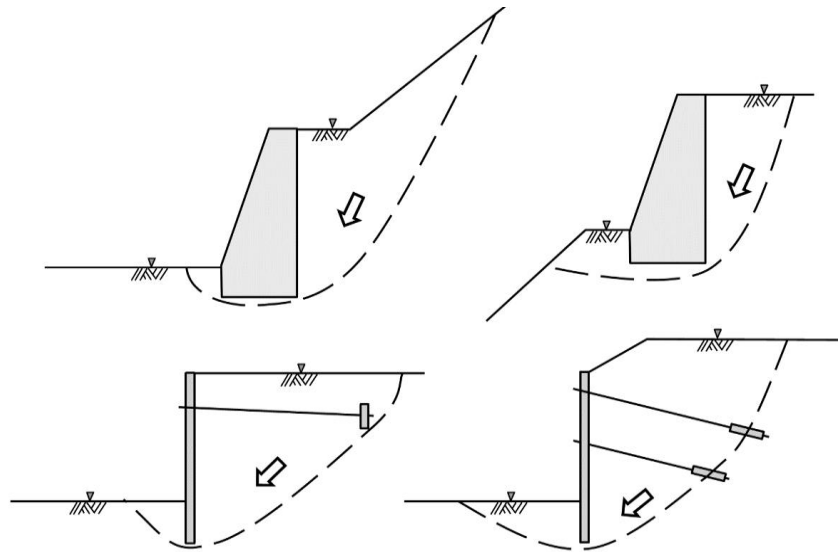
Figure 1.16 Examples of overall instability for gravity and anchored retaining

walls. (Redrawn from Clayton, C. et al., Earth Pressure and Earth-Retaining

Structures, Second Edition, Taylor & Francis, Jan 7, 2014.)
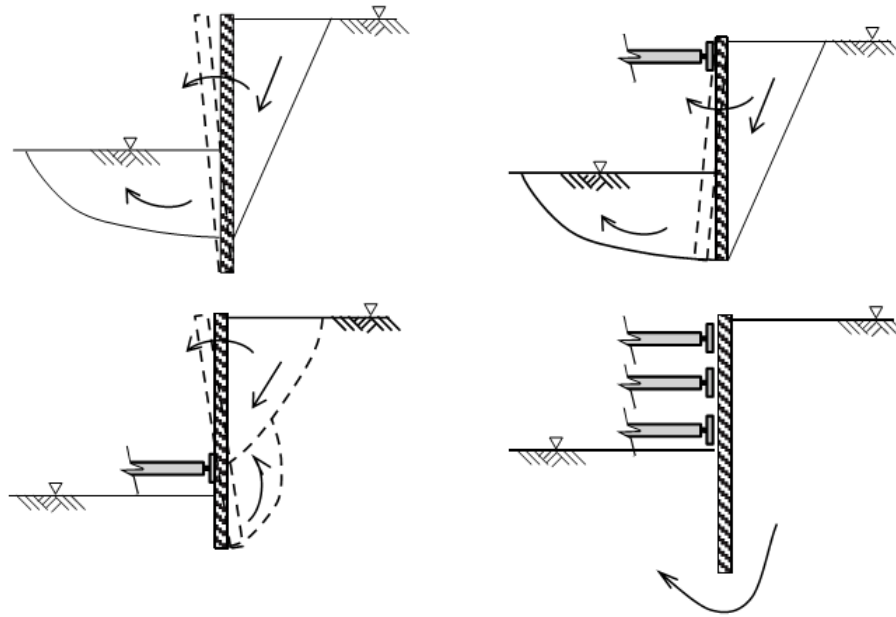
Figure 1.17 Examples of failure modes for a range of embedded walls. (Redrawn from Clayton, C. et al., Earth Pressure and Earth-Retaining Structures, Second Edition, Taylor & Francis, Jan 7, 2014.)

1.8.5. Introduction to analysis

The system of retaining structure may be analysed in many different ways and a variety of methods are available to the designer. Each has a valuable place in the 'tool box' and it is up to the engineer to appreciate the assumptions and limitations of each in order to select the most appropriate for a given task. They range from such simple one (can require only hand calculations) to the much complex (can require significant computational power).

1.8.5.1 closed-form solutions

In mathematics, a proper expression of a closed-form solution is one that can be expressed analytically in terms of a bounded number of certain elementary functions. A closed-form solution would include by most engineers to be one that can be computed without the need for iteration and expressed by an explicit equation; for example, the collapse load of a strip footing on clay based on the solution for a rigid punch indenting a metal surface Prandtl, L. (1921). It is the mode of application rather than the mode of derivation that determines whether or not it is closed-form. The term closed-form will be used in this section for solutions to governing equations that have been obtained by analytical means.

A severe closed-form solution in continuum mechanics is one that persuade the compatibility, the equations of equilibrium and constitution (i.e. stress-strain relationships) in which the two main theories that have furnished solutions of practical use in retaining wall design are the theory of elasticity (Love 1927) and the theory of plasticity (Hill 1950).

1.8.5.2. Solutions based on elasticity theory

When strains are reversible—deformation is fully recovered upon the removal of load, the situation goes to the essential characteristic of elastic behaviour. Elastic behaviour must not be linear, although the wide majority of closed-form solutions be supposed linearity (probably because there is no universally accepted way of describing non-linear stiffness in a simple manner).

1.8.5.2.1. Excavation heave

The suitable estimates of excavation heave that have been suggested by Butler (1975) can be made using simple charts, derived with Steinbrenner's method—initially planned for estimating settlement (Steinbrenner 1934). In Figure 1.18 one of Butler's charts is reproduced for an excavation square in plan (L/B = 1) and for undrained loading conditions ($v = 0.5$), appropriate for estimating short-term heave.

In Butler's charts, Young's modulus, E, varies linearly with depth according to

$$E = E_0(1 + k.z/B)$$

$$[1.29]$$

where E_0 is Young's modulus at the surface and k expresses its rate of increase with respect to the depth/foundation width ratio *(z/B)*. *H* (on the vertical axes of the charts) is the thickness of the layer in which the excavation is made and $I\rho$ is an influence factor for vertical movement. The heave is estimated from the equation

$$\rho = I\rho \left[\frac{q.B}{E_0} \right]$$

$$[1.30]$$

where q is the amount of vertical stress reduction due to excavation. Using undrained Young's modulus values derived from undrained triaxial compression tests on 102 mm diameter specimens, on the basis that

$$E_u = 220c_u$$

$$[1.31]$$
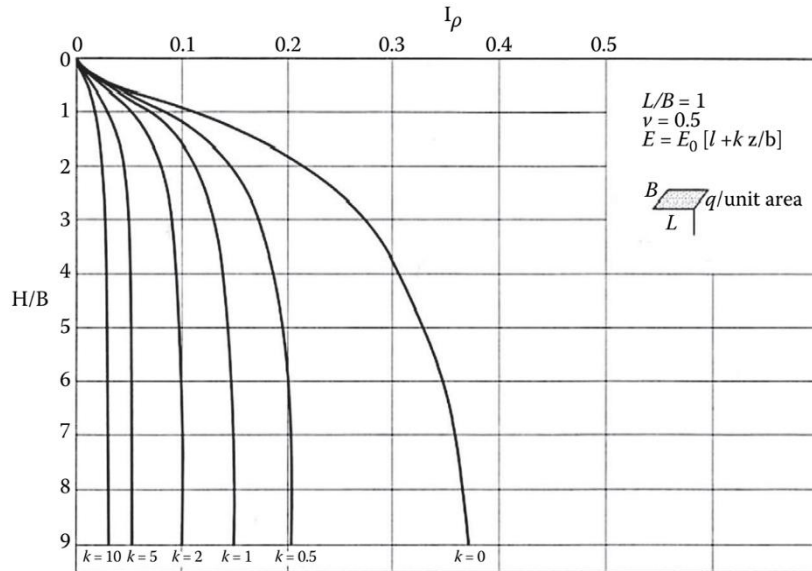
Figure 1.18   Chart for estimating undrained heave and reloading settlement. (From Clayton, C. et al., Earth Pressure and Earth-Retaining Structures, Second Edition, Taylor & Francis, Jan 7, 2014.)

1.8.5.2.2. Wall bending

Based on elastic theory, bending deformation is another important type of calculation (i.e. the deflections and curvature of the wall under working conditions). The beam theory of Euler and Bernoulli (nowadays referred to simply as engineering beam theory) is described in a number of standard texts (e.g. Gere and Timoshenko 1991). In Figure 1.19, the governing fourth-order equation is derived from the standard result linking the principal quantities, namely,

$$\frac{\sigma_x}{y} = \frac{M}{I} = \frac{E}{R}$$

$$[1.32]$$

From which

$$M = -EI\frac{d^2v}{dx^2}$$

$$[1.33]$$
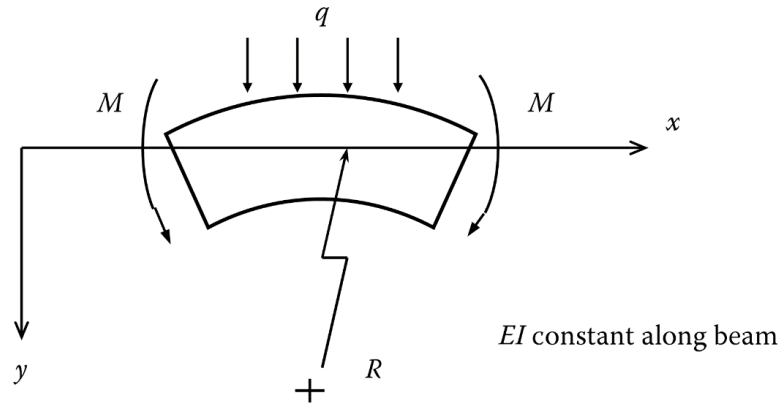
Figure 1.19 Simple beam bending. . (From Clayton, C. et al., Earth Pressure and Earth-Retaining Structures, Second Edition, Taylor & Francis, Jan 7, 2014.)

Other considerations of vertical equilibrium and moment lead to the familiar fourth-order equation relating loading intensity *q* and deflection *v*:

$$EI \frac{d^4 v}{dx^4} = q$$

$$[1.34]$$

It is possible for relatively simple boundary conditions (i.e. for rotation, loading, and displacement), to solve Equation 1.32 analytically to obtain distributions of shear, deflection, and moment along the beam. By considering the earth pressures as the applied loading intensity and the retaining wall as a vertical beam, it would be possible to adapt these solutions to a retaining wall context. However, many of earth retaining structures are statically indeterminate, rendering simple considerations of equilibrium inadequate. Furthermore, earth pressure distributions depend on wall deflection, so unless the interaction between soil and structure is incorporated, this approach is of limited usefulness.

In bending, the same deflection and curvature on any vertical section implied by application of beam theory to the retaining wall (for example, a cantilever wall propped at excavation level by a continuous concrete slab). Many walls are in fact 'two-way spanning' and exhibit curvature in the vertical direction as well as the horizontal. For this, plate bending theory is required (see, Timoshenko and Woinowsky-Krieger 1959), for which the governing equation is

$$\frac{\partial^4 w}{\partial x^4} + \frac{2\partial^4 w}{\partial x^2 \partial y^2} + \frac{\partial^4 w}{\partial y^4} = \frac{q}{D}$$

$$[1.35]$$

where $D = Et^3/12(1 - v^2)$ and w is the deflection. Direct application of Equation 1.35 to earth-retaining structures is not workable and, as with beam theory, not particularly meaningful unless including the soil-structure interaction effects.

1.8.5.3. Solutions based on plasticity theory

The essential characteristic of plastic behaviour is that deformations are permanent and are not recovered upon the removal of load, further, strains are irreversible. Plastic deformation can be accompanied by the elastic deformation, usually termed as 'elastic-plastic behaviour'. There are three essential ingredients to a model of plastic behaviour as following; flow rule, the yield function, and hardening law.

1.8.5.3.1. Active and passive stress states (Rankine)

A mathematical theory of the frictional stability of a granular frictional mass has been presented by Rankine working from first principles wherein based only on the principle that sliding resistance was the outcome of the tangent of the friction angle and the normal stress. This led to the now well-known expressions for the active and passive earth pressure coefficients:

$$K_a = \frac{(1 - \sin\phi')}{(1 + \sin\phi')}; \quad K_p = \frac{(1 + \sin\phi')}{(1 - \sin\phi')}$$

$$[1.36]$$

Rankine's approach was based on failure occurring and uniform states of stress at all points simultaneously within the retained soil mass, so was very different to Coulomb's wedge analysis nearly a century earlier. Rankine's analysis is restricted to a soil surface that is either horizontal or sloping at an angle of β to the horizontal (such that $\beta \leq \phi'$) and to a vertical back of wall ($\theta = 90°$).

1.8.5.4. Limit analysis

It is difficult to gain the exact solutions but via plasticity theorems can be handled to set bounds for the failure (collapse) loads. However, to obtaining the collapse load for a given case without having to solve the full boundary value problem, limit analysis is the required way. This is done by 'bracketing' the true solution with estimates that can be refined and brought closer together. By ignoring the equilibrium condition, an unsafe-upper bound to the failure load may be

calculated; by ignoring the compatibility condition a safe-lower bound may be calculated: the true failure load must lie between these bounds. If the bounds are equal, the exact solution has been found.

The bound theorems can only be proved for materials that show perfect plasticity and have an associated flow rule, which guarantee that failure loads are unique and independent of loading path.

1.8.5.5. Limit equilibrium analysis

With semi-empirical limit equilibrium analysis have a chance for obtaining solutions to a more general range of problems, which combine features of lower and upper bound calculations. The limit equilibrium method is like an upper bound calculation in that it considers a mechanism of failure and it is like a lower bound calculation in that it considers conditions of static equilibrium, but it does not satisfy the requirements of the proofs of the theorems. Although there is no proof that the limit equilibrium method leads to the correct solution, it is a very known used method in practice and experience shows that the solutions obtained often in good agreement with in situ observations.

1.8.5.6. Discrete spring models

If it is required to calculate internal forces, wall displacements, and the possible movements in the adjacent ground, a soil-structure interaction analysis is required. There are several different approaches to modelling surrounding ground and the retaining wall,(Figure 1.20).

The physical problem in (a) is governed by fundamental equations of equilibrium, compatibility and constitution. Where the soil is replaced by discrete springs, in (b), that are independent and have no interaction with each other. The wall can be modelled by engineering beam theory modified to take the springs in consideration, or by dividing it up into finite elements on spring supports. Finally, full interaction between soil and structure, in (c), is represented; complex stress-strain behaviour is possible, equilibrium and compatibility are fully satisfied. It should be clear that (c) is a more faithful representation of reality than (b), but it comes with the penalty of greater modelling complexity (and hence cost). Solution of problems based on (b) can be achieved with a simple spreadsheet, whereas (c) will require specialist software either capable of formulating and solving large systems of simultaneous equations, or of iterating to an equilibrium solution. If wall displacements, shears, and moments alone are sought, calculations

based on (b) may be perfectly adequate. However, if other ground movements and surface settlements are required, calculations using (c) will be necessary. below, a brief discussion of the theories and some involved solution procedures.
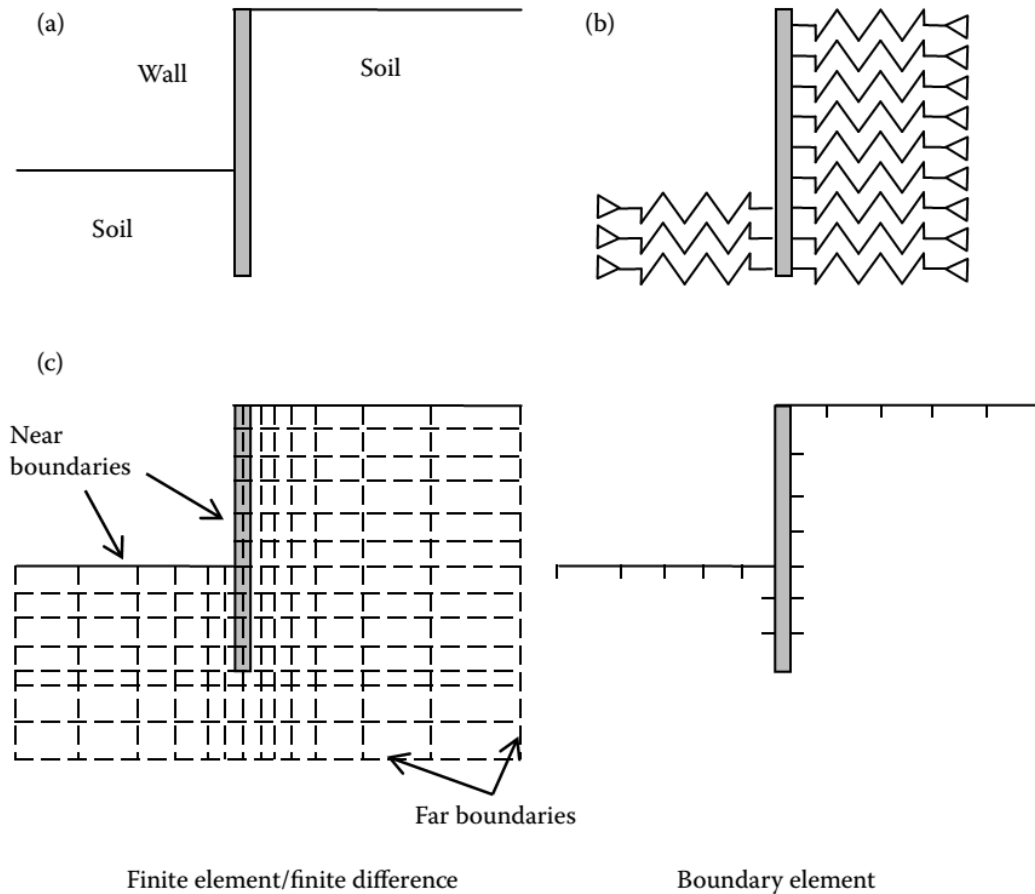
Figure 1.20   Different representations of a retained excavation. (a) Physical problem. (b) Discrete spring model. (c) Full continuum models. . (From Clayton, C. et al., Earth Pressure and Earth-Retaining Structures, Second Edition, Taylor & Francis, Jan 7, 2014.)

1.8.5.7. Continuum models

Continuum models (also termed 'numerical models') simplify the geometry of the soil-structure interaction problem by dividing the soil and any structural members (such as a retaining wall) into elements or zones. Within each element or zone, the properties of the structure or the soil are taken to be constant. Thus, property variations and geometry can be simplified, allowing

a solution to be calculated for each zone. With the quick growth of computing power, these methods are increasingly used for retaining wall design.

1.8.5.7.1. Finite element method

In Figure 1.20 'c', The finite element method (FEM) is a numerical technique for solving the differential equations governing a boundary value problem (Zienkiewicz 1977). The region of interest is divided into elements or discrete areas, often triangular or rectangular, defined by node points located at the vertices and sometime along the element edges (see Figure 1.21). Within each element, the behaviour is idealised, with the 'principal quantity of interest' constrained to vary in a prescribed mode (linear or quadratic). The value of this quantity at any interior point in the element is related to its values at the nodes, through interpolation or shape functions, *N*, based on the element geometry

$$\theta = \sum_{i=1}^{i=n} N_i \theta_i$$

$$[1.37]$$
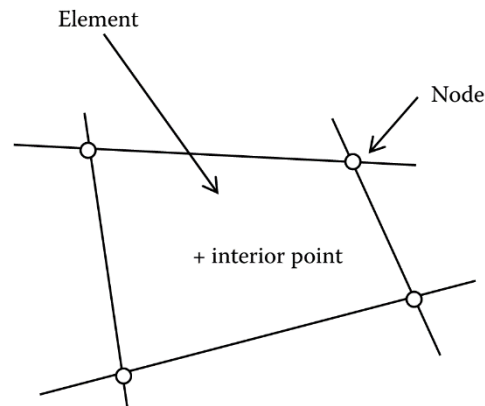
Figure 1.21 Finite element. (From Clayton, C. et al., Earth Pressure and Earth-Retaining Structures, Second Edition, Taylor & Francis, Jan 7, 2014.)

where θ is the quantity and *n* the number of nodes. In retaining wall analyses, the displacement is the main of interest and differentiation of the shape functions yields expressions for the strain vector ε in terms of the vector of nodal displacements *a*:

$$\varepsilon = Ba \qquad [1.38]$$

where *B* depends on the element geometry. Then, an appropriate constitutive relationship can be used to relate stresses σ and strains ε within the element:

$$\sigma = D\varepsilon = DBa \qquad [1.39]$$

where *D* depends on the properties of the material. Applying virtual basis theorems, element stiffness relationships can be established between applied loads *F* and resulting displacements at the nodes:

$$F = Ka = \int \left(B^T DBd(vol) \right) a$$

$$[1.40]$$

After all, a global stiffness matrix is obtained by assembling the contributions from each individual element. After applying boundary conditions, such as known displacement and forces 'fixities', the global system of equations is solved to yield the unknown nodal displacements. Internal strains in any element may be calculated from these displacements (Equation 1.38), followed by stresses using the constitutive relationships (Equation 1.39). For an intensive treatment of the FEM in relation to geotechnical engineering in general and earth retaining structures in particular (check David and Zdravkovic 1999 and 2001). Clayton, C. R et al (2014).

1.8.5.7.2. Finite difference method

In the finite difference method (FDM) shown in Figure 120c, materials are demonstrate by zones, defined between a grid of points. The user generates a grid to fit the geometry of the physical problem to be modelled. Each zone follows a prescribed pattern of stress-strain behaviour (elastic or plastic) and when yielding occurs the grid distorts to update the geometry of the grid points.

The explicit FDM (Cundall 1976) uses the basic equations of motion and a time-stepping process to calculate incrementally the accelerations (and hence by integration the displacements and the velocities) of the zone mass, which is collected at the grid points. The strains obtained from this are then used in a constitutive law, to determine the corresponding stress increment for the zone. The stress increments are then summed to obtain a new out-of-balance force and the calculation cycle is repeated. The dynamic response of the system is numerically damped, so that with increasing time steps, the problem reaches equilibrium and the required solution. Note that in

such an application of the finite difference method, the time-steps are used to obtain a solution, rather than to model time-dependent material behaviour, Clayton, C. R et al (2014).

1.8.5.7.3. Boundary element method

The boundary element method (BEM) is another numerical method for solving boundary value problems governed by differential equations (Banerjee and Butterfield 1981). The principal difference between this method and FEM/FDM is that the differential equations are transformed into equivalent integral equations prior to solution. Typically, the integral equations link boundary stresses to boundary displacements and so the method is particularly suited to those problems where the surface area to volume ratio is low, such as in many three-dimensional foundation problems. BEM requires only the boundary of the domain to be discretized into segments or elements (Figure 120c), not the interior (i.e. surface rather than volume discretization). The number of physical dimensions to be considered is effectively reduced by one, resulting in a smaller system of equations and significant savings in computing time (10 times faster than FEM for the same problem is quite typical).

This simplification is made possible by taking advantage of a so-called fundamental or singular solution, which gives the stresses and displacements at some point B due to a load or displacement acting at another point A. In geotechnical work, Mindlin's solution for a point load within a semi-infinite solid, or Boussinesq's solution for a point load acting on the surface of a half-space, are commonly used. By distributing the fundamental solution over the surface of the domain, a general solution is obtained in terms of a boundary density function. Boundary conditions are imposed by requiring the density function to satisfy an integral equation on the boundary. The solution is obtained first at the boundary and then at points within the region using the boundary solution, Clayton, C. R et al (2014).

1.9. Conclusion :

The flow of water can therefore fundamentally modify the reaction of the ground to the digging of excavations, in particular by considerably increasing the risks of instability in the short term. Hence the need to take into account the effects of water flow in the calculation and in the analysis of the behaviour of retaining structures.

The first consideration in selecting the most suitable method is whether the construction of the retaining wall is possible under the local geological conditions. The second is how well the retaining wall is capable of supporting. Last, deformation and stress analyses are required to ensure the safety of the retaining wall.

Depending on the nature and conditions of their environment, retaining structures have always presented important features that vary greatly from one type to another. The behaviour of a support structure cannot be accurately assessed without also considering the behaviour of the soil in contact and of their "soil-structure interaction" interface.

Conventional calculation methods (at limit states) remain well suited for the sizing of the vast majority of sheet pile walls. They give superabundant results. With these methods, the deformation of the screen is not involved in the calculation. It was recognized early on that this simplification is not acceptable in many cases where structural strain has to be considered when calculating contact pressures. In the absence of a representative theory, semi-empirical methods were first proposed to evaluate the loads that these structures had to support.

Continuum methods (finite elements or finite differences) are enjoying undeniable success in all areas concerned with soil-structure interaction. Then, they serve as a research, design and dimensioning tool. They allow the interaction between the soil and the structure to be reproduced in a realistic way. The kinematic and static compatibility between the soil and the structure is implicitly checked if the support structure and the soil are considered in the analysis and if their interface is modelled by suitable contact elements. Their successful use, however, requires the experience of the modeller and validation of the results by observations on similar works or by comparison with other proven methods. The choice of the boundary conditions, in particular with regard to the dimensions of the model (geomodel), must be made in such a way as to correctly reproduce the behaviour. The limits of the model must in particular be evaluated by a sensitivity analysis to verify whether or not they influence the behaviour in the vicinity of the structure.

Although it is now possible, with the development of computer tools and numerical calculation methods, to obtain a fairly realistic representation of the behaviour of the support structures of excavations, significant efforts are still necessary to better understand phenomena, such as the effects of water flow in the soil and their consequences on the stability of excavations and the sizing of supports. And thus really grasp the issues of soil-structure interaction.

Chapter 2

Methods for evaluating the stability of excavation bottoms
with respect to hydraulic failure: literature review

Chapter 2: Methods for evaluating the stability of excavation bottoms with respect to hydraulic failure: literature review

2.1. Introduction:

With the development of high rise buildings and other civil engineering constructions, deep excavations under retaining walls are profoundly connected to urban sites, whether it is for basements construction, underground parking, or tunnels. Excavations construction, and corresponding walls and retaining situations, as all geotechnical construction in general, requires a lot of empiric knowledge, only possible to obtain through hard investigation and data analysis.

One of the main problems in this type of excavation is the water flow around the walls, which may cause instability problems, and consequently dangerous situations and, therefore, deep studies are needed to carry out excavations as safe as possible. These excavations are often near buildings, and sensitive zones, which implies that their design should be careful and well planned in order to make sure that no dangerous situations occur while and after excavations are made.

This work bases itself in a specific type of deep excavation failure known as bottom failure. This type of failure often occurs because of the water seepage from the highest water level to the lowest where the excavation bottom lies. This is a very complex issue, since the type of soils and soil parameters are never the same. The excavation phases are rather diverse, and also the wall stiffness and interface are variable.

The various methods proposed in the literature for the analysis of the stability of excavation bottoms with respect to hydraulic failure are based on fairly restrictive assumptions, by defining a safety factor with respect to bottom failure of excavations caused of the seepage phenomenon or the lifting of the bottom of the excavation (hydraulic failure). These methods take only the role of retaining wall water-tightness, the effect of seepage water flow forces (hydrodynamic forces) causing the reduction of passive pressure in the downstream side of the screen is ignored.

This chapter presents a review of previous work published in the literature (state of art) on the stability of cofferdams and deep excavations invaded by the flow of water around the retaining screens, and having a direct connection with the cases considered in this study. This chapter is punctuated by deductions, discussions and comparisons of the different approaches and methods proposed in the literature. And ends with a conclusion.

2.2. Review of the literature (previous work):

In the following, the findings on hydraulic bed failure described in the literature are summarized.

2.2.1. Basic calculation approaches

The basic calculation approaches described in the literature to prove the safety against hydraulic heave are described in chronological order below.

2.2.1.1. Calculation approach according to Terzaghi, Terzaghi and Jelinek as well as Terzaghi and Peck

Terzaghi 1954 and K. Terzaghi 1925 differentiated in his earlier works between two types of failure which can be caused by flowing water below a dam: the earth pressure bottom failure and the erosion bottom failure.

According to Terzaghi, erosion can be ruled out if the exit gradient on the downstream side is less than the critical specific hydraulic gradient i_{crit}.

Terzaghi initially used the expression "earth pressure ground failure" instead of the term "hydraulic failure". In later works, e.g. in Terzaghi and Peck 1961, the term "earth pressure ground failure" no longer occurs. Terzaghi initially treated the hydraulic failure as an earth pressure problem, which could not be solved using earth pressure theory Terzaghi 1954. For Terzaghi, the crucial question was at what state of stress the structural change in the soil is so significant that the permeability coefficient k_f is noticeably influenced. According to Terzaghi (Terzaghi 1954 and K. Terzaghi 1925), this is the case when the "compressive strength" of the soil is exceeded. Terzaghi explained the "compressive strength" of the soil using the active earth pressure wedge behind a retaining wall. According to this, there is a risk of hydraulic ground failure only when the stress condition causes a structural change and thus an increase in permeability. This very complex process was not pursued by Terzaghi in later works. For a detailed description, the interested reader is referred to Terzaghi K. Terzaghi 1925.

In later works (K. Terzaghi 1961 and K. Terzaghi)1954 Terzaghi greatly simplified his procedure for verifying safety against hydraulic heave. During tests, he was able to observe a rise in the sand next to the construction pit enclosure over a width of $b = t / 2$. On the basis of these

observations, Terzaghi assumes that the sand is loosened over a width of $b = t / 2$ next to the construction pit enclosure (Fig. 2.1, a).
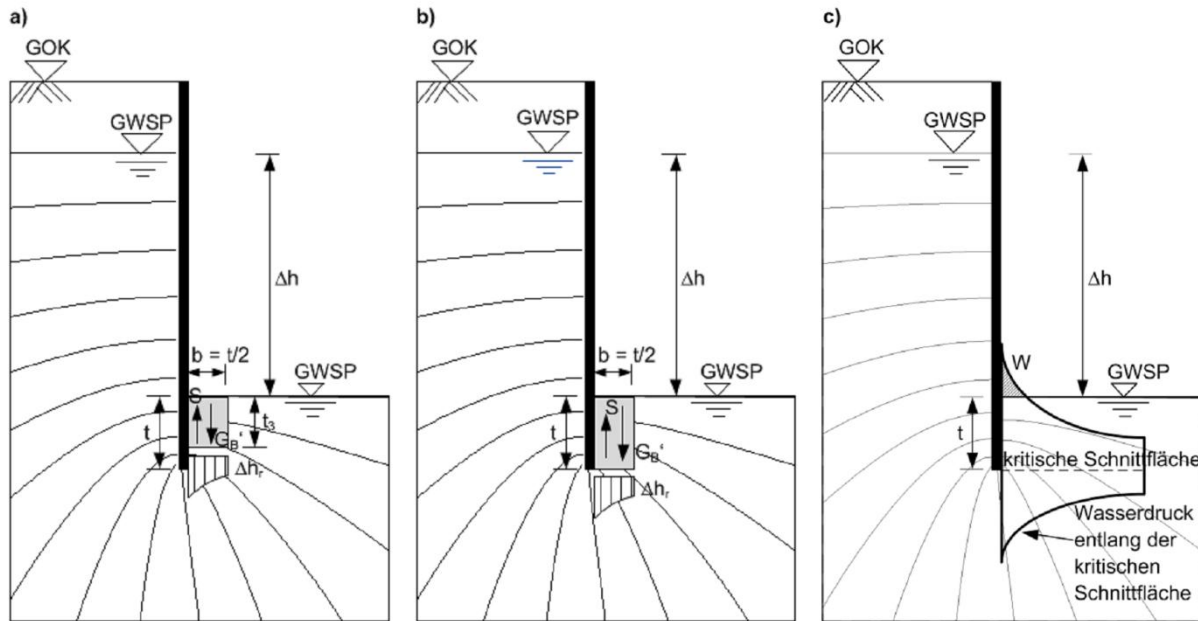
Figure 2.1: Calculation approaches according to Terzaghi (according to K. Terzaghi 1954 and K. Terzaghi 1961)

To calculate the safety against hydraulic ground failure, Terzaghi therefore considers a soil prism whose width b corresponds to half the embedment depth $t / 2$ (Fig. 2.1, a). The height of the prism t_3 results from the position of the most unfavorable cut surface. The prism is pushed up when the related flow force S in the prism becomes equal to or greater than its weight under buoyancy GB '. Other restraining forces (e.g. frictional forces) are neglected. The safety against hydraulic ground failure is accordingly verified if equation 2.1 is fulfilled.

$$S < G_B' \text{ bzw. } S < G'$$

[2.1]

According to Terzaghi and Jelinek K. Terzaghi 1954, the effective horizontal stresses and thus the frictional forces at the side edges of the prism are practically zero at the moment of failure. There are therefore no restraining frictional forces acting along the side walls of the prism.

The relative flow force S acting over a meter width in the floor prism is calculated according to the following equation (equation 2.2):

$$S = \gamma_W \cdot \Sigma \Delta h_r \cdot b$$

$$[2.2]$$

The stabilizing weight under buoyancy GB 'per meter of width is calculated according to equation 2.3.

$$G_B' = \gamma_B' t_3 \cdot b$$

$$[2.3]$$

In the case of a sheet pile wall surrounded by a flow (enclosure of a construction pit), it is indicated in Terzaghi and Jelinek K. Terzaghi 1954 that the height of the soil prism is equal to the embedment depth t, therefore $t_3 = t$ (Figure 2.1, b). For all other cases, e.g. B. an underflow weir, the most unfavourable value for t_3 must be determined.

Terzaghi and Jelinek 1954 also presented a new method for sizing the charge filter. If the water pressure acting along the critical cut surface at depth $t3$ ($t3 = t$ applies to the walls of the construction pit with flow around), multiplied by the ratio γ_B '/ γ_W, is plotted upwards, we obtain line W (Figure 2.1, c), which corresponds to an imaginary bed of earth equal to the hydrostatic water pressure. In order to create an equilibrium, that part of the curve W which is located above the base of the excavation must now be compensated by means of a load filter.

In tests, however, Terzaghi found that a uniformly applied filter has the same effect as an adapted load filter. According to Terzaghi and Peck 1961, the load filter should therefore only be taken into account in the area of the critical floor prism, i.e. H. on a width of b = t / 2. The weight of the load filter under buoyancy G_A' acts on the width b as an additional restraining force (equation 2.4).

$$G' = G_B' + G_A' = \gamma_B' t_3 \cdot b + \gamma_A' d_A \cdot b$$

$$[2.4]$$

In equation 2.4, G' is the total weight under buoyancy per meter of width and d_A is the thickness of the load filter. The related flow force S can still be calculated according to equation 2.2, unaffected by the load filter.

2.2.1.2 Calculation approach according to Baumgart and Davidenkoff

The calculation approach described below for calculating the safety against hydraulic heave was first published in Russian in 1929 by Davidenkoff and Baumgart 1929.

According to Davidenkoff 1970, proof of safety against hydraulic soil failure is provided by considering a ground prism placed on the construction pit lining, the width b of which is negligible (flow path, Figure 2.2). The length of the prism t_3 should be chosen for verification such that the most unfavorable ratio results between the associated flow force S acting in the filament and the restraining weight force under the buoyancy G_B'.

Taking into account the current line along the enclosure of the construction pit represents the worst case, because the hydraulic gradient i and therefore the flow force S are the most important along the wall. Assuming negligible width b of the replacement body, Baumgart and Davidenkoff assume that in a failed state there is no friction in the soil and between the soil and the wall.

The related flow force S acting on the flow path is calculated according to equation 2.5.

$$S = \gamma_W \cdot \Delta h_r \qquad [2.5]$$

In equation 2.5, Δh_r is the residual potential level at the lower end of the flow path under consideration. The stabilizing weight under buoyancy G_B' is calculated using equation 2.6.

$$G_B' = \gamma_B' \cdot t_3 \qquad [2.6]$$

Stabilizing frictional forces are not taken into account in this approach. The proof of safety against hydraulic ground failure is carried out according to equation 2.1.

According to Davidenkoff 1970, the most unfavorable length of the flow path is equal to the embedment depth ($t3 = t$; Figure 1.4, b) in the case of underground excavation enclosures in homogeneous soil.

Davidenkoff also indicates how the calculation approach can be applied in the event that a load filter is applied to the excavation base (Figure 2.2). In this case, the flow path is lengthened

by the thickness of the load filter d_A. The restraining weight under buoyancy G' then results from equation 2.7.

$$G'=\gamma_B' \cdot t_3 + \gamma_A' \cdot d_A$$

[2.7]

Since it is not influenced by the load filter, the related flow force S can still be calculated according to equation 2.5.
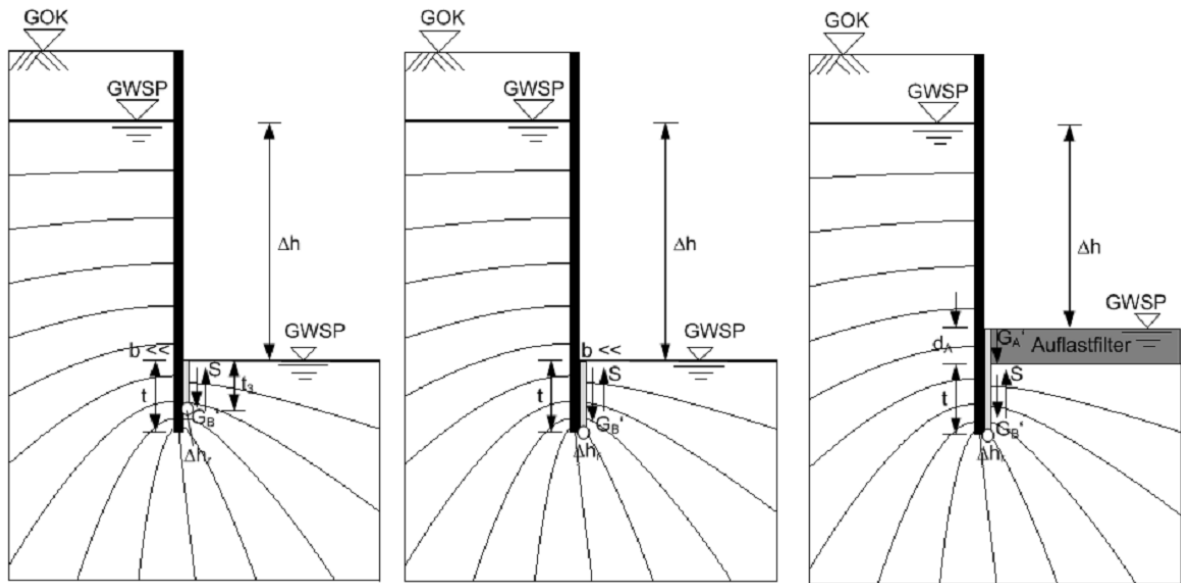
Fig. 2.2: Calculation approach according to Baumgart / Davidenkoff (according to Davidenkoff 1970)

2.2.1.3. Calculation approach according to Harza

According to Harza 1935, failure due to hydraulic ground failure occurs when the hydraulic gradient i, multiplied by the weight of the water γ_W, overcomes the weight at any point on the base of the excavation with the uplift of the soil γ_B'. This is the case when the exit gradient i at the base of the excavation is equal to the critical specific hydraulic gradient i_{crit}.

According to Harza, the proof of security against hydraulic ground failure is fulfilled if:

$$i \cdot \gamma_W < \gamma_B'$$

[2.8]

In the case of excavation pit enclosures with a flow, the greatest hydraulic discharge gradient i is always directly on the wall.

2.2.1.4. Calculation approach according to Bažant

On the basis of numerous tests on hydraulic basal failure, Bažant (1940) developed a new theory to prove the safety against hydraulic basal failure, which is also included in its own investigations.

As a result of his experiments, Bažant comes to the conclusion that the hydraulic ground failure is caused by changes in the structure of the sand on the air side of the construction pit enclosure. The vertical specific hydraulic gradient at the base of the wall is always greater than the vertical specific critical hydraulic gradient in the moment of failure ($i_z > i_{z,crit}$). In the area in which the vertical critical specific hydraulic gradient $i_{z,crit}$ is exceeded, the grains are pushed upwards by the water pressure and the structure of the soil is disturbed. However, the ground only starts moving when the specific flow force f_S is not only greater than the weight of the ground under buoyancy at the point of the greatest gradient i, but also when the related flow force S is also greater than the weight of the one above and below Grains polluting, soil is. Bažant concludes from this that exceeding the specific critical gradient i_{krit} at one point does not necessarily lead to a disturbance of equilibrium and thus to hydraulic ground failure.

As a new equilibrium condition, Bažant 1940 initially suggests contrasting the forces that act directly along the wall (equation 2.9). The proof of security against hydraulic ground failure is therefore fulfilled if:

$$G_B' \geq S \Rightarrow t \cdot \gamma_B' \geq \Delta h_r \cdot \gamma_W \qquad [2.9]$$

In equation 2.9, Δh_r is the residual potential height at the base of the wall. This calculation approach corresponds to the calculation approach according to Baumgart / Davidenkoff. For his theoretical explanations, Bažant considered a sheet pile wall with a flow around it, which is embedded equally deep in an isotropic subsoil on both sides (see Figure 2.3). In this case, equation 2.9, with $\Delta h_r = \Delta h_{crit} / 2$, gives the critical potential difference to

$$\Delta h_{krit} = 2 \cdot t \cdot \gamma_B' / \gamma_W \qquad [2.10]$$

The calculated critical potential difference then results from $\gamma_B' = 9 \ kN/m^3$ and $\gamma_W = 10 \ kN/m^3$ to $\Delta h_{crit} = 1,8 \cdot t$.

In his experiments, however, depending on the storage density D of the test sand, he determined critical potential differences between $\Delta h_{crit} = 2.3t$ and $3.6t$. Bažant concludes from this that, in addition to the weight of the soil itself, other restraining forces must act in the sand and that it is not sufficient to only consider the forces along the wall.

Therefore, in his further investigations, Bažant no longer only considered the forces along the construction pit enclosure, but all forces that acted in a certain area in front of the construction pit wall. This area is composed of that sub-area in which the related flow force S is smaller than the weight force under buoyancy $G_B{}'$, i.e. in which equation 2.11 is fulfilled for each point. In any vertical line, this applies from the y-axis (excavation base) to point Z_1 (dark gray area in Figure 2.3, a).

$$z \cdot \gamma_B{}' \geq \Delta h_r \cdot \gamma_W \qquad [2.11]$$
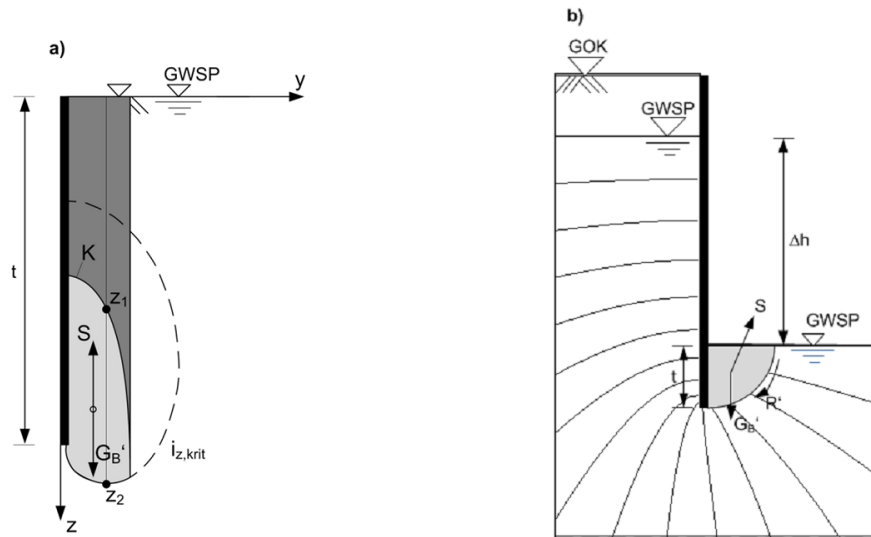
Fig. 2.3: a) equilibrium consideration (according to . Bažant 1940), b) calculation approach (according to Bažant 1953)

The second sub-area is that area (fault area) in which equation 2.11 is no longer fulfilled (light gray area in Figure 2.3, a). This sub-area is bounded by point z_1 at the top and at the bottom by point z_2 in any vertical line. The point Z_2 lies at that point of the vertical section, in which $i_z = i_{z,crit}$. The fault area is therefore limited towards the bottom by the line along which the vertical specific hydraulic gradient corresponds to the critical specific hydraulic gradient i_{crit}. If the point

z_1 lies in the vertical section on the $i_{z,crit}$ line, the equilibrium verification according to equation 2.9 is fulfilled over the entire height. This point represents the maximum lateral limitation of the area under consideration.

For the disturbance range, Bažant extends the equilibrium condition (equation 2.9) by a further term T, which represents the forces that must also act with restraint (equation 2.11) in order to create a state of equilibrium.

$$G_B' + T \geq S \qquad\qquad [2.12]$$

If equation 2.11 is not fulfilled, an additional force acts on the area above the point z_1, which is in equilibrium, and the hydraulic breakdown occurs.

By means of analytical studies, in which he describes the potential reduction by means of confocal hyperbolas, Bažant defines the fault area as a function of the embedment depth t and the potential difference Δh. The derivation of his equilibrium consideration is not given here in full, see Bažant 1940.

However, Bažant found that it is not possible for him to determine the restraining force T, which in his opinion consists largely of the friction between the sand and the wall. He therefore did not conduct any further investigations into this equilibrium consideration.

Later Bažant 1953 and Bažant 1963 presented a new calculation approach to prove the safety against hydraulic ground failure (Figure 2.3, b). Bažant investigates the equilibrium of all forces acting on a body bounded by a cylindrical line (flow force S, weight under buoyancy G_B', friction force R).

2.2.1.5. Calculation approach according to Knaupe

For special boundary conditions, Knaupe 1968 analytically solved Laplace's differential equation to describe laminar, steady flow when flow around the wall and was thus able to calculate the residual potential height Δh_r at any point in the flow area. The proof of equilibrium between the related flow force S and the weight force under buoyancy G_B' (equation 2.13) was carried out on a narrow strip, between the streamline directly at the construction pit enclosure ψ_1 and the

streamline Ψ_2 (Figure 2.4, a). Knaupe calculated the critical potential difference Δh_{crit}, which leads to failure due to hydraulic ground failure in wide construction pits, using equation 2.12.

$$\Delta h_{krit} = \frac{\gamma_B{}'}{\gamma_W} \cdot \omega_3 \cdot t$$

$$[2.13]$$

The proportionality factor ω_3 is a function for recording the geometry of the construction pit and takes into account the ratio of the hydraulic dimensions of *(t + Δs) / T* and *Δs / t* (Fig. 2.4, b). The dimensions of the broken body depending on the hydraulic boundary conditions are therefore defined according to Knaupe using the proportionality factor ω_3. To determine the proportionality factor, Knaupe developed dimensioning diagrams for various boundary conditions ω_3 (Knaupe 1968).
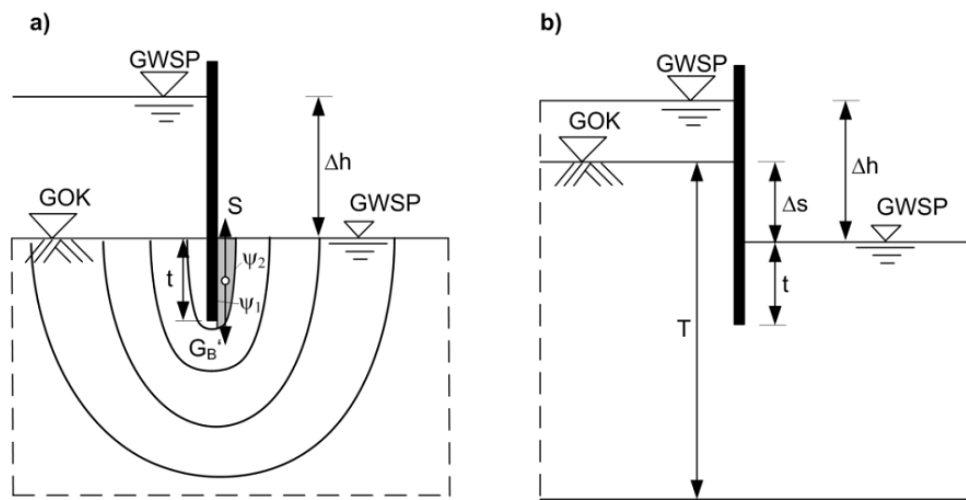
Figure 2.4: Knaupe's calculation approach (after Knaupe 1968)

In his test series with various hydraulic boundary conditions and soil materials, he found that the measured critical pressure heads were always greater than the critical potential differences *Δh_{crit}* calculated analytically according to equation 2.13. He explained this as the effect of frictional forces in the ground. For this purpose, Knaupe introduced a further factor ω_z, with which the restraining friction component can also be taken into account as a function of the irregularity coefficient U and the effective friction angle φ_B' of the soil. The equation 2.14 was determined empirically through experiments

$$\omega_z = 0,45 \cdot U \cdot \tan \varphi_B'$$

$$[2.14]$$

Taking into account the internal friction, the critical potential difference Δh_{crit} at wide construction pits is then calculated according to equation 2.15.

$$\Delta h_{krit} = \frac{\gamma_B'}{\gamma_W} \cdot (\omega_3 + \omega_z) \cdot t$$

$$[2.15]$$

A detailed description of this calculation approach is given in Knaupe 1968.

2.2.1.6. Calculation approach according to Tanaka

Tanaka 1996 also presents a new calculation approach for the verification of safety against hydraulic ground failure, which the authors call "the prismatic failure concept".

Tanaka found that the shape of the failure body in hydraulic failure in anisotropic and stratified soils as well as in the base of excavation pit with load filter does not correspond to the equivalent body according to Terzaghi 1954. Tanaka therefore developed its own calculation approach for these cases.

The replacement body, which is used in the "prismatic failure concept", has a prismatic shape with height t_3 and width b (Figure 2.5). The upper edge of the prism is always the base of the excavation. By varying the dimensions t_3 and b, depending on the hydraulic boundary conditions, the prism for which the lowest safety factor F_S (equation 2.16 or 2.17) results, with a constant potential difference Δh, can be determined.

Two different variants of the calculation approach are considered:

- Prismatic failure, no friction

- Prismatic failure, friction

If no friction forces R at the edges of the prism are taken into account (no friction), the safety factor F_S is calculated as the quotient of the weight of the soil prism under buoyancy G_B' through the related flow force S acting in the prism .

$$F_S = \frac{G_B'}{S}$$

$$[2.16]$$
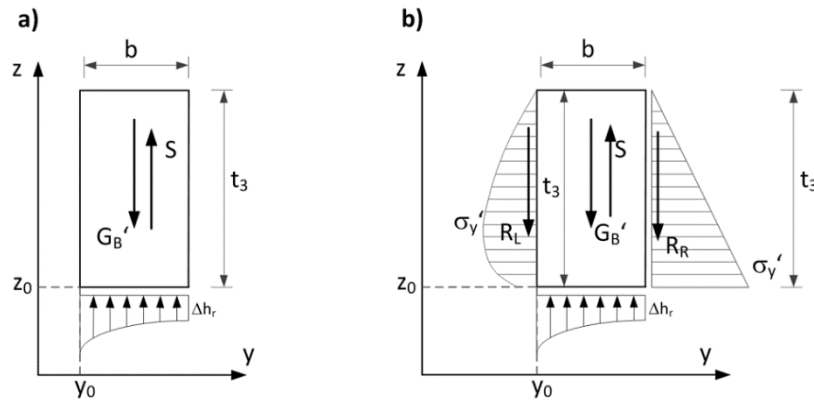
Figure. 2.5: Calculation approach according to Tanaka (according to Tanaka 1996) a) without friction, b) with friction

If the friction forces R_L and R_R along the side surfaces are taken into account (friction, Figure 2.5, b), the safety factor F_S is calculated according to equation 2.17.

$$F_S = \frac{G_B' + R_R + R_L}{S}$$

[2.17]

According to Tanaka, the frictional forces acting along the right and left side surfaces of the prism (R_R and R_L) result from the horizontal effective stress σ_y' multiplied by the tangent of the friction angle φ_B' or with the tangent of the wall friction angle δ_B' (equation 2.18 and 2.19).

$$R_R = \int_{z_0}^{z_0 + t_3} \sigma_y' \cdot \tan \varphi_B' \cdot dz$$

[2.18]

$$R_L = \int_{z_0}^{z_0 + t_3} \sigma_y' \cdot \tan \delta_B' \cdot dz$$

[2.19]

According to Tanaka, there is a passive earth pressure condition on the downstream side of the construction pit enclosure. The effective horizontal stresses σ_y' can therefore be calculated using equation 2.20.

$$\sigma_y' = K_{pgh,B} \cdot \sigma_v'$$

[2.20]

In equation 2.20, $K_{pgh,B}$ is the passive earth pressure coefficient of the soil. When applying his calculation approach to a construction pit enclosure surrounded by a flow, Tanaka found that the prismatic substitute body in the homogeneous subsoil and without the application of friction forces R (no friction) has in the worst case no width b ($b = 0$) and extends below the wall base. The prismatic equivalent body without taking into account frictional forces along the side surfaces therefore corresponds to the expanded stream filament according to Odenwald and Herten.
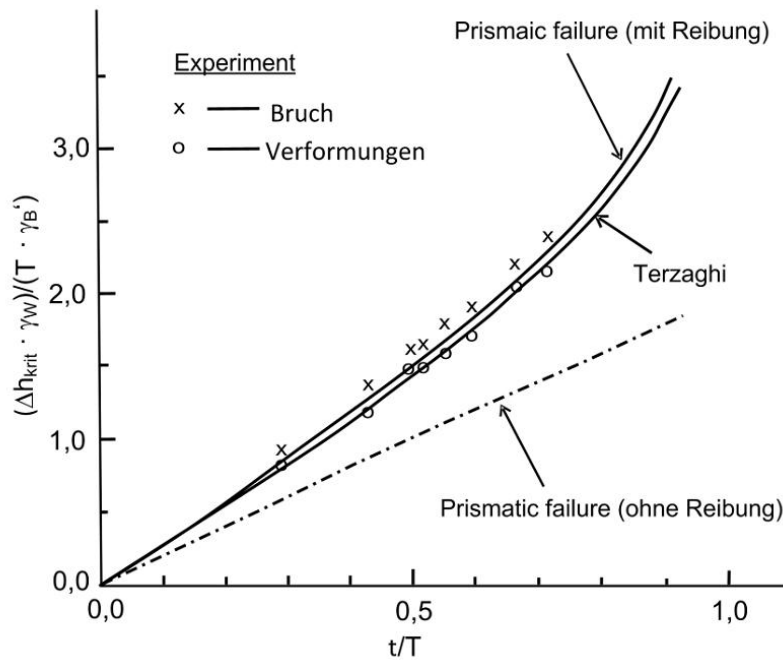
Figure 2.6: Comparison of calculation results and test results (according to Tanaka 1996)

However, if the frictional forces R along the side surfaces are taken into account (friction), the width b of the prism, for which the least security results, is not negligibly small. The widths b of the most unfavorable prism determined by Tanaka are slightly smaller than the equivalent body width according to Terzaghi ($b = t / 2$) when the building pit enclosures flow around them.

Tanaka also compares the results of his calculation method with the results of his tests on hydraulic ground failure Tanaka 1999 as well as with the results obtained with the Terzaghi calculation approach. This is shown in Figure 2.6. For the tests, the sand was installed with a medium density ($D \approx 0.5$).

Two very interesting findings can be obtained from the comparison. On the one hand it can be seen that the results according to Tanaka (friction) almost correspond to the results according

to Terzaghi. This means that in the Terzaghi approach, the neglect of frictional forces along the side surfaces as well as the substitute body that only extends to the base of the wall is compensated by a larger width b of the substitute body. On the other hand, the calculation results according to both approaches agree very well with the test results.

First approaches to taking a load filter into account when applying the "prismatic failure concept" are given in Hirose et al. Tanaka 1999.

2.2.1.7. Calculation approach according to Odenwald and Herten

Odenwald and Herten extended the Baumgart / Davidenkoff streamline to the depth at which the vertical specific hydraulic gradient i_z is equal to the critical vertical specific hydraulic gradient $i_{z,crit}$. The length of the prism with negligible width results from equation 2.21.

$$t_3 = t + \Delta z \qquad [2.21]$$

In equation 2.21, in addition to the already known quantities Δ_z, the vertical distance between the wall tip and the line that defines the area with the critical specific vertical specific hydraulic gradient $i_{z,crit}$ (see Figure 2.7, a).

In the area in which the vertical specific hydraulic gradient $i_{z,crit}$ is greater than the vertical specific hydraulic gradient i_z, the specific flow $f_{S,z}$ is always greater than the specific weight of the soil under buoyancy $\gamma_B{}'$. Thus, the vertical specific flow force $f_{S,z}$ is taken into account wherever it is greater than the specific weight of the ground under buoyancy $\gamma_B{}'$. The consideration of a stream filament with a negligible width b, which extends below the wall base, is therefore the most conservative calculation approach.

The related flow force S acting in the extended stream filament is calculated according to equation 2.22.

$$S = \gamma_W \cdot \Delta h_z \qquad [2.22]$$

The stabilizing weight under buoyancy G_B' is calculated according to equation 2.23.

$$G_B{}'\gamma_B{}'t_3 = \gamma_B{}'\cdot(t + \Delta z) \qquad [2.23]$$

Figure 2.7: Calculation approach according to Odenwald / Herten

If a load filter is placed on the base of the excavation (Figure 2.7, b), the weight of the load filter also acts as a retaining weight (Figure 2.7). The restraining weight force under buoyancy G is then calculated according to equation 2.24.

$$G'= G_B'+G_A'=\gamma_B' \cdot t_3 + d_A \cdot \gamma_A'=\gamma_B' \cdot (t+\Delta z)+d_A \cdot \gamma_A \qquad [2.24]$$

The calculation approach according to Odenwald / Herten corresponds to that of Tanaka without the application of frictional forces, since the most unfavorable prism according to Tanaka in this case is equivalent to the extended stream filament according to Odenwald / Herten.

2.2.2. Findings from model tests

The findings from the experiments described in the literature are summarized below. A distinction is made between the influence of the hydraulic boundary conditions, the observed fracture process and the measured critical potential differences Δh_{crit}.

2.2.2.1. Influence of geometric and hydraulic boundary conditions

The magnitude of the related flow force *S*, which acts in front of the construction pit enclosure, can be determined using the current and equipotential line network. The current and equipotential line network in homogeneous soils depends exclusively on the hydraulic boundary conditions of the model under consideration. Some authors therefore examined the influence of the hydraulic boundary conditions on the current and equipotential line network and thus on the safety against hydraulic ground failure.

In particular, the influence of the relationship between the embedment depth and the thickness of the water-bearing layer *t / T* and the construction pit width B was examined.

- **Influence of the ratio of the embedment depth to the thickness of the water-bearing layer *t/ T***

Sentko 1961 found in his investigations that the higher the *t / T* ratio, the greater the safety against hydraulic heave. This can be explained using the potential distribution. If the ratio of t / T is high, more potential is already dissipated in the area below the wall. This results in a somewhat reduced potential in the downstream area next to the wall (Figure 2.8, right).
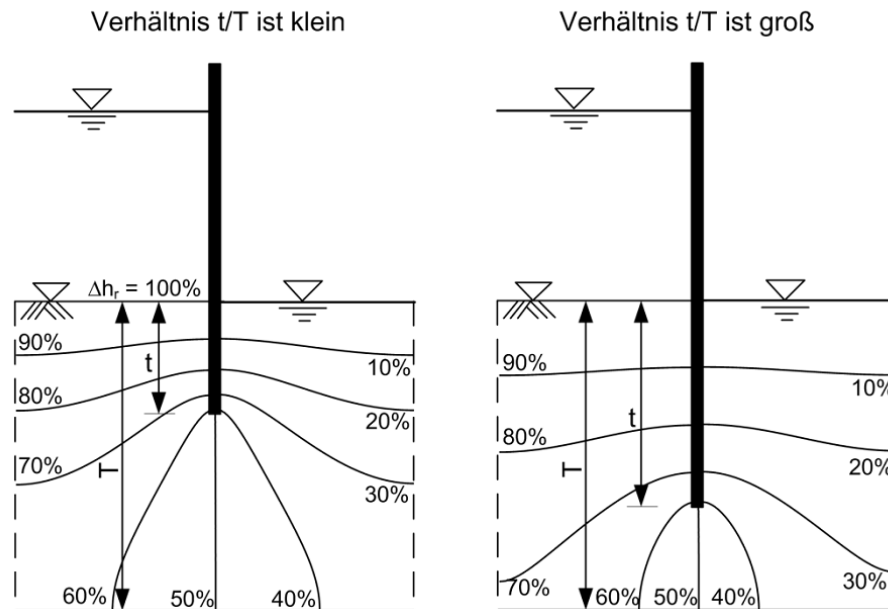
Figure 2.8: Potential reduction depending on the ratio t / T

With a small ratio of t / T, however, more potential is dissipated along the wall. The hydraulic gradient i and thus the related flow force S are greater in this case along the construction pit enclosure.

Tanaka et al. 1996 from his model tests. He also noted an increase in the critical potential difference Δh_{crit} with an increasing ratio of t / T.

- **Influence of the excavation width B**

With regard to the influence of the excavation width B, Sentko 1961 found that the critical potential difference Δh_{crit} is smaller with a narrow excavation width B than with wider excavations. The reason for this is, as shown in Figure 2.9, the concentration of the equipotential lines on the area relevant for the hydraulic ground failure at small widths B of the construction pit.
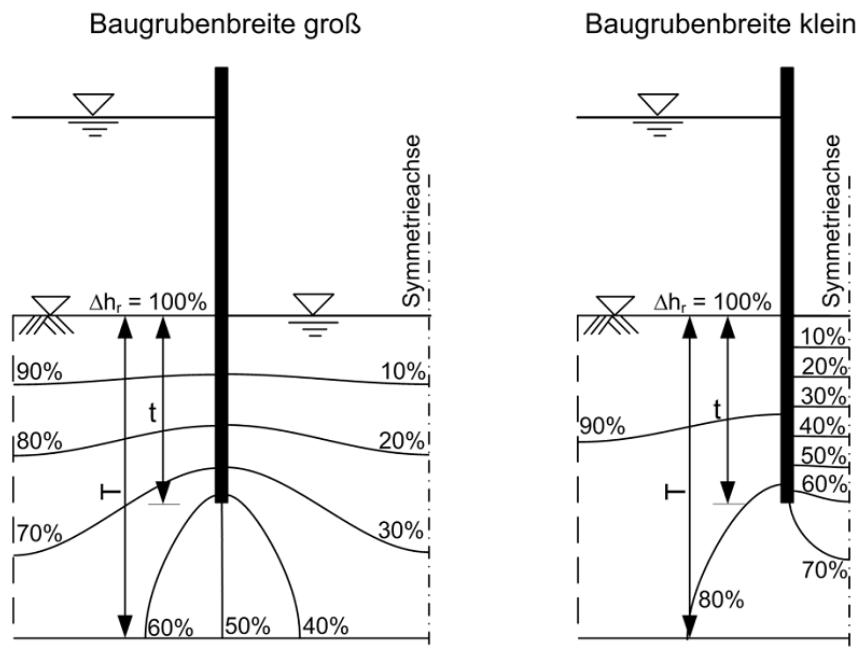
Figure 2.9: Potential reduction depending on the construction pit width

In the example shown in Figure 2.9, the residual potential Δh_r at the tip of the wall increases by reducing the width B of the construction pit from around 40% to around 60% of the potential difference Δh. By increasing the residual potential height Δh_r along the construction pit enclosure, a larger related flow force S acts and hydraulic ground failure occurs even with lower potential differences Δh.

Knaupe 1968 also dealt with the influence of the excavation width on the safety against hydraulic ground failure. During his investigations, Knaupe came to the same conclusions as Sentko.

2.2.2.2. Observed failure process from model tests

The experiments under consideration, with the exception of the experiments by Marsland 1953 and Knaupe 1968, had the same boundary conditions to the effect that the respective surfaces of the test soil on the air and water side have the same height (Figure 2.10). However, the distance between the partition wall and the model edges as well as the test sand used varied.
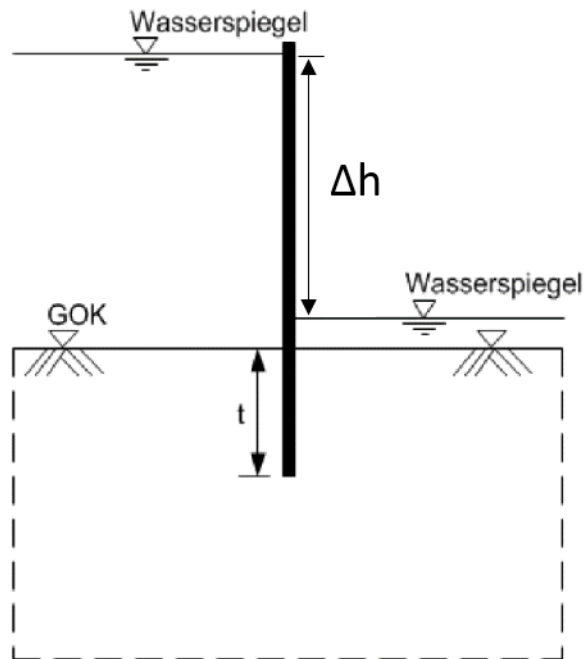
Figure 2.10: Boundary conditions for the experiments from the literature

Bažant 1940 describes the failure process most extensively, which he observed in numerous experiments with different storage densities. Only his observations are detailed below. A detailed summary of all experiments without a load filter described in the literature is given in Boley and Schober 2013.

Bažant found that the first sand movements occurred near the sheet pile wall, starting at around $\Delta h = 2 \cdot t$ (state a, Figure 2.11). According to Bažant, the new structure of the sand is in a

stable equilibrium. With a further increase in the potential difference Δh, he observed a loosening and extensive uplift of the test sand on the air side. The subsidence on the water side was smaller than the rise on the air side (state b, Figure 2.11). A further increase in the potential difference Δh then led to sand movements in a strip directly next to the sheet pile wall, which was initially only very narrow, but quickly became wider (state c, Figure 2.11). Then the entire loosened part of the test sand started to move, which quickly led to hydraulic ground failure (condition d, Figure 2.11). In state c in Figure 2.11, the sand was no longer in stable equilibrium, and the occurrence of the hydraulic ground failure could then no longer be prevented.

Bažant also states that the observed course of the failure was sometimes accompanied by subordinate sand movements that did not lead to the hydraulic ground failure. In the case of loosely stored sand, condition b is not so clear and condition c occurs immediately. Furthermore, by varying the storage density D, Bažant found that higher potential differences Δh could actually be achieved with a higher storage density. In a long-term experiment with a duration of 16 hours, the same result was achieved as in the experiment with a short experiment duration. With that he justified the short test duration of 10-30 minutes.
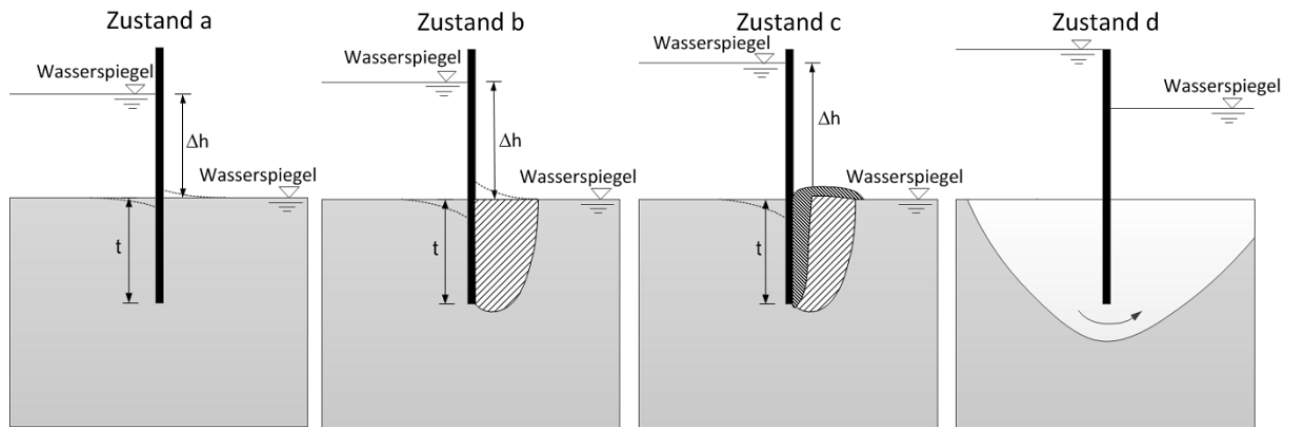
Figure 2.11: Failure sequence in the event of hydraulic ground failure
(according to Bažant 1940)

In summary, from all the experiments described in the literature (cf. Boley and Schober 2013), it can be stated with regard to the failure process that the loosening begins with the hydraulic failure at the base of the wall and propagates to the surface. The width of the loosened area and the loosening time depend on the storage density D of the test soil. However, the first sand

movements / loosening do not lead directly to the hydraulic ground failure, this required a further increase in the potential difference Δh in all experiments. The flow time at constant potential difference Δh does not seem to have any relevant influence on the equilibrium.

Attempts at hydraulic ground failure with air-side protection by a load filter are known to the author only from Terzaghi and Jelinek 1954 or Terzaghi 1954 as well as from Marsland 1953.

Terzaghi carried out his tests with load filters to verify his theoretical considerations. He did not provide a detailed description of the observed failure process. He merely noted that a uniformly distributed load in the uplift area has the same effect as a filter which is distributed like the gray area in Figure 2.1.

Marsland investigated with his experiments the influence of a load filter on the critical potential difference and thus on the safety against hydraulic bottom failure. During his experiments, he found a broken body in the shape of a circle, the center of which is the intersection between the excavation pit and the excavation base (base material). Further information on the failure sequence is not given.

2.2.3. Recent research works

2.2.3.1. Kodaka & al. (2001):

From experiments on a reduced model testing in the laboratory, with a fixed wall, the plane hydraulic failure (figure 2.12), the results of Kodaka & al. (2001) show that when the hydraulic head loss (H) reaches 17.2 cm, corresponding to $(H / D)_{crit} = 3.44$, the sand deposit adjacent to the wall on the downstream side and having a relative density $Dr = 60\%$ is gradually raised. The sand heaving seepage phenomenon was observed for a water height difference (H) of 18.5 cm, ie $(H / D)_{crit} = 3.70$ (Figure 2.13).
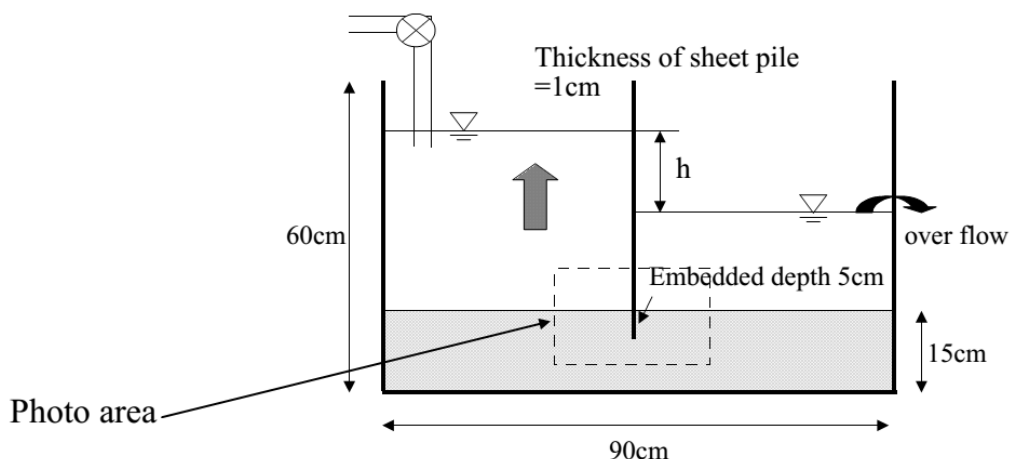
Figure 2.12: Model test apparatus and boundary conditions (From Kodaka & al. (2001))
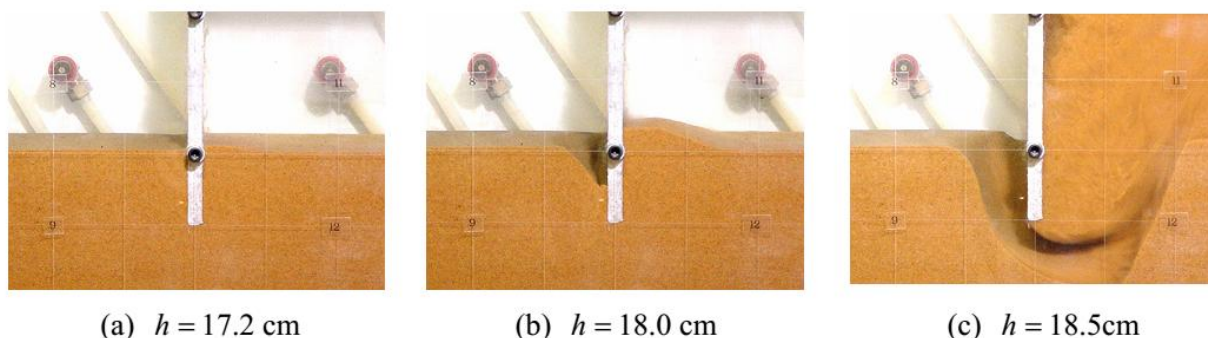
(a) $h = 17.2$ cm   (b) $h = 18.0$ cm   (c) $h = 18.5$cm

Figure 2.13: Deformation of sand deposit with different water head difference h [From Kodaka & al. (2001)]

Table 2.1, below, clearly shows the differences observed between the values of $(H/D)_{crit}$, corresponding to the two types of hydraulic failure, given by Terzaghi (1943), Tanaka & al. (1999) and Kodaka & al. (2001). The values of Kodaka & al. (2001) exceed the values of Terzaghi (1943) by $\approx 22\%$ and $\approx 18\%$, and those of Tanaka & al. (1999) by 31.30% and 31.21% for uplift and seepage phenomenon respectively. We can see that the values of Tanaka & al. (1999) are the most critical compared to the others.

Table 2.1 Comparison of the values of *(H / D)crit*, inducing a hydraulic failure for a fixed wall, given by Terzaghi (1943), Tanaka & al. (1999) and Kodaka & al.

Hydraulic failure type	(H/D)crit			Deviations (2) from (1)	Deviations (3) from (1)	Deviations (3) from (2)
	Terzaghi (1943) (1)	Tanaka & al. (1999) (2)	Kodaka & al. (2001) (3)			
uplift	2.82	2.62	3.44	- 7.63%	+21.99%	+31.30%
seepage	3.14	2.82	3.70	-11.35%	+17.83%	+31.21%

2.2.3.2. Benmebarek & al. (2005):

Using the explicit finite difference method implemented in the FLAC code and examining a fixed wall (Figure 2.14) which can represent a shored (butted) sheet pile wall, Benmebarek & al. (2005) identified different failure mechanisms on the downstream side of the
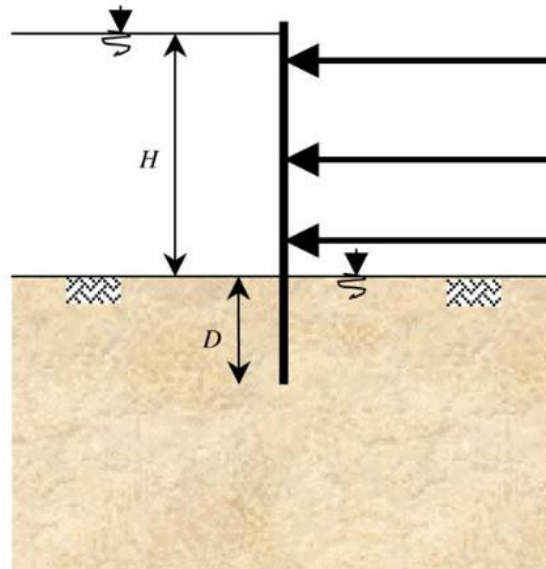
Figure 2.14: Case of a fixed wall studied by Benmebarek & al. (2005)

Table 2.2: Critical pressure drop (H / D)$_{crit}$ for various parameters $\phi, \psi / \phi$, and δ / ϕ For a fixed wall. [From Benmebarek & al. (2005)]

δ/ϕ	ψ/ϕ	H/D limit				
		$\phi = 20°$	$\phi = 25°$	$\phi = 30°$	$\phi = 35°$	$\phi = 40°$
0	0	2.63*	2.68*	2.74*	2.77*	2.8*
	1/2	2.64**	2.70**	2.79**	2.82**	2.90**
	1	2.64**	2.71**	2.82**	2.84**	2.93**
1/3	0	2.67*	2.78*	2.84*	2.90*	2.93*
	1/2	2.68**	2.82**	2.88**	2.94**	2.98**
	1	2.68**	2.84**	2.91**	2.97**	3.03**
2/3	0	2.72*	2.81*	2.90*	2.92*	2.97*
	1/2	2.73**	2.83**	2.92**	2.97**	3.12**
	1	2.73**	2.84**	2.93**	3.04***	3.16***
1	0	2.73*	2.84*	2.90*	2.93*	2.99*
	1/2	2.73**	2.87**	2.94**	3.03**	3.13**
	1	2.73**	2.90**	2.98**	3.05***	3.16***

Failure by bulk heave of rectangular (*) or triangular (**) soil prisms, or by boiling (***).

wall, occurring for critical hydraulic head losses *(H / D)$_{crit}$* in the range 2.63 to 3.16 (see Table 2.2), which depend on the conditions and characteristics of the soil and the soil/wall interface.

2.2.3.3. Houlsby (2006):

Following the publication of the results of the research work of Benmebarek & al. (2005), G. T. Houlsby, of the University of Oxford, was able to confirm, validate and disclose his results in the discussion published in Benmebarek & al. "Discussion" (2006). That he found them in 1975 as part of his graduation project at Cambridge University, dealing with the calculation of the stability of sheet pile walls simply embedded at the ground in a non-cohesive, homogeneous and isotropic sand, by taking taking into account the variation of the pore pressures upstream and downstream of the curtain. Its results have not been published before due to lack of validation support [Benmebarek & al. "Discussion" (2006)].

In his work, published in [Benmebarek & al. "Discussion" (2006)], Houlsby (2006) employed the method using a standard application of the characteristic method for effective stresses, as described by Sokolovski (1965) cited in [Benmebarek & al. "Discussion" (2006)]. By

substituting the effective stresses and the pore pressures for the total stresses in the equilibrium equations, the latter are then written as follows:

$$\frac{\partial \sigma'_{xx}}{\partial x} + \frac{\partial \tau_{xy}}{\partial y} = -\frac{\partial u}{\partial x}$$

$$[2.25]$$

$$\frac{\partial \tau_{xy}}{\partial x} + \frac{\partial \sigma'_{yy}}{\partial y} = -\gamma' - \frac{\partial u}{\partial y} = -\left(\gamma' + \frac{\partial u}{\partial y}\right)$$

$$[2.26]$$

The volume force in the opposite direction to the y axis is therefore increased by the term $\partial u / \partial y$, and there is also a volume force $\partial u / \partial x$ in the opposite direction to the *x* axis. As long as the volume change in pore pressure (*u*) is specified, the resulting problem can be treated simply as a problem involving a variable volume force. Houlsby (2006), published in [Benmebarek & al. "Discussion" (2006)], used the computer tool while programming the method in Fortran language, and the pore pressure could be indicated by an analytical expression or by interpolation between the mesh points. He used for the distribution of pore pressures, the analytical solution presented by Schofield and Wroth (1968), cited in [Benmebarek & al. "Discussion" (2006)].

Houlsby (2006), obtained values of Active and passive earth coefficients for φ = 30 ° and φ = 40°; for a ground / screen interface friction angle (δ) equal to 0, φ / 2 and φ, and for a variety of hydraulic head (H). For the sake of simplicity, the author has considered just the case $\gamma'=\gamma_w$ (similar to the work of Benmebarek et al. (2005)).

The author conducted his study in terms of maximum hydraulic gradient i_0 at the soil surface, which is related (using the analytical expression for pore pressures) to the water height (hydraulic head) by l 'expression: $H/D = \pi \, i_0$, as used by Benmebarek & al. (2005). And by making comparisons, he found that his values are in very satisfactory agreement with those given by Benmebarek & al. (2005). He conducted the study in a further step, and examined in two different ways the critical water height (critical hydraulic head), on the upstream side of the sheet pile wall, which would cause the failure [Houlsby (2006), published in Benmebarek & al. "Discussion" (2006)]:

➢ The first method consists in plotting as a function of the maximum hydraulic gradient i_0 the curves representative of the horizontal components of the active and passive earth pressure forces, also including the terms of the water pressure above and below the ground surface. The maximum value i_0 allowed was simply that corresponding to the point of intersection of the two curves. For low values of i_0 the calculated active forces are lower than the maximum passive resistance. This calculation must be appropriate for a purely translational failure mechanism.

➢ The second calculation was the same in principle, but involves checking the equilibrium of moments with respect to the assumed centre of rotation, by Houlsby (2006), published in [Benmebarek & al. "Discussion" (2006)], located at the lower end of the curtain (twist-breaking mechanism). This represents a more realistic mechanism (although it is not always necessarily the most critical).

The results of the two calculations, presented as a function of H/D_{crit} (Critical Relative Hydraulic Head Loss), are given in Table 2.3 below. These results clearly show that the rotational failure mechanism is more critical.

Table 2.3: Critical values of H/D for the failure of a sheet pile wall, simply embedded at the bottom, presented by Houlsby (2006) in the discussion published in [Benmebarek & al. "Discussion" (2006)].

φ	δ/φ	$(H/D)_{crit}$ (mécanisme de translation)	$(H/D)_{crit}$ (mécanisme de rotation)
30°	0	0.83	0.52
	1/2	1.09	0.67
	1	1.28	0.78
40°	0	1.17	0.69
	1/2	1.65	1.00
	1	2.05	1.25

The work of Houlsby (2006) presented in the discussion published in [Benmebarek & al. "Discussion" (2006)], being the only one which gives the numerical values of the critical relative hydraulic load H/D_{crit} causing a fracture mechanism by rotation of a sheet pile screen simply embedded at the foot (free screen), will serve as our means of comparison in the present study for the case of a free sheet pile screen simply embedded at the foot in a homogeneous and isotropic sand.

2.2.3.4. Wudtke & al. (2008) :

Wudtke & al. (2008) examined different situations concerning hydraulic uplift. They showed that the safety against hydraulic uplift was influenced by the specific properties of the soils, the existing geological stratification, and the type and extent of the structure.

2.2.3.5. Mozò & al. (2014) :

By adopting the digital approach, Mozò & al. (2014) analyzed the stability against hydraulic failure of an excavation supported in a homogeneous, non-cohesive and isotropic granular soil, with a comparison with the case of anisotropy of the soil in permeability, considering the problem a plane flow around a diaphragm wall with a total height $H_w = 20$ m and a thickness of *0.80 m*, during the various sequences of the excavation. The level of the water table behind the wall is located 2 m below the level of the natural ground (figure 2.15).

The authors used the numerical code GGU-SS-FLOW 2D (2008) based on the finite element method and specialized in the calculation of plane flows. This software allows the analysis of permanent flows and the calculation of parameters such as: hydraulic gradient, flow rate, flow velocity and hydrodynamic pore pressure against the wall. They calculated these parameters during the various excavation and drying sequences. The level of the water table in front of the wall on the downstream side is therefore a function of the geometry of the excavation, the permeability of the soil and the characteristics of the surrounding aquifer. Figure 2.16 shows the flow network around the diaphragm wall of the case considered by the authors.
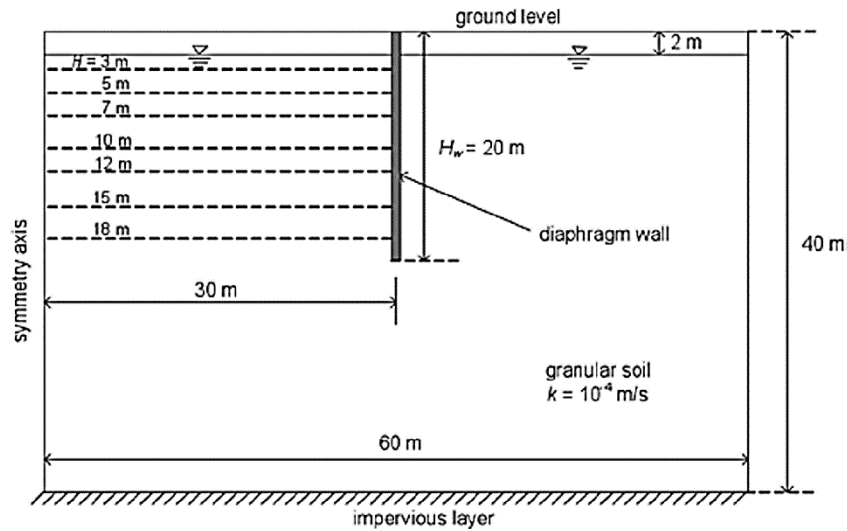
Figure 2.15: Boundary conditions and excavation sequence for the diaphragm wall analysis [From Mozò & al. (2014)]

The permeability coefficients used, representing the case of alluvial and fluvial soil deposits, are as follows:

— For the isotropy case $(k_h/k_v=1)$: $k = k_h = k_v = 10^{-4}$ m / s;

— For the case of anisotropy: $k_h = 10^{-3}$ m / s and $k_v = 10^{-4}$ m / s, that is: $(k_h / k_v = 10)$

The authors considered for the chosen soil, a saturated density $\gamma_{sat} = 20$ KN / m3; and a planed density $\gamma' = 10.2$ KN / m3; with a density of water $\gamma_w = 9.81$ KN / m3; And they adopted an overall safety factor $F_S = i_c / i \geq 2$ based on the criterion of the critical hydraulic gradient approach according to the Terzaghi method, i.e. to verify the safety of the excavation against the risk of hydraulic failure by uplift or by the seepage phenomenon. They also took into account the effect of the planed density of the soil γ'.

The methodology of Mozò & al. (2014) consists of evaluating the hydraulic stability of the diaphragm wall by defining the maximum admissible depth (H_{max}) for excavation and the minimum embedment depth (D_{min}) of the wall to avoid rupture. Figure 2.17 shows the equipotential lines and the velocity vectors resulting from the calculation carried out by the authors using the numerical code cited above.
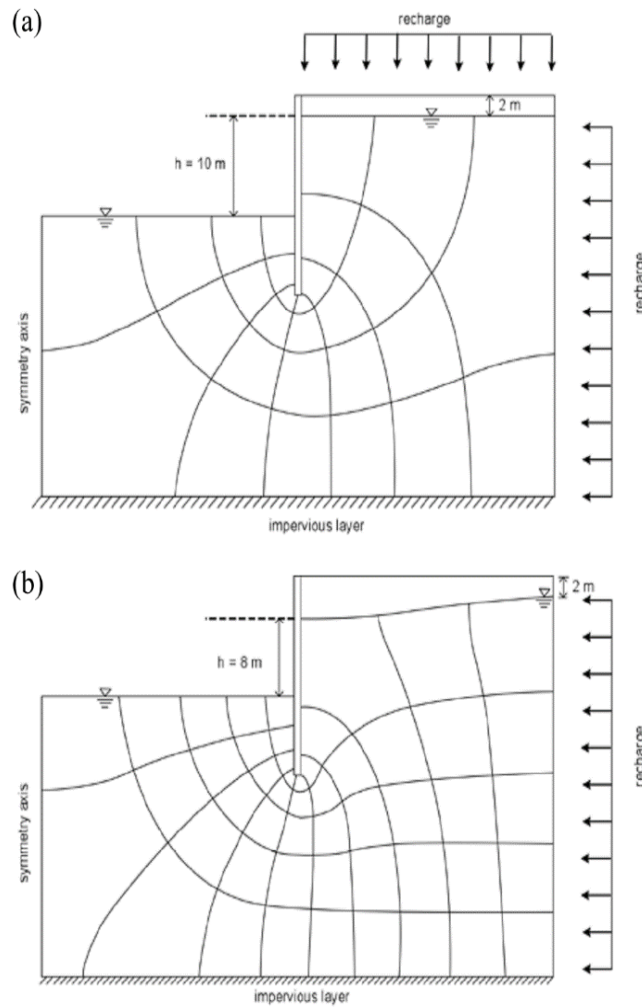
Figure 2.16. Flownets around a diaphragm wall when the excavation
is 12 m deep, showing the effect of: a) steady vertical and lateral
recharges and b) only lateral recharge from an unconfined aquifer, [From Mozò & al. (2014)]

Figure 2.18 shows the distribution of the hydraulic gradient (i) around the diaphragm wall when the depth of the excavation reaches 12 meters. We can deduce that this depth corresponds to a hydraulic head loss $\Delta h = (12-2) = 10\ m$, and an embedding depth (sheet) $D = 8\ m$. let $\Delta h / D = 1.25$ [similar to the value given by Houlsby (2006) published in Benmebarek & al. "Discussion" (2006); for $\phi = 40\ °$ and $\delta / \phi = 1$, considering a rotation mechanism (table 2.2)].

The authors have shown that the high values of the hydraulic gradient *(i)* are manifested under the foot of the wall, but also that the concentration of *(i)* is of particular interest at the level

of the bottom of the excavation next to of the diaphragm wall on the downstream side, where *(i)* reaches an average value of 0.6; *(i_{moy} = 0.6)*. But, just below the toe of the wall *(i)* approaches values slightly greater than 1.

Figure 2.17: Equipotential lines and flow velocity vectors for an excavation of 12 m, [From Mozò & al. (2014)]

Figure 2.18: Distribution of hydraulic gradients around the diaphragm wall, [From Mozò & al. (2014)]

Once the value of (i) is close to unity, corresponding to the critical hydraulic gradient $(i_{cr}=1.04 \approx 1)$, it should be checked that this zone having (i_{cr}) close to unity does not propagate up to at the surface of the ground thus causing a hydraulic rupture by the phenomenon of seepage. Since the value of *(i)* is about 0.3 in the soil below the excavation and next to the wall, then it is not necessary to check the spread of the seepage phenomenon.

The authors have pointed out that Harr (1990) cited in [Mozò & al. (2014)] indicated that the values of 4 and 5 are reasonable for the safety factor with respect to hydraulic failure defined by *Fs= i_{cr}/i,* when using graphical methods. While Powrie (2004), cited in [Mozò & al. (2014)], suggested MSF values of between 1.25 and 1.5 for fine sand from Norway for a design based on the excavation's damping system.

By repeating the analysis for each excavation sequence shown in Figure 2.16 (evolution of excavation depth), Mozò & al. (2014) were able to draw graphs showing, as a function of the depth of the excavation H and of the *H / H_w* ratio, (H_w being the total height of the wall), the variations of the hydraulic gradient and of the safety factor at level of the bottom of the excavation and the toe of the wall with comparisons between the cases of isotropy and anisotropy in soil permeability (Fig. 2.19 and Fig. 2.20).
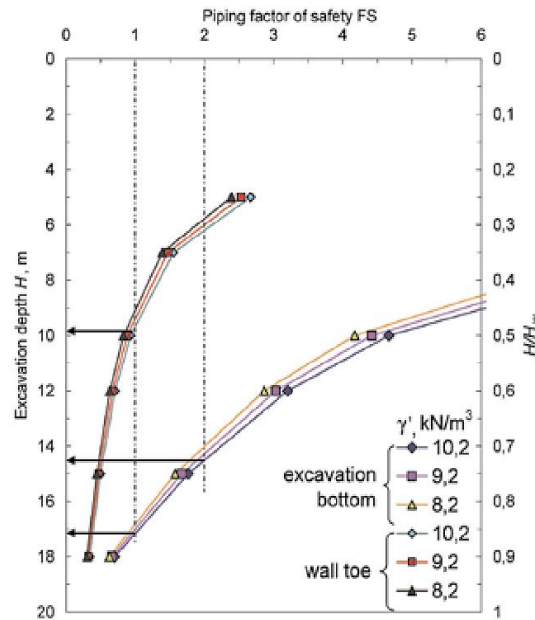
Figure 2.19 Hydraulic gradient *i* versus excavation depth *H* in an isotropic granular soil (H_w is the wall height)
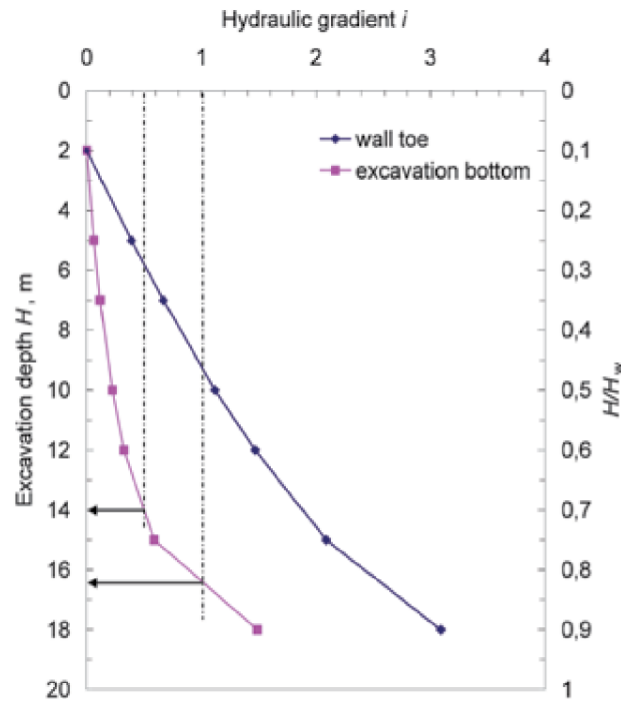
Figure 2.20 Piping factor or safety Fs versus excavation depth H,
showing variation with buoyant unit weight

2.2.3.6. Pane & al. (2015)

Pane & al. (2015), reported that hydraulic uplift failure is one of the most feared ultimate limit states in geotechnical engineering practice, and that such failure often occurs with little or no warning, and that is extremely difficult to stop the phenomenon once it has started. The rise of particles from powdery soils by upward flow of water (i.e. 'heave' or 'seepage phenomenon') can lead to relatively sudden catastrophic failures of the elements structures, support structures and earthworks such as dams and embankment.

The authors said that some of these failure have been reported in recent times; to cite just a few examples, numerous collapses of embankment and ground protection sheet piles produced during recent catastrophic events (Example: Hurricane Katrina in New Orleans in the United States of America in 2005; the soil of the Elbe River in Germany in 2013) were attributed to this rupture mechanism. For these reasons, and for the difficulties of adopting effective countermeasures once it is raised or the seepage phenomenon has been triggered, the safety margins associated with this type of hydraulic failure are traditionally quite high.

In their work, the authors recalled and discussed the traditional approaches most used for checking resistance to uplift, namely:

a) The critical gradient approach,

b) The Terzaghi Approach (1943).

While describing and highlighting some of their limitations. These approaches are generally based on an Overal Factor of Safety (OFS).

With the advent of "Eurocodes", these approaches have been significantly modified by the introduction of "partial safety factors (γ_{stb} and γ_{dst})" to stabilizing and destabilizing actions. The two approaches prescribed in the current version of Eurocode 7 (EC7) (standard EN 1997-1-2003), were also examined by the authors, namely:

c) The effective stress approach, expressed by equation 2.9b of EC7;

d) L'approche en contrainte totale, formulée par l'équation 2.9a of EC7.

However, Pane et al. (2015) have shown that the two approaches to EC7 do not provide a consistent assessment of safety against uplift failure, and in some cases can lead to illogical and erroneous results.

Based on these considerations, the authors even recommended the rewrite of EC7 and suggested an approach modifying those of EC7, with the aim of providing a more generalized and rational approach for checking uplift [Pane & al. (2015)].

2.2.3.7. Serdar KOLTUK & al. (2019)

Serdar KOLTUK & al (2019) performed experimental and numerical investigations to clarify the seepage failure by heave in sheeted excavation pits in stratified cohesionless soils in which a relatively permeable soil layer (k_{upper}) lies above a less permeable soil layer (k_{lower}) between excavation base and wall tip.

In their work, a test apparatus was designed, taking advantage of symmetry, to investigate the failure mechanism in two-dimensional seepage flows around a wall embedded in stratified cohesionless soils.

The test apparatus was made of acrylic glass, and its dimensions were: length x width x height = 530 mm x 200 mm x 680 mm. A partition panel with a thickness of 27 mm and a height of 500 mm was used to model the excavation wall (see Figure 2.21). At the beginning of the test, the water levels on both sides of the partition panel were equal. During the test, the water level at the left side of the test apparatus was lowered stepwise by 10 mm while the water level at the

1: upper soil layer, 2: lower soil layer, 3: filter layer, 4: non woven fabric, 5: partition panel, 6: standpipes, 7: deaerator (reservoir), 8: water inlet, 9: overflow, 10: water outlet
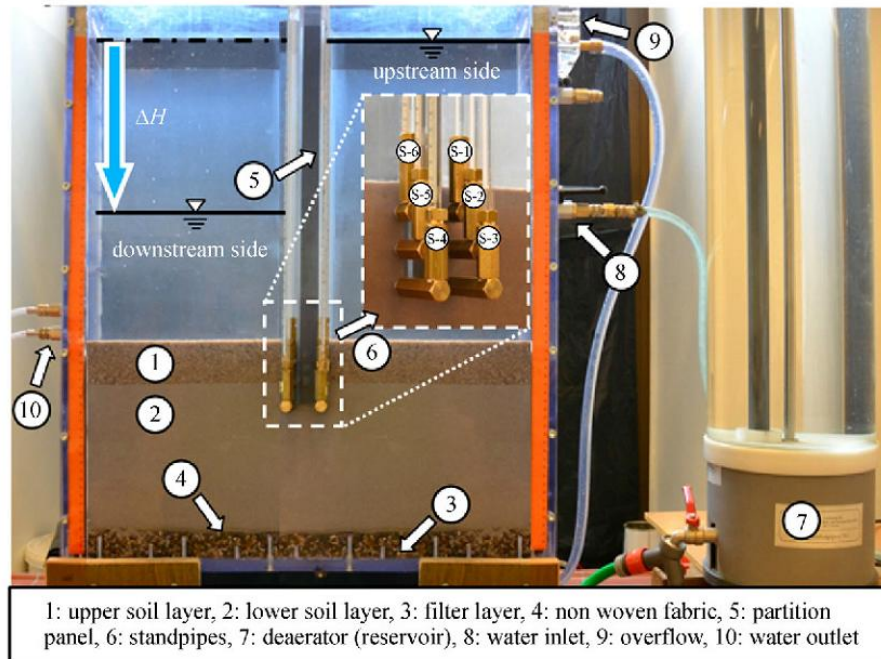
Figure 2. 21 Test apparatus. [From Serdar KOLTUK & al. (2019)]

right side was kept constant through a continuous water supply and overflow. After the potential difference between up- and down-stream sides *ΔH* reached the value required for the development of seepage failure by heave according to Terzaghi and Peck's approach, it was lowered stepwise by 5 mm. After each lowering of the water level, any change in the test soils was carefully observed. In case of appearance of first deformations on the soil surface or a remarkable change of water heights in the standpipes, the lowering of the water level was stopped and it was waited as long as, until the system reached a new equilibrium of forces and entered into a new stable state. Accordingly, each test took 2–3h.

The test configurations and their results are listed in Table 2.5. $\Delta H_{collapse(exp)}$

represents the potential difference between up- and down-stream sides that led to total collapse in the performed model tests while $\Delta H_{Terzaghi\&Peck}$ represents the critical potential difference calculated according to the approach of Terzaghi and Peck.

To determine the value of $\Delta H_{Terzaghi\&Peck}$, the average hydraulic head $\Delta h_{av,failure}$ at the bottom of heave zone suggested by Terzaghi and Peck was first calculated by using Equation (2.28), which corresponds to Equation (2.27) with Fs=1:

$$FS = (Dx\gamma'_{upper} + dx\gamma'_{lower})/\Delta h_{av}x\gamma_w, \tag{2.27}$$

$$\Delta h_{av,failure} = [Dx(\gamma_{sat,upper} - \gamma_w) + dx(\gamma_{sat,lower} - \gamma_w)]/\gamma_w. \tag{2.28}$$

Subsequently, $\Delta H_{Terzaghi\&Peck\,required}$ for the development of $\Delta h_{av,failure}$ was determined by means of steady-state ground-water flow analysis.

Table 2.5 Test configurations and the corresponding potential differences in the limit state

test No.	embedment depth, $D+d$ (cm)	upper layer No.	D of the upper layer (cm)	D_r of the upper layer	γ_{sat} of the upper layer (kN/m³)	k_{upper}/k_{lower}	$A = \Delta H_{collapse(exp)}$ (cm)	$B = \Delta H_{Terzaghi\&Peck}$ (cm)	A/B
1	5.0	2	2.5	42%	19.6	2.3	20	16.2	1.23
2	5.0	2	2.5	97%	20.7	1.1	17.5	15.6	1.12
3	7.5	2	5.0	42%	19.6	2.3	31 (31.5)	23.1	1.34
4	7.5	2	5.0	97%	20.7	1.1	26 (26.5)	22.3	1.17
5	5.0	3	2.5	33%	19.1	9.3	24	16.8	1.43
6	5.0	3	2.5	98%	20.1	5.6	25.5 (26)	17.6	1.45
7	7.5	3	5.0	33%	19.1	9.3	37.5	25.4	1.48
8	7.5	3	5.0	98%	20.1	5.6	40.5 (40)	26.3	1.54
9	5.0	4	2.5	58%	20.6	1.3	25 (24.5)	15.9	1.57
10	7.5	4	5.0	58%	20.6	1.3	40 (39)	22.9	1.75
11	5.0	5	2.5	53%	20.3	7.8	26 (27)	17.9	1.45
12	7.5	5	5.0	53%	20.3	7.8	– a)	27.3	– a)

Note: a) No total collapse occurred for the maximum reached potential difference in the test box.

Therefore, Serdar KOLTUK & al (2019) found that in all conducted tests, the values of $\Delta H_{collapse(exp)}$ were higher than $\Delta H_{Terzaghi\&Peck}$. On the other hand, in respect of failure behaviour, the same observations were made in all tests. The various stages of seepage failure by heave observed in Test No. 10 are shown in Figure 2.22. The potential difference that led to a theoretical failure according to Terzaghi and Peck's approach ($\Delta H_{Terzaghi\&Peck}= 22.9\ cm$) caused heaves of about 2 mm on the downstream side (see Figure 2.22(b)). Further increasing of the potential difference ΔH

led to further heaves on the downstream side. However, when the lowering of the water level was stopped, soil reached a new equilibrium of forces and entered into a new stable state. Settlements on the upstream side were appeared shortly before the total collapse occurred (see Figure 2.22(c)). The seepage failure by heave (total collapse) took place as a result of progressive deformations that developed under a constant potential difference of $\Delta H_{collapse(exp)}= 40$ cm (see Fig. 2.22(d)). Serdar KOLTUK & al (2019) simulated the model tests presented above by means of numerical analyses using finite element (*FE*) software PLAXIS 2D—Version 2017, (Figure 2.23).
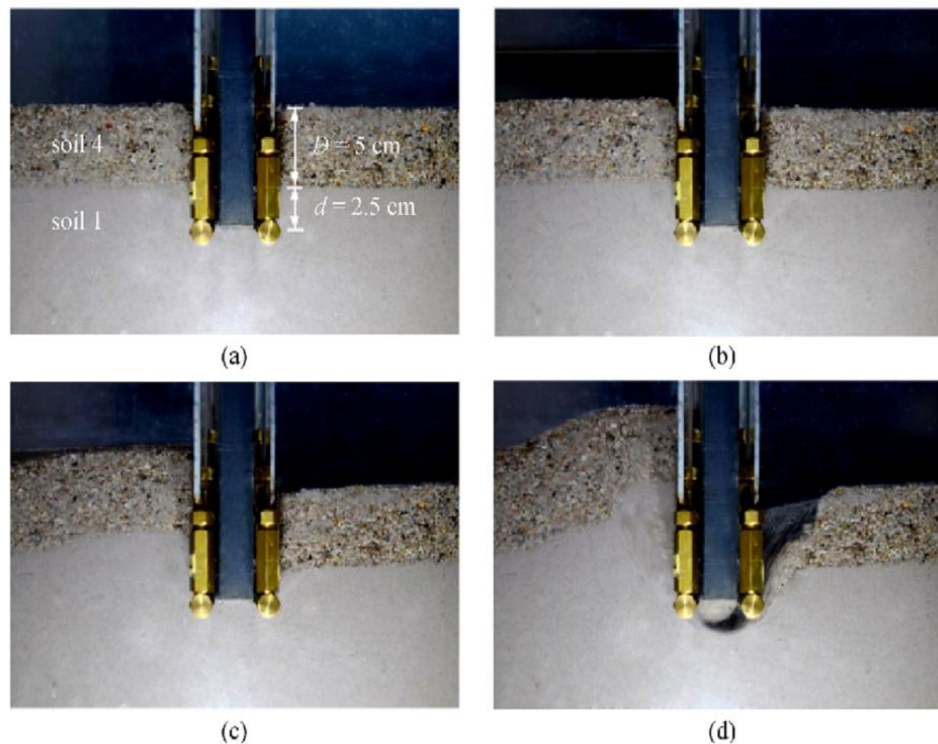
Figure 2.22 Development of seepage failure by heave in Test No. 10: (a) $\Delta H<\Delta H_{Terzaghi\&Peck}$;(b) $\Delta H=\Delta H_{Terzaghi\&Peck}$; (c) $\Delta H_{Terzaghi\&Peck}<\Delta H<\Delta H_{collapse(exp)}$; (d) total collapse, $\Delta H=\Delta H_{collapse(exp)}$. [From Serdar KOLTUK & al. (2019)]

Table 2.6 shows the critical potential differences $\Delta H_{collapse(num)}$ that led to a numerical limit state in the performed finite element analyses. In addition, the ratios of $\Delta H_{collapse(exp)} /\Delta H_{collapse(num)}$ and $\Delta H_{collapse(exp)} /\Delta H_{Terzaghi\&Peck}$ are given for comparison.
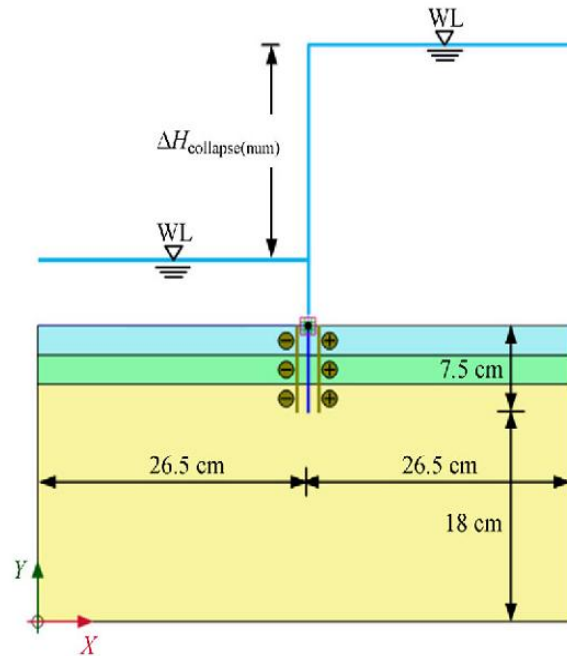
Figure 2.23: Numerical simulation of the performed model tests with an embedment depth of 7.5 cm. [From Serdar KOLTUK & al. (2019)]

In all tests, Serdar KOLTUK & al (2019) found that the critical potential differences obtained from the model tests were higher than those obtained from the numerical analyses and Terzghi and Peck's approach ($\Delta H_{collapse(exp)}/\Delta H_{collapse(num)} > 1$ and $\Delta H_{collapse(exp)}/ \Delta H_{Terzaghi\&Peck} > 1$). Compared to the approach of Terzaghi and Peck, the numerical analyses showed a better agreement with the results of the model tests.

Table 2.6: Results of the finite element analyses and their comparison with experimental results

Test No.	upper layer No.	k_{upper}/k_{lower}	$\Delta H_{collapse(num)}$ (cm)	$\Delta H_{collapse(exp)}/\Delta H_{collapse(num)}$	$\Delta H_{collapse(exp)}/\Delta H_{Terzaghi\&Peck}$
1	2	2.3	18.1	1.10	1.23
2	2	1.1	17.0	1.03	1.12
3	2	2.3	26.2	1.18	1.34
4	2	1.1	24.2	1.07	1.17
5	3	9.3	19.9	1.21	1.43
6	3	5.6	20.9	1.22	1.45
7	3	9.3	29.7	1.26	1.48
8	3	5.6	31.5	1.29	1.54
9	4	1.3	17.2	1.45	1.57
10	4	1.3	24.4	1.64	1.75
11	5	7.8	20.9	1.24	1.45
12	5	7.8	31.8	_ [a]	_ [a]

Note: a) No total collapse occurred for the maximum reached potential difference in test box.
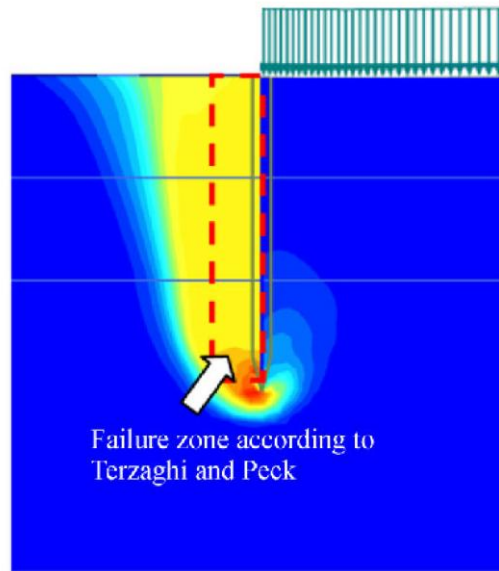
Figure 2.24: Numerical simulation of Test No. 10: failure zone.
[From Serdar KOLTUK & al. (2019)]

Figures 2.24 illustrate the corresponding distribution of the incremental displacements for Test No. 10. A significant difference between the shapes of the failure zones obtained from the numerical analysis and Terzaghi and Peck's approach is clearly visible where a triangle-shaped heave zone with a larger width was obtained from the numerical analysis, in contrast to the rectangular-shaped heave zone suggested by Terzaghi and Peck. The triangle-shaped heave zone obtained from the numerical analysis is in good agreement with the failure zone shown in Figure 2.22(d).

2.2.3.8. ZHAO Guo-qing & al. (2020)

ZHAO Guo-qing & al. (2020) conducted full-scale field tests and numerical analyses to study the failure mechanism of the circular shaft subjected to hydraulic uplift.

They established an axisymmetric two-dimensional finite element model using the finite element software PLAXIS 2D 2015 in accordance with the circular shaft character on site. The numerical model of the excavation shown in Figure 2.25.

The results of the FE software showed that the soil body seems to collapse when the excavation reached 3.6 m below the surface. The location of the maximum incremental displacement changed from the centre of the shaft to the soil-wall interface when the

excavation depth varies from 3.2 m to 3.6 m (see Figure 2.26(a)). It implied that the displacement persistently increased at the soil-wall interface at this moment. As shown in Figure
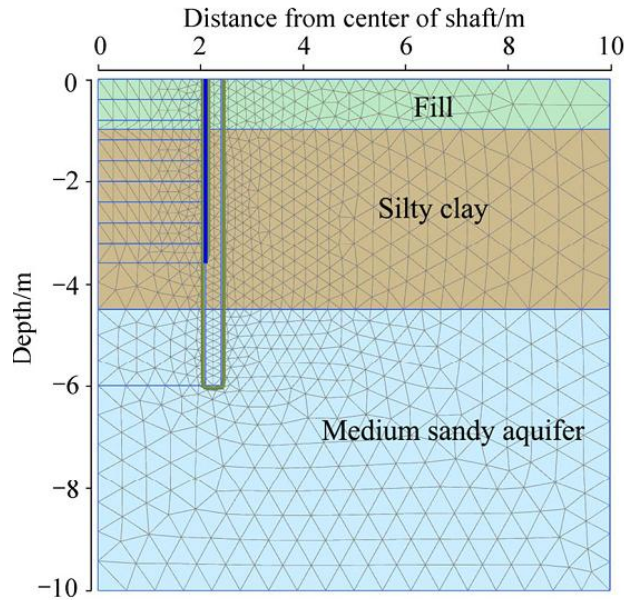
Figure 2.25 Numerical model of test shaft [From ZHAO Guo-qing & al. (2020)]
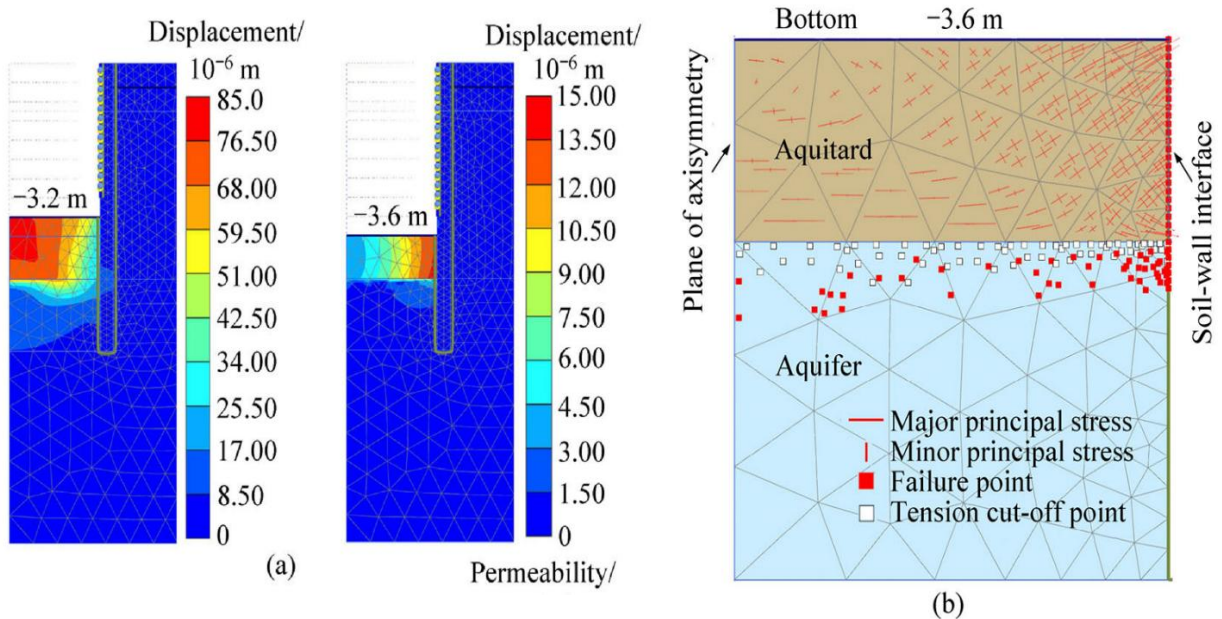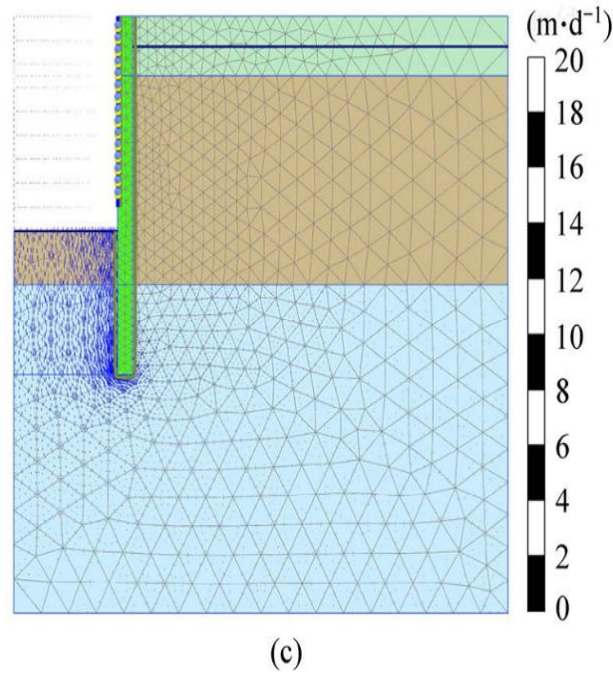
Figure 2.26 Computed water inrush process of shaft: (a) Incremental displacements; (b) Failure of soil-wall interface; (c) Groundwater flow; [From ZHAO Guo-qing & al. (2020)]

2.26(b), the failure points cut through the soil-wall interface, which illustrated that the soil reached the limit of the destruction at the interface.

The authors concluded that the finite element analysis results are in good agreement with the observed phenomena on site, implying that the present FEM model can be used for stability evaluation of similar shaft subjected to hydraulic uplift.

2.3. Conclusion :

Several methods dealing with the evaluation of the stability of excavation bottoms have been proposed in the literature, which are generally based on a fairly high safety factor with respect to the failure of the excavation bottom by the seepage phenomenon or the heaving at the bottom of the excavation (hydraulic failure), which are unexpected phenomena and can occur suddenly, with little or no warning, inside the cofferdams. They take only the role of waterproofing wall, the effect of flow forces causing the passive pressure reduction in front of the wall embedment is ignored. And the values of the critical hydraulic head loss causing failure also proposed in the

literature sometimes show critical differences. These methods often suffer from limitations and lack of generalization, rendering their use ineffective and sometimes leading to illogical and erroneous results. In addition, they are unable to predict deformations and failure mechanisms essential for understanding the behaviour of retaining walls. And cannot deal with complex cases, excavations and their surrounding environments, in their entirety.

Second part

Numerical modelling of excavation basal stability

Chapter 3

Presentation of numerical modelling tool

Chapter 3: Presentation of numerical modeling tool

3.1. Introduction

There are many books which deal in great detail with the application of numerical methods usually finite element methods to engineering problems in general or to geotechnical problems in particular (eg Zienkiewicz and Taylor, 2000; Cook, Malkus and Plesha, 1989; Cook, 1995; Livesley, 1983; Smith and Griffiths, 1988; Britto and Gunn, 1987; David and Zdravkovic, 1999). It is intended here to provide merely a brief introduction to numerical modelling: enough for the reader to be able to understand some of the language of numerical modelling, some of the issues that need to be confronted when setting about numerical modelling of a geotechnical problem, and some of the pitfalls that may confront the numerical modeller.

We start by deriving the governing equations for mechanical and flow problems in one dimension. This apparently trivial beginning allows us to illustrate the development of a number of aspects of the finite element approximation which can be readily extended to two and three dimensions. The governing equations are also presented for the two-dimensional problem: parallels with the one-dimensional equations will be drawn.

3.2. Plaxis code

After a review of the State of Art, and other proper literature about the seepage problem in underwater excavations, much more studies about this complex subject were needed, with the use of more updated technologies, such as commercial geotechnical software. These studies will help to learn more properly the behaviour of bottom failure in deep excavations, and that will bring increased safety to their design and construction. Consequently, a way of studying this soil behaviour was imagined by trying to correlate the results of previous works with the use of a finite element method (FEM) geotechnical software. The chosen program was PLAXIS, which is a very powerful and well-known geotechnical software, with a friendly interface. The aim of this study is to try a new approach to the bottom stability problem in deep excavations, and therefore to have a better knowledge of that important subject, because deep excavations are increasing with the rehabilitation of urban sites. Nowadays, underground parking is becoming a great concern, in an attempt of getting rid of public parking, which occupies large areas. To apply PLAXIS program to this study, some modifications are needed to achieve the proper results. In addition, different programs have different features, and, as it was said, different input parameters should be introduced. In FEM software application, the mesh generator works in different ways,

which means that the final result may not be exactly the same. Therefore, proper result analysis is needed, so the data can be compared and studied appropriately. On the other hand, physical models are a different subject: they are much harder to reproduce in software, because there are a lot of variables which may not be considered in the physical model, or are not very accurate, which may lead to different results. Therefore, this part of the work will take more time than any of the other ones, because it is also very hard to reproduce the exact same conditions, in terms of stress, strain and water conditions, such as permeability and constant water head.

3.3. Development of plaxis

The development of PLAXIS began in 1987 at Technical University of Delft, as an initiative of the Dutch Department of Public Works and Water Management. The initial goal was to develop an easy way to use 2D finite element code for the analysis of river embankments on the soft soils of the lowlands of Holland. In the subsequent years, PLAXIS was extended to cover most other areas of geotechnical engineering. Because of continuously growing activities, a company named PLAXIS b.v. was formed in 1993.

The main objectives of this program are intended to provide a tool for practical analysis to be used by geotechnical engineers who are not necessarily numerical specialists. Many engineers frequently consider non-linear finite element computations which take a lot of time and effort. On the contrary, PLAXIS has robust and theoretically sound computational procedures, which have a friendly interface. Development of PLAXIS would not be possible without worldwide research at universities and research institutes. To ensure that the high technical standard of PLAXIS is maintained, the development team is in contact with a large network of researchers in the field of geomechanics and numerical methods.

3.4. Plaxis 2d

PLAXIS 2D is a finite element package intended for the two dimensional analysis of deformation and stability in geotechnical engineering. Geotechnical applications require advanced constitutive models for the simulation of the non-linear, time dependent and anisotropic behaviour of soils and/or rock. In addition, since soil is a multi-phase material, special procedures are required to deal with hydrostatic and non-hydrostatic pore pressures in the soil. Although the modelling of the soil itself is an important issue, many tunnel projects involve the modelling of structures

and the interaction between the structures and the soil. PLAXIS is equipped with features to deal with various aspects of complex geotechnical structures.

The input of soil layers, structures, construction stages, loads and boundary conditions is based on convenient CAD drawing procedures, which allows for a detailed modelling of the geometry cross-section. From this geometry model, a 2D finite element is generated. PLAXIS allows for automatic generation of unstructured 2D finite element meshes with options for global and local mesh refinement, and the 2D mesh generator is a special version of the Triangle generator . In this program, it can be used quadratic 6-node and 4th order 15-node triangular elements to model the deformations and stresses in the soil. Many elements can be inserted in the model such as plates, anchors, geogrids, tunnels, with a lot of definition options available.

In this software, special beam elements are used to model the bending of retaining walls, tunnel linings, shells, and other slender structures. The behaviour of these elements is defined using a flexural rigidity, a normal stiffness and an ultimate bending moment. Plates with interfaces may be used to perform realistic analysis of geotechnical structures. In addition, joint elements are available to model soil-structure interaction. Values of interface friction angle and adhesion are generally not the same as the friction angle cohesion of the surrounding soil. To model anchors and struts, elastoplastic spring elements are used. The behaviour of these elements is defined using a normal stiffness and a maximum force. A special option exists for the analyses of prestressed ground anchors and excavation supports.

The PLAXIS program offers a convenient facility to create circular and non-circular tunnels using arcs and lines. Plates and interfaces may be used to model the tunnel lining and the interaction with the surrounding soil. Fully isoparametric elements are used to model the curved boundaries within the mesh. Various methods have been implemented to analyse the deformations. PLAXIS uses various soil models such as the well-known Mohr-Coulomb model, which is based on notorious soil parameters in engineering practice. In addition, it has advanced soil models of many types as elastoplastic hyperbolic models, and time-dependent models. This program has a soil test option, which permits to check the behaviour of the selected soil material model with the given material parameters.

With the help of the Staged construction feature, it is possible to make a realistic simulation of construction and excavation processes by activating and deactivating clusters of

elements, application of loads, changing of water tables, etc. In this study, this feature is very helpful, because in every calculation the excavations or the rise of the water level is phased. The decay of excess pore pressure with time can be computed using a consolidation analysis, which requires the input of permeability coefficients in the various soil layers. Automatic time stepping procedures make the analysis robust and easy to use.

The safety factor is usually defined as the ratio of the failure load to the working load. This definitions is suitable for foundation structures, but not for sheet -pile walls or embankments. For this latter type of structure it is more appropriate to use the soil mechanics definition of a safety factor, which is the ratio of the available shear strength to the minimum shear strength needed for equilibrium. PLAXIS can be used to compute this factor of safety using a phi-c reduction procedure, which will be explained later. The PLAXIS postprocessor has enhanced graphical features for displaying computational results. Values of displacements, stresses, strains and structural forces can be obtained from the output tables. Plots and tables can be sent to output devices to export them to other software. A special tool is available for drawing load-displacement curves. The visualisation of stress paths provides a valuable insight into local soil behaviour which allows a detailed analysis of the results of a PLAXIS calculation.

In summary, PLAXIS is an excellent tool for a lot of geotechnical problems, with various features which allow a good and safe evaluation of the majority of the geotechnical constructions, and because it has a friendly interface, not hard to use, and for that matter there is not so much chance for error.

3.4.1. Mesh

In order to perform the calculations the mesh in Plaxis has to be generated. When Plaxis creates the mesh, it automatically divides the geometries into finite elements. It is important to generate a sufficiently fine mesh in order to get accurate results from Plaxis.

In this case this means that a finer mesh should not generate any differences in the factor of safety compared to the previously used mesh. It is important to notice that the finer the mesh, the longer the calculation will take to perform. Hereby an unnecessarily fine mesh should be avoided due to long calculation times. This is however, a relatively small problem in Plaxis 2D and of much more concern in Plaxis 3D. Plaxis generates the elements in the mesh by using a triangulation procedure (PRM, 2015).

3.4.2. Elements

In this section the different ways to model soil elements are presented, later on in this work the possible structural and interface elements are described. In Plaxis it is possible to use 6-nodal or 15-nodal triangular elements for the soil, as seen in Figure 3.1 and 3.2. It is important to point out that the default mode is 15-node elements, this provides a fourth order integration for displacements and the numerical integration uses 12 gauss points. The 15-node elements result in a finer distribution of nodes and therefore more accurate calculations in comparison to the 6-nodal elements. This is more time consuming, but is assessed as necessary to get accurate results and used in this work (PRM, 2015).
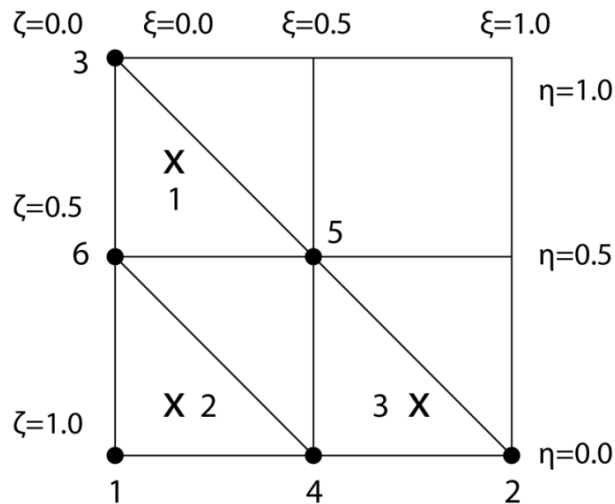
Figure 3.1 Local numbering and positioning of nodes and integration points (x) of a 6 node triangular element (PSM, 2015).

Plaxis automatically generates a mesh depending on the target element size, le which is a global entity generated by the dimension of the outer geometry and the element distribution factor selected in Plaxis. The element distribution factor is a factor that states which quality the mesh should be generated with. The target element size is a function of: (PRM, 2015):

$$l_e = r_e 0.06\sqrt{(x_{max} - x_{min})^2 + (y_{max} - y_{min})^2}$$

[3.1]

Where
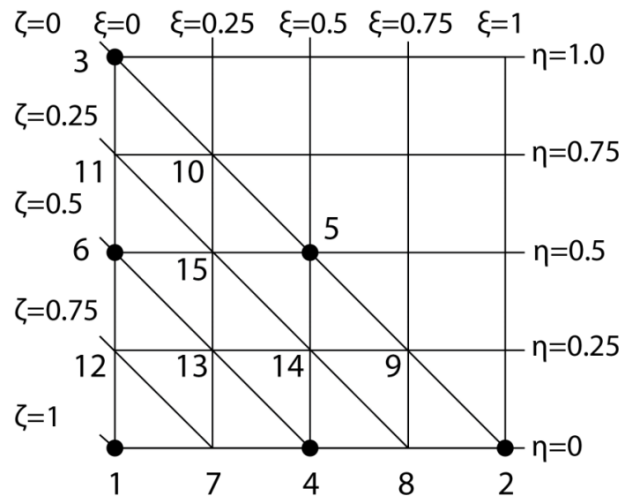
Figure 3.2 Local numbering and positioning of nodes of a 15-node
34 triangular element (PSM, 2015).

r_e Relative element size factor, the values for different element distributions can be seen in the reference manual for Plaxis (PRM, 2015).

l_e Average element size

After this automatically generated mesh, it is possible for the user to do local refinement of the mesh around points of interest or regions that are considered to be difficult to calculate correctly due to large stress concentrations caused by corners or edges of structural elements. Plaxis automatically makes the structural elements compatible with the soil elements (PRM, 2015).

3.4.3. Plate elements

In Plaxis plates are used to model slender geotechnical structures with a substantial bending stiffness and normal stiffness. In order to model these correctly the most important parameters are bending stiffness, EI, the axial stiffness, EA, and the thickness of the element, deq (PRM, 2015).

The 6-node soil elements are compatible with the 3-node plate elements and in analogy the 15-node soil elements are compatible with the 5-node plate elements as seen in Figure 3.3. In two-dimensional modelling these nodes have three degrees of freedom per node, one rotational and two translational. The Gaussian stress points seen in the plate elements below

are used to calculate bending moment and axial forces, for the case with the 5-node plate element there are four pairs of stress points (PRM, 2015).
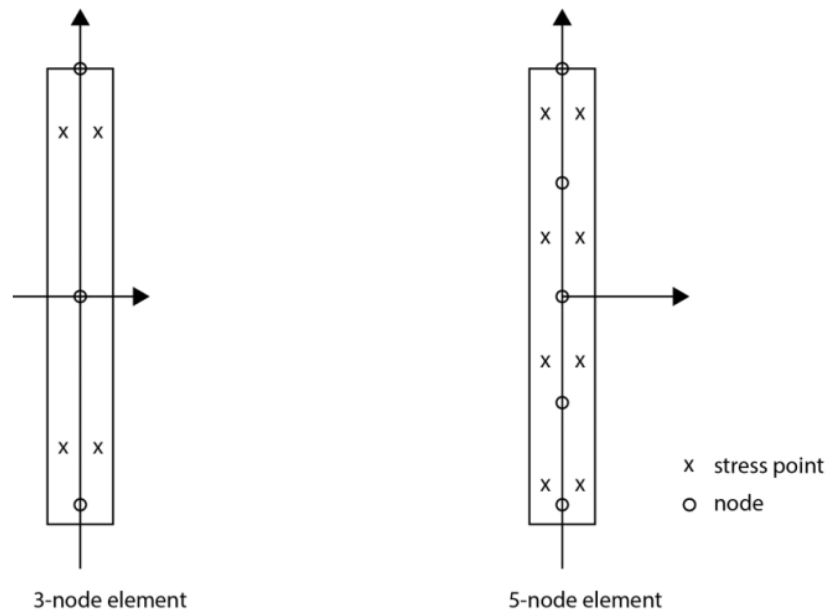
Figure 3.3 Position of nodes and stress points in embedded beam
row elements (PRM, 2015).

3.4.4. Interfaces and interface elements

The interfaces in Plaxis 2D are applied to plates or geogrids to enable accurate modelling of the interaction between the soil and structures. They can e.g. simulate the contact zone between a plate and soil, were the shearing is intense. An interface is usually assigned to both sides of the plate element (PRM, 2015).

When 15-node soil elements are used, the interface element consists of 5 pair of nodes with three translational degrees of freedom in every node (ux,uy,uz). The three degrees of freedom enable the node pair to have different displacements relative to one another.

Figure 3.4 shows the interface elements, in this figure the interface elements look similar to the plate elements. However the difference is that the interface elements consist of pairs of nodes, where the node coordinates are equal to one another. Hereby the thickness of the elements is zero. In the point where the interfaces end, the node pair is collapsed to a single node. These elements are numerically integrated using six Gauss points (PRM, 2015).
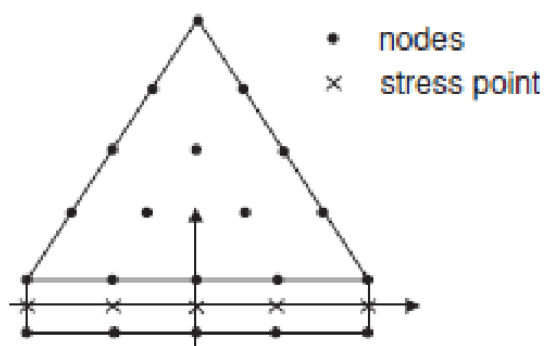
Figure 3.4 Distribution of nodes and stress point sin 6-node deem
elements and their connection to soil elements

3.4.5. Fixed-end anchors

Fixed end anchors are modelled as point elements in Plaxis 2D. They have an axial stiffness but no bending stiffness. These are used to model the shoring supporting the retaining structure in one of the excavations (PSM, 2015).

3.4.6. Boundary conditions

Plaxis offers a number of different ways to set the boundary conditions for each phase. Plaxis 2D automatically assigns general boundary conditions to the geometry model. In Plaxis the vertical model boundaries are fixed in the x-direction, which means that $ux=0$ (no deformation) and free to move in the y-direction. It also automatically fixes the bottom boundary in all direction, i.e. $ux=0$, and $uy=0$. In contrast the boundary of the ground is set as free to move in all directions to enable modelling of soil movements. Plaxis provides the option to turn off or change these boundary conditions, but by doing so boundary conditions need to be set manually (PRM, 2015). During the modelling in Plaxis it is of importance to ensure that the selected geometry boundaries do not affect the critical slip surface and the factor of safety in the model. Therefore it has been ensured that both the depth of the soil layer and the length of the surface boundary outside the excavation pits (on both sides) are sufficient so that the slip surface is not affected by the outer boundaries.

In order to perform a Fully coupled flow-deformation analysis correctly the groundwater flow boundaries and hydraulic conditions need to be set. Plaxis 2D enables the user to

determine which of the outer geometry boundaries that is open or closed in the model condition window. By default Plaxis sets the bottom boundary to closed and the three other boundaries to open, the definition of a closed boundary is that it does not allow groundwater flow across the boundary. Besides the default conditions the two vertical geometry boundaries are also set to closed in this work. In a Fully coupled flow-deformation analysis these boundaries are very important, since these control where the pore water may flow and therefore these properties influence the total pore pressures.

These hydraulic boundary conditions always override the ones that are specified in the model conditions (PRM, 2015).

Plaxis also provides the possibility to enter hydraulic boundary conditions manually in several other ways; one is to define a groundwater head boundary condition to one of the other geometry boundaries. When this is done Plaxis will automatically generate external water pressures. During the deformation analysis Plaxis will work with the external water pressures as traction loads which are taken into consideration with the weight of the soil and the pore pressures (PRM, 2015).

3.4.7. Drainage

In Plaxis there are several ways to model the drainage situation in the soil, drained or undrained behaviour. One of the most important parameters during an FE -analysis of soil is the pore pressure, since this significantly influences the time-dependent behaviour of the soil. The pore pressures are generated in correspondence to the drainage types. In this work Plaxis 2D is used to generate the pore pressures. The used material is assumed to have a drained behaviour. This is based on a comparison of a drained and an undrained analysis in Plaxis 2D. The drained situation is suited for long-term situations and the undrained situation is suited for short-term situations without the time dependent development of pore pressures. In this drainage type excess pore pressures are a consequence of stress changes and the undrained analysis can be dived into three cases A, B and C (PRM, 2015). The drainage type Undrained A is chosen based on, that this model uses effective parameters to model the undrained behaviour and that it is assumed that the shear strength of the clays does not increase with the depth, which suits this model perfectly. The comparison for two identical excavation pits shows that the

drained analysis provides a lower factor of safety and to avoid overestimating the factor of safety, the drained analysis is used in the rest of the FE-analysis.

The drained analysis is only available for the plastic calculations and the safety analysis. During the Fully coupled flow-deformation analysis the behaviour of the soil is determined by the saturated permeability and therefore the drainage type is disregarded in this calculation type. The saturated permeability is in this case a direct input parameter chosen in the flow parameters tab sheet (PRM, 2015). Plaxis 2D provides a number of predefined hydraulic models, as van Genuchten or Approximate van Genuchten.

Due to the fact that the *Fully coupled flow-deformation analysis* is used to model most of the phases in this thesis, the selection of the drainage type will not have a significant impact on the results. For that, we chose the standard type.

3.4.8. Initial stress generation

The initial stresses in soil are affected by the water conditions, the weight of the soil and the history of the formation of the soil. Plaxis offers two different ways to generate the initial stresses, the k0 -procedure and Gravity loading. In this work, the k0 -procedure is used, which is a direct input procedure in Plaxis 2D. k0 provides the initial ratio between horizontal effective stress and vertical effective stress, $\sigma'h / \sigma'v$ but does not consider external loads. The k0- procedure is especially suited to generate the initial stresses for horizontal surfaces (PRM, 2015).

3.4.9. Safety calculations

Plaxis 2D uses a c/φ reduction to make a safety analysis which for the *Mohr-Coulomb material* model mean that the safety calculation reduces the strength parameters tan φ and c successively until failure occurs. This is done according to Equation 3.2 as

$$\sum M_{sf} = \frac{\tan \varphi_{input}}{\tan \varphi_{reduced}} = \frac{c_{input}}{c_{reduced}} \qquad [3.2]$$

The strength reduction performed in Plaxis introduces out-of-balance forces in the model. The out-of balance forces will in turn result in additional deformations (that does not have a physical meaning). However, the probable failure mechanism of the model is determined by the

incremental displacements and/or the incremental shear strains during the last step of the calculations (PK, 2015).

The safety calculations are performed using the load advancement number of steps procedure in Plaxis 2D. In the first step the multiplier $\sum Msf$ is set to 1.0 and Msf specifies the increment of strength reduction during this step (PRM, 2015).

As the soil strength is gradually reduced until failure occurs, the factor of safety corresponds to the strength reduction factor. The failure is recognized by the small reduction in strength which leads to large change in displacements or strains (PK, 2015).

$$FS = \frac{available\ strength}{strength\ at\ failure} = \text{value of } \sum M_{sf} \quad \text{at failure} \qquad [3.3]$$

It is important to note that the value of $\sum$Msf needs to have become steady in the end of the safety calculation, otherwise the factor of safety will not be a representable value.

3.4.10. Fully coupled flow-deformation

The significance of the Fully coupled flow-deformation analysis (FCFD) is used to calculate deformations simultaneously with pore pressures caused by time dependent

changes in the hydraulic conditions. During the FCFD analysis, the total pore pressures (the sum of steady state and excess pore pressures) are calculated. In order to correspond with the previously described calculations types, P-steady is calculated based on the hydraulic conditions at the end of the calculation phases. This enables the excess pore pressures to be calculated from the total pore pressures. Because of this unsaturated soil behaviour and suction can be considered in a Fully coupled flow deformation analysis (PRM, 2015).

3.4.11. Pore pressures

In general Plaxis 2D is used for effective stress analysis, where the sum of the effective stresses, σ' and the active pore pressure p_{active} results in the total stresses, σ, formulated as:

$$\sigma = \sigma' + p_{active}$$

$$[3.4]$$

The active pore pressure can in turn be divided into the product of the effective saturation, p_{steady} and excess pore pressure, p_{excess} . The steady state pore pressures represent the stable

pore pressure state, which shall not change during a deformation analysis. There are several ways to generate these pore pressures, by selecting different pore pressure calculation types in the phases window. In the *Fully coupled flow-deformation analysis* the pore water pressure and the displacements are calculated simultaneously and therefore the steady state pore water pressures are a result of a preliminary steady-state groundwater flow calculation. This calculation type uses the hydraulic boundary condition in the end of the calculation phase (PRM, 2015) Stress changes in undrained materials, which result in deformations lead to the generation of excess pore pressures. However, excess pore pressure can occur in any material (excluding non-porous) during a FCFD analysis.

In situations when the degree of saturation differs from unity (unsaturated soil) the pore water pressure is not equal to the active pore pressure. In these cases selection of a soil water retention curve, which relates the positive pore water stress (suction) to the degree of saturation, is needed. Plaxis carries a number of predefined data sets to model the flow of water in the unsaturated zone.

3.4.12. Predefined data sets

In Plaxis there are a number of predefined data sets to model the soil water retention curve, which is used to model the unsaturated flow of groundwater. This curve is generated with standardized soil classification systems, which in Plaxis are named as USDA, Hypres, Standard and Staring.

3.4.13. Suction

In Plaxis 2D there is an option to either ignore or allow suction during the FE-analysis. This option inflicts several properties on the pore pressures in the soil and regardless if ignore suction is used or not, this option is used in all phases during modelling in Plaxis. The initial stress generation, plastic calculation, Fully coupled flow-deformation and the safety calculation all supports this option.

3.4.14. Ignore suction

When this option is used the soil is considered fully saturated below and completely dry (ideally unsaturated) above the phreatic level. In the plastic calculation step the phreatic level is defined manually by the user but during the Fully coupled flow-deformation analysis it is

generated as a calculation result from Plaxis. Ignore suction means that the positive steady state pore stresses will be set to zero (suction will be ignored) but excess pore pressure (positive and negative) both under and over the phreatic level, will be taken into account.

- In drained materials the effective saturation will be set to, $S_{eff} = 1$. This will reject any previous value.

- The steady-state pore pressure on or below the phreatic level is set as:

$$P_{steady} \leq 0 \; S = 1, S_{res} = 0, S_{sat} = 1 > S_{eff} = 1$$

Ignore suction will not affect stresses and related quantities that has previously been defined in the FE-analysis (except for the above mentioned). For the Fully coupled flow deformation analysis the situation is different

3.4.15. Allow suction

This option allows suction to be included in the active pore pressure and pore water pressure. Now the soil saturation depends on the soil water retention curve, SWRC. In analogy with the ignore suction option, stresses and previous quantities still apply.

3.4.16. Material models

To be able to model geotechnical problems correctly a suitable material model must be used in Plaxis. There are a number of predefined material models that best suit various types of soil and the user is also given the possibility to create a user-defined model.

3.4.16.1. Linear elastic model:

This model represents Hooke's law for linear and isotropic elasticity. It has two elastic stiffness parameters, the Young's modulus E, and the Poisson's ratio ν. The elastic linear model is very limited to simulate the behaviour of a soil. It is mainly used for massive rigid structures placed in the ground.

3.4.16.2. Mohr-Coulomb model:

This well-known model is generally used as a first approximation of the behaviour of a soil. It has five parameters: Young's modulus, E, Poisson's ratio, ν, cohesion, c, friction angle, φ, and dilatancy angle, ψ.

3.4.16.3. Model for fractured rock (Jointed Rock Model):

It is an anisotropic elastoplastic model, for which, plastic shear can occur only in a limited number of shear directions. This model can be used to simulate the behaviour of stratified or fractured rocks.

3.4.16.4. Hardening Soil Model:

It is an elastoplastic type hyperbolic model, formulated in the framework of plasticity with strain hardening in shear. In addition, this model takes into account compression strain hardening, to simulate the irreversible compaction of a soil under the first compressive loading. This model can simulate the behaviour of sands, gravel, and even soft soils, such as clays and silts.

3.4.16.5. Model for soft soils (Soft Soil Model):

It is a Cam-Clay type model, which simulates the behaviour of soft soils, such as normally consolidated clays or peat. This model is applicable very well to situations where primary consolidation is preponderant.

3.4.16.6. Model for soft soil with creep (Soft Soil Creep Model):

It is a second-order model, formulated in the context of viscoplasticity. It simulates the behaviour of soft soils, such as clays or normally consolidated peats, as a function of time. This model takes into account the logarithmic compression.

3.4.16.7. User-defined model:

This option allows you to define and use behaviour laws other than the standard PLAXIS models.

Note :

All the modelling supposed an elastoplastic behaviour, answering the model with fracture criterion of Mohr-Coulomb, which is the model most commonly used in soil mechanics. The elastoplastic behaviour can be represented by the one-dimensional model (figure 3.5) includes a spring of stiffness K to symbolize elasticity, and a threshold shoe S_o.
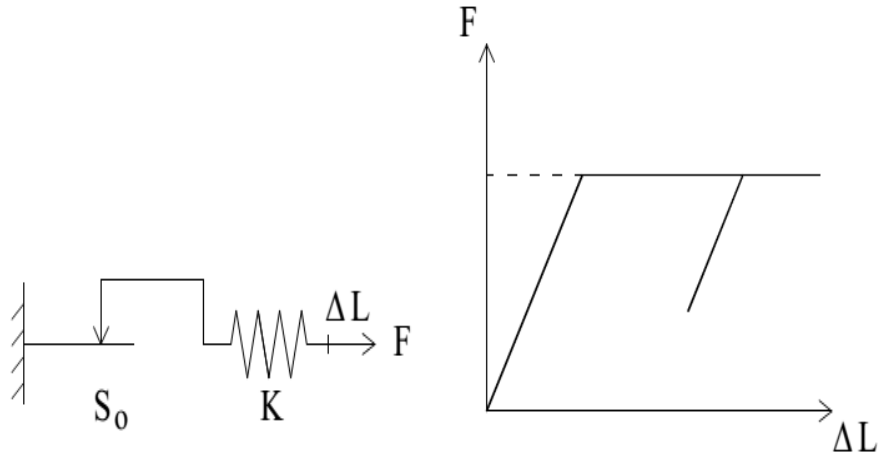
Figure 3.5 One-dimensional representation of the elastoplastic behavior.

| σ_1 | Contrainte axiale | ε_1 | Déformation axiale |
| σ_3 | Contrainte constante de confinement | ε_v | Déformation volumique |
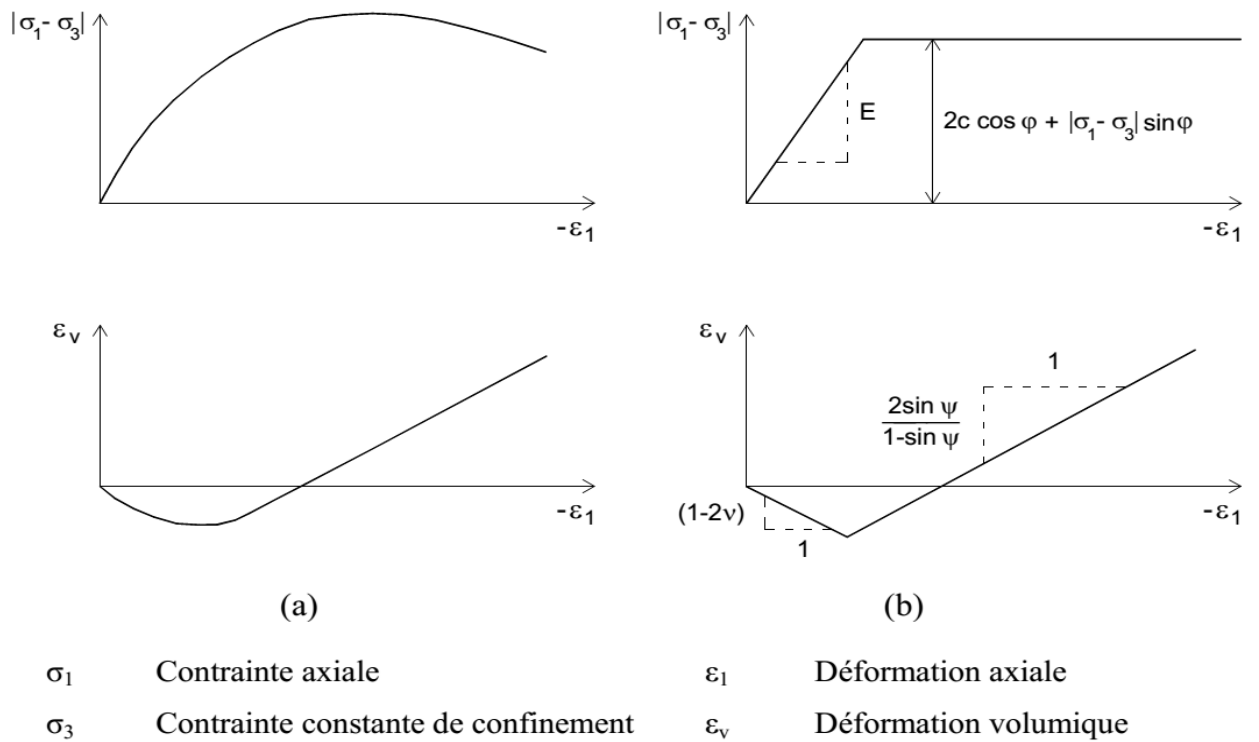
Figure 3.6 Standard triaxial test results (a) and elasto-plastic model (b).behavior.

The elasto-plastic model "Mohr-Coulomb" is characterized by five parameters, which are:

in elasticity;

E Young's modulus of elasticity,

υ Poisson coefficient,

in plasticity;

φ friction angle,

ψ dilatancy angle.

Under triaxial stress, the parameters of the model are shown in figure 3.6.

3.5. Conclusions

We presented at the beginning of this chapter a certain number of concepts and tools, relating to modelling, to draw attention to the role, importance and necessity of modelling in hydro-geotechnics. Which have led, with the development of the computer tool, to remarkable advances in the field of calculation of retaining structures and the analysis of their behaviour, which is often very complex and difficult to identify and take charge with conventional tools analytical. Modelling allows, starting from a design of a problem on the basis of the assumptions and models adopted (geometric-mechanical - statistics), the understanding, prediction and knowledge of the phenomena studied. And to test the influence of certain parameters (parametric study) using different numerical techniques.

The use of modelling to understand the structures and their environment is becoming essential. It is necessary to define a goal for modelling, to clarify it and translate it into a language understood by all those who are interested in the targeted modelling. Because this is the decisive phase and an important step to take towards quality.

Models should be employed while fully expressing the assumptions they imply and the limits within which they were developed and can be used. All plastic models potentially involve

certain degrees of parameters (constants), paths on which the strains (fracture) depend, a consequence of the non-linearity of the relationships between stresses and strains in soils.

The elastoplastic model of Mohr-Coulomb, conventional for soils whose failure mechanisms are governed by shear, will be used in the present study for the first case of study, since the soil considered is purely powdery, where Hardening soil model wiil be used for the second case of study. In addition, the model has the advantage of requiring few parameters, the meaning of which is well represented.

In geotechnics, it is impossible to always obtain complete data on the soils or rocks of the site, for example: the initial stress state, the properties and the discontinuities can only be partially well known. Consequently, the digital simulation tool should not be a black box which only offers a solution to the data entered. But rather, it must also allow digital experiments "Numerical Laboratory". The Plaxis code respects this particularity by offering the user the possibility to test his ideas, to introduce his own models of behaviour and to model the construction sequences.

The richness of the code in incorporated models of soil and rock behaviour, in load changes, in orders (making it possible to manufacture modelling procedures adapted to geotechnical problems), in interface elements and in structural elements (beam, cable ...) makes this simulation tool very competitive in geotechnics. This justifies the choice of this code in the present numerical analysis of the behaviour of the soil-screen interaction under the effect of water flow to study the stability of excavations against hydraulic failure.

Chapter 4

Numerical analysis of the excavations stability in the presence of flow

Chapter 4: Numerical analysis of the excavations stability in the presence of flow

4.1. introduction

The design of cofferdams and deep excavations supported by sheet pile walls or diaphragm walls is often dominated by the flow of water around the retaining wall. The flow of infiltration water, from the upstream side to the downstream side of the wall induced by the lowering of the water table (for the removal of water or the drying up of the excavation), influences the overall wall stability and the stability of the base and / or bottom of the excavation. Where a lifting of a block of soil "heaving" in front of the sheet (embedding length of the wall), a phenomenon of seepage "uplift", a liquefaction of the soil, or a mechanical rupture by reduction of the passive pressure of the Soil (abutment) can occur depending on soil properties and the conditions and types of the support structure.

There are many methods published by Terzaghi (1943), McNamee (1949), Marsland (1953) and Davidenkoff & Franke (1965), for the evaluation of the stability of the bottom of the excavation against failure. soil hydraulics, based on a factor of safety with respect to failure by the seepage phenomenon or uplift, but the rupture sometimes occurs even in deep excavations designed by these methods Tanaka (2002). The characteristics of seepage water flow and hydraulic breakdown of the soil under different flow conditions were also discussed by Tanaka & al. (2009). These methods proposed in the literature for the analysis of stability are based on fairly restrictive assumptions. They only take on the role of waterproofing sheet piles, the effect of reducing passive earth pressure is ignored. Other failure mechanisms very dependent on hydraulic and mechanical boundary conditions can occur with hydraulic head losses lower than the values corresponding to the failure of the bottom of the excavation.

For a consequent review of the referential literature, more detailed descriptions and more developed discussions relating to previous work (state of the art) published in the literature, dealing with methods for evaluating the stability of excavation bottoms with respect to -vis of the hydraulic rupture, and having a direct relation with the cases considered in the present study, the reader will be able to refer to " chapter 2 " in the first part (bibliographical synthesis ...) of this thesis.

This chapter is devoted to the present numerical modelling of the excavations stability of a real case located in Germany with the presence of flow around the waterproof retaining wall. The present work took a tranche from an 80 km long open sewer located in the Ruhr area, Germany as an example to establish a hydro geological model and analyse the instability of the excavation base

surface caused by the groundwater flow using the powerful geotechnical software, Plaxis v 2012. The maximum achieved depth of the excavation and the failure mechanism before applying the drainage system was checked out and compared with previous research. As a next step, this study presented the affectivity of the adopted drainage system inside the excavation pit to relax the pore-water pressure in order to achieve the required excavation depth. Also, optimising the length of the adopted drainage system and studied its position effect from the wall, taking into consideration the economic and safety aspects.

finally, use the stone columns technic to test the column installation effect on the improvement of excavation base stability where the columns installation technics modifies the properties of the surrounding natural soil in which can give a good result of our problematic.

The following flowchart (Figure 4.1) presents the methodology employed in this study.
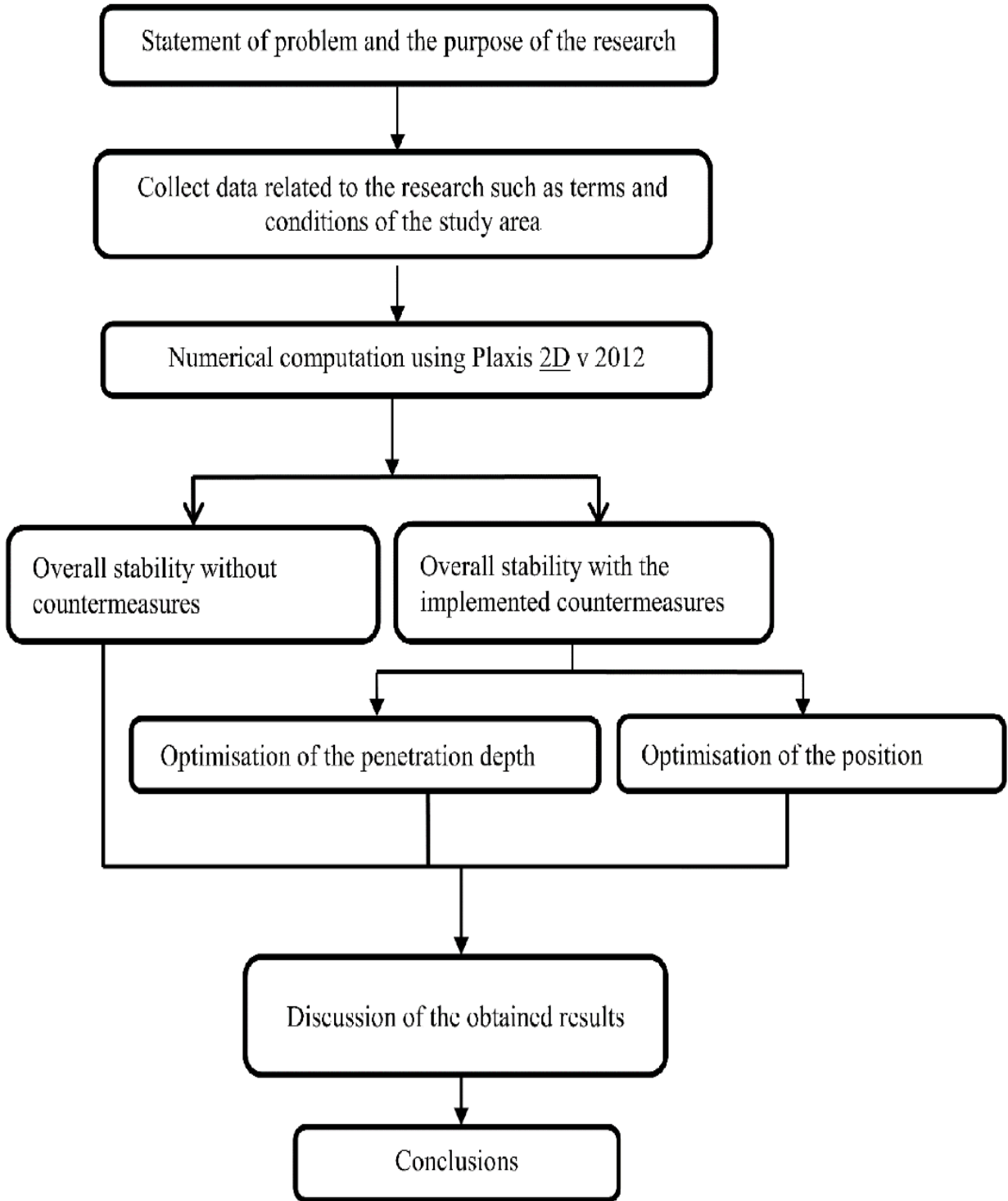
Figure 4.1. Research methodology flow chart

4.2. Using sandy columns for drainage system

- **Case of study**

Since the period of industrialisation, wastewater in the Ruhrgebiet in Germany has drained into the east–west river of Emscher. Now, due to the world's most modern sewage system, the river of Emscher will be converted into a near-natural body of water in order to restore the natural condition of the Emscher and its tributaries. The overall project is over a length of 51 km, between Dortmund-Deusen and the mouth of the Emscher in Dinslaken, where the wastewater will flow in closed piped channels of about 400km of sewer tunnels with a maximum outside diameter of 4.20 metres that are up to 40 m deep.

In the area of section 40 (Figures 4.2 and 4.3), data from laboratory investigations have been collected where 300 boreholes were drilled to a depth of about 70m in order to investigate the soil characteristics. The information gained mostly showed that the site consists of two main layers, Quaternary sand, predominantly with underlying cohesive soils such as marl. Figure 4.4 shows the schematics of the systematised geotechnical longitudinal section of construction section 40.

Figure 4.2. The main course of the Emscher project

Figure 4.3. The site of the study area in section 40
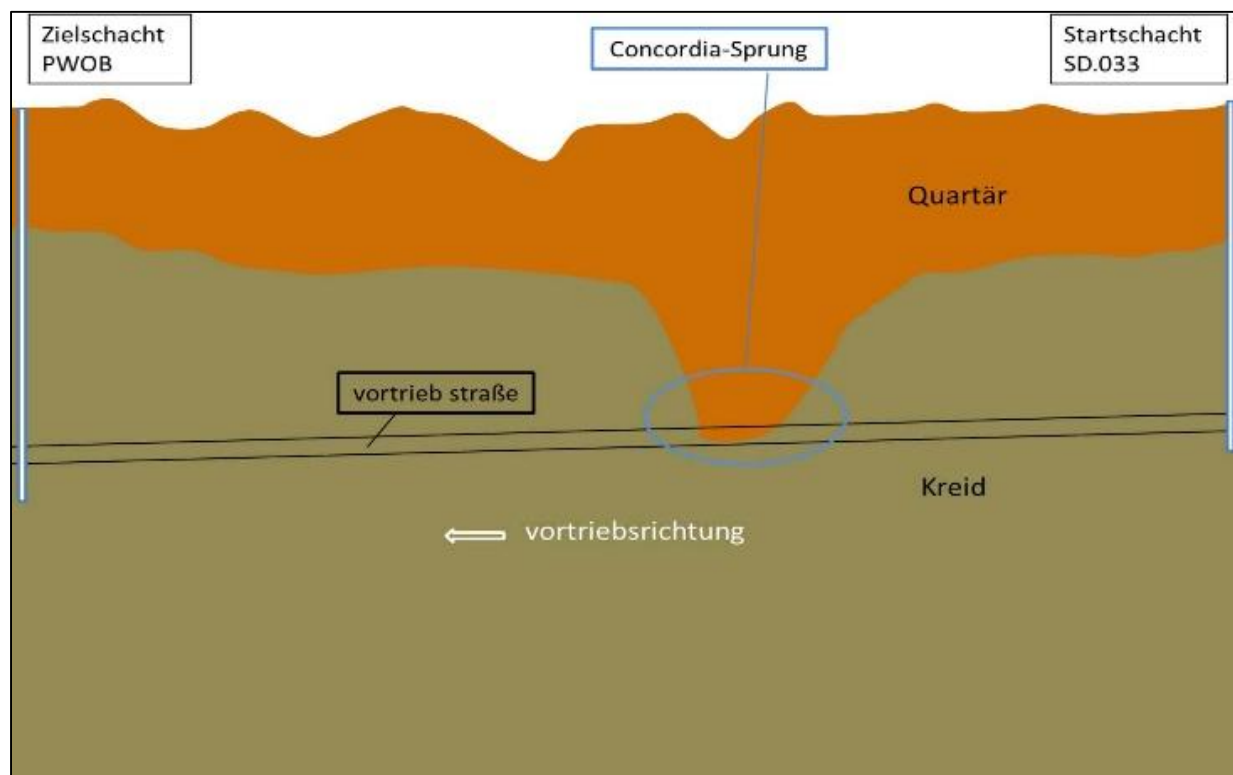
Figure 4.4. The systematised, geotechnical longitudinal section of construction section 40

Figure 4.5 shows the grain size range of the Cretaceous ground (solid lines) passed through in the west half of section 40 and the grading distribution of the material of the Concordia-Sprung in the east half of section 40 (dashed lines).

Various types of marl can be distinguished along the route of construction section 40 (Route of the Interceptor SD.033-PW OB). The Emscher marl is the predominant deposit and consists of calcareous silty fine sands, clayey silts, calcareous and glauconitic, which are consolidated to calcareous marlstone or sand marl and clay or caly. Above the Emscher marl are the Osterfeld beds, which consist of marly and silty fine sands, mostly with a considerable medium sand content, as well as very sandy silts. The Bottrop beds, which partly overlie the Osterfeld beds, consist of grey-green glauconitic fine sand marlstone, which transitions at the base from marly fine to medium sands. The upper part of the Bottrop beds consists of marlstones and fine sandy clay marlstones. At its surface, the marl is mostly softened and weathered. The Cretaceous beds dip flatly to the north-northwest. Additional tectonic faults lead to all these Cretaceous strata being

passed through by the tunnel drive. In this paper, the western half of section 40 (PW OB) was taken as a case study, where the Emscher marl is the predominant deposit, falling under mostly a considerable medium sand.
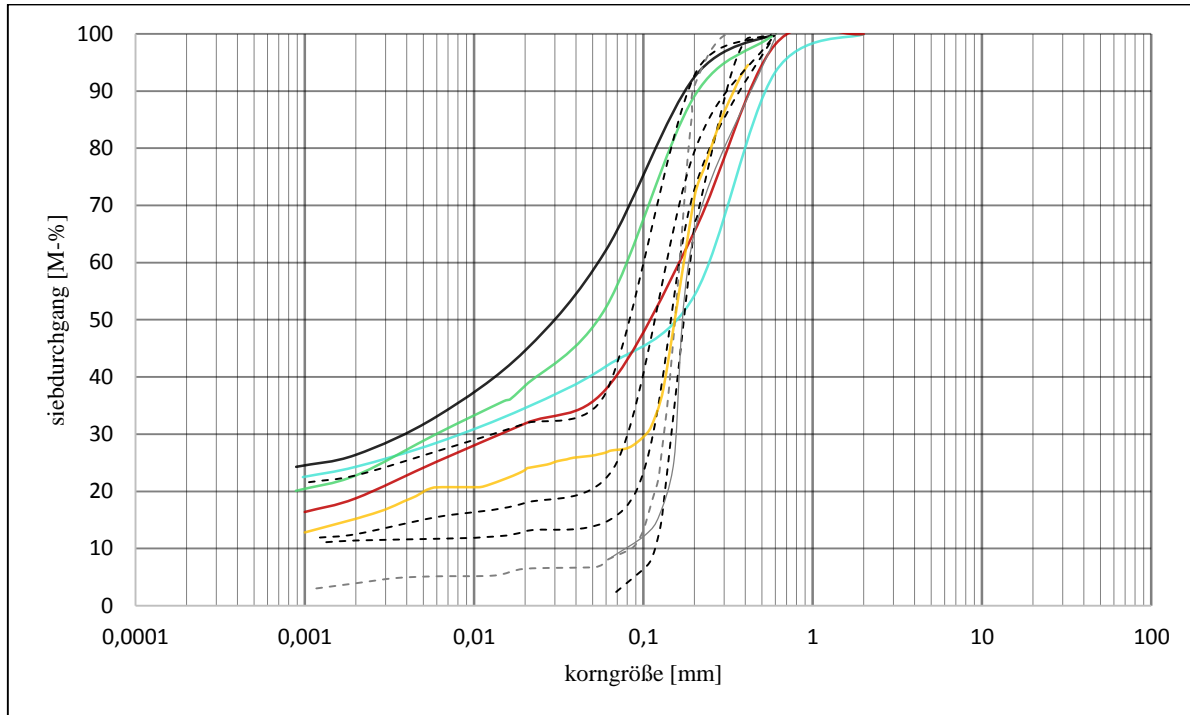
Figure 4.5 Typical grading curves in the Cretaceous determined in the site investigation (solid lines) and typical grading curves in the Concordia-Sprung fault zone (dashed lines)

4.2.1. Numerical Simulation of the Case Study

In both cases – cohesive soil and groundwater relaxing system – the classical method fails. Here, numerical simulations based on the FEM appear to be a helpful tool, since they present the relevant failure mechanism as a result of the calculation. The FE modelling method using the Plaxis 2D-V2012 computer program has been applied to the case study of a deep excavation PWOB located in section 40.

Using the numerical method advantages, an axisymmetric model is used where the FE mesh consists of 15-nodes of triangular elements. The size of the calculation model was chosen so that the boundaries do not influence the deformation behaviour of the model. Theoretically, the tensile stresses that can be absorbed by the ground are cut-off. In order to simulate the excavation and construction process as a real case, the calculation was divided into several groups based on

the actual excavation planning. According to the data of the previous on-site investigation and the laboratory tests, the parameters, such as the permeability, the modulus and so on, for every soil are determined with the Mohr-Coulomb model used for all soil layers. The soil parameters for the simulation are summarised in Table 4.1.

Table 4.1. Main hydraulic and mechanical properties of the soils

Parameter	Quaternary sand	Marl	Clean Sand
Unsaturated unit weight γ_{unsat} (kN/m³)	19	20	19
Saturated unit weight γ_{sat} (kN/m³)	20	22	20
Friction angle (°)	30	25	30
Cohesion (kN /m²)	0	40	0
Dilation angle (°)	0	0	0
Poisson's ratio	0.3	0.25	0.33
Wall-friction and -adhesion R	0.5	0.2	1
Permeability (m/s)	1×10^{-4}	1×10^{-6}	1×10^{-3}
Young's modulus (kN /m²)	29,700	40,000	20,200

The next step is to define the plate. In this analysis, the plate was considered rigid, so its stiffness has a great value to make sure it does not deform itself, since this is not being studied in this work. In addition, the plate is fixed, so the option Total fixities were applied, to make sure that the wall does not move at all. To the whole model Standard fixities were applied too, which means that in the bottom of the model horizontal and vertical fixities were applied, and in the sides only vertical fixities. Another feature that had to be taken in consideration was the application of the interfaces in both sides of the plate.

After the application of the material to all the clusters, the mesh is ready to run. It was consider a medium global coarseness as a good choice for the mesh, but close to the plate and its tip it was refined, since it is close to those locations that the failure will take place. In

Figure 4.6 a global view of the model with the mesh generated can be seen. As it was said before, the mesh is much finer close to the plate and tip.

Figure 4.7 presents the project where the case study was chosen for this paper. It shows a circular excavation with an inside diameter B=46 m and a depth d=45 m (see Figure 4.8).The surrounding soil is retained by an impermeable wall of 2 m in thickness. The wall is inserted by D=6 m beneath the final excavation.
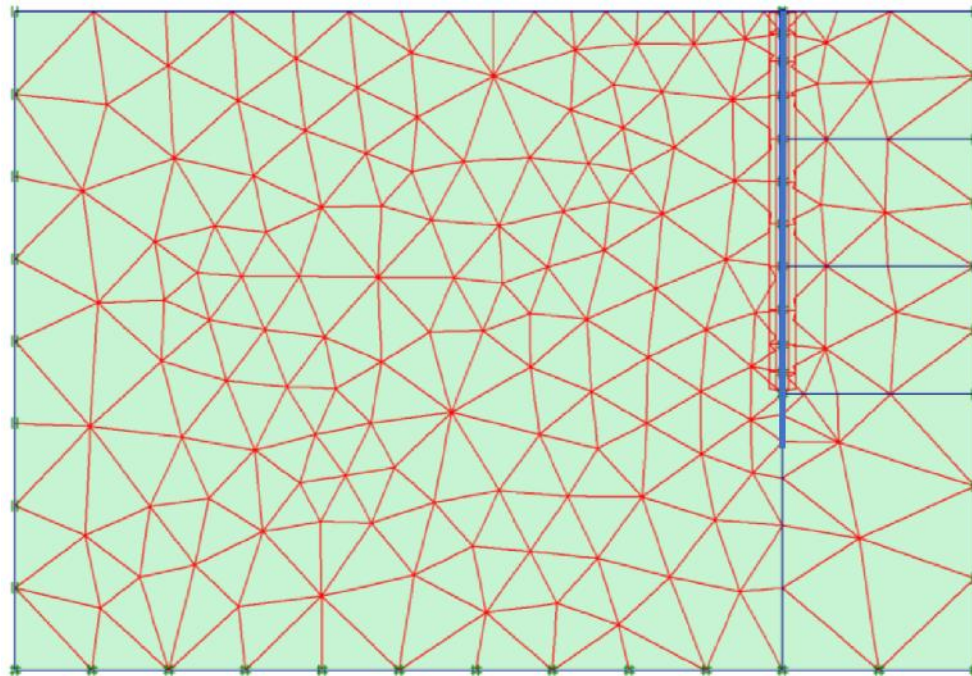
Figure 4.6 General view of the model with mesh generated

Following this, the Initial water conditions can be entered. The ground water level was considered to be located at 6m bellow the ground surface. One phase of the Calculation Program was the introduction of the plate in the soil, so in the Initial conditions only the soil appeared. Now, the model is ready for the Calculation program where the different stages are going to be introduced.

For the phased model, 5 stages were made:

- Phase 1: apply the weight of soil and the soil stress;
- Phase 2: activation of the plate;
- Phase 3: start the excavation process;

- Phase 4: take out the failure stage;

- Phase 5: phi-c reduction.
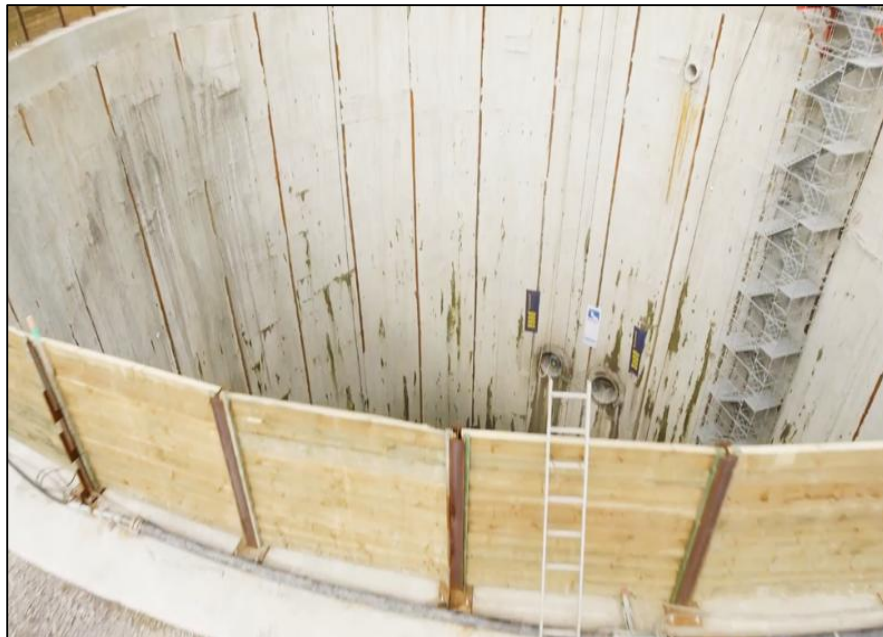
Figure 4.7. Presentation of the pit chosen for this paper (PWOB).
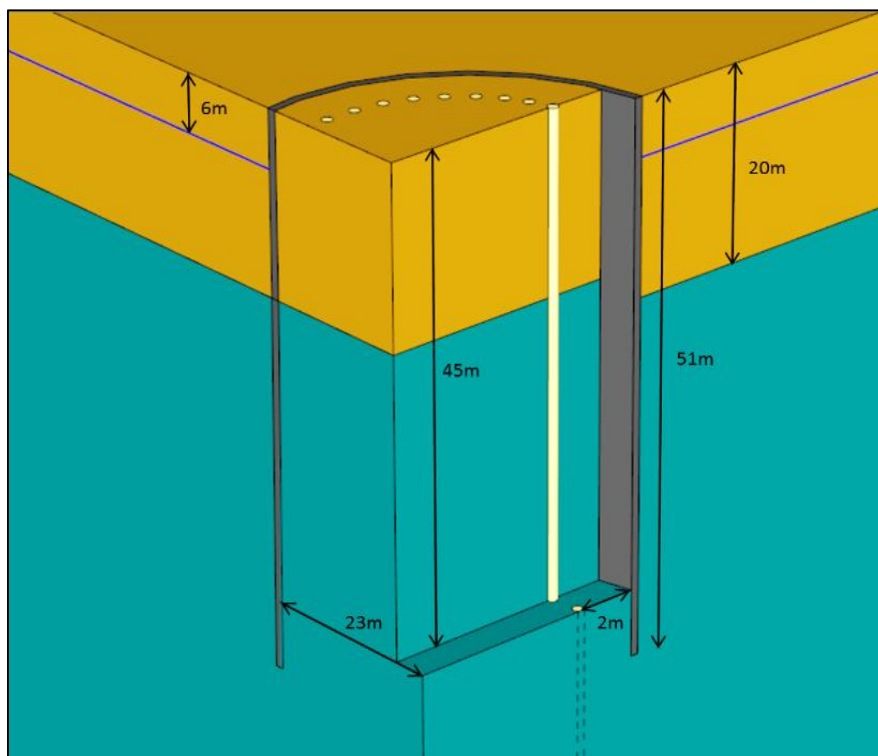
Figure 4.8. Three-dimensional model of relatively wide circular-shaped excavation pit

4.2.2. Phi-C reduction

In the software PLAXIS, the shear strength reduction procedure is called phi-c reduction, and is used to compute safety factors. This option can be selected as a separate Calculation Type in the General tab sheet. In the phi-c reduction approach the strength parameters tan Φ (phi) and c of the soil are successively reduced until failure of the structure occurs. The strength of the interfaces, if used, is reduced in the same way. The strength of structural objects like plates and anchors is not influenced by *phi-c reduction*.

The total multiplier $\sum Msf$ is used to define the value of the soil strength parameters at a given stage in the analysis:

$$\sum \text{Msf} = \frac{\tan\varphi_{input}}{\tan\varphi_{reduced}} = \frac{c_{input}}{c_{reduced}}$$

where the strength parameters with the subscript „input" refer to the properties entered in the material sets and parameters with the subscript „reduced" refer to the reduced values used in the analysis. $\sum$Msf is set to 1.0 at the start of a calculation to set all material strengths to their unreduced values.

A phi-c reduction calculation is performed using the Load advanced number of steps procedure. The incremental multiplier Msf is used to specify the increment of the strength reduction of the first calculation step. This increment is by default set to 0.1, which is generally found to be a good starting value. The strength parameters are successively reduced automatically until all Additional steps have been performed. By default, the number of additional steps is set to 100, but a larger value up to 1000 may be given here, if necessary. It must always be checked whether the final step has resulted in a fully developed failure mechanism. If that is the case, the factor of safety is given by:

$$SF = \frac{\text{available strength}}{\text{strength at failure}} = \text{value of} \sum \text{Msf at failure}$$

If a failure mechanism has not fully developed, then the calculation must be repeated with a larger number of additional steps.

To capture the failure of the structure accurately, the use of Arc-length control in the iteration procedure is required. This feature enables accurate computations of collapses loads and failure mechanisms to be carried out. In conventional load-controlled calculations the iterative procedure breaks down as soon as the load is increased beyond the peak load. With arc-length control, however, the applied load is scaled down to capture the peak load and any residual loads. The use of a Tolerated error of no more than 3% is also required. Both requirements are complied with when using the Standard setting of the Iterative procedure.

4.2.3. Groundwater relaxation system

The boundary conditions for the groundwater relaxation system taken into account can be derived from the verifications. In the calculation, the groundwater relaxation system is simulated as a circumferential drainage ditch due to the rotational symmetry. The groundwater relaxation system is implemented in the construction work by means of boreholes filled with filter sand; the dimensions of the boreholes are carried out taking into account the calculated maximum water flow.

In addition to the specifications for number, diameter and final depth, the deepest excavation level that can be reached without a groundwater relaxation system must also be taken into account during execution. For construction-related reasons, the relief bores can also be made from a higher level. The maximum distance between adjacent bores was set between about 2 m and 6 m in order to achieve the assumed rotationally symmetrical group effect.

A 39 clean sand columns with a diameter of 30 cm reaching down to a depth of te=90 m from the ground surface, and 2 m away from the wall were modelled as a concentric thin slot (figure 4.9). Sandy columns with relatively high permeability ($k=10^{-3}$ m/s) are an appropriate measure to improve the hydraulic situation at the bottom of the excavation. For the initial state, the groundwater was set at 6 m below the top of the site. The effectiveness of the relief wells is ensured until the groundwater rises as planned; Particular attention should be paid to the free drainage of water from the boreholes into the drainage layer installed on the final excavation level. The water that accumulates in the drainage layer is collected via pump sumps and pumped to the receiving water.
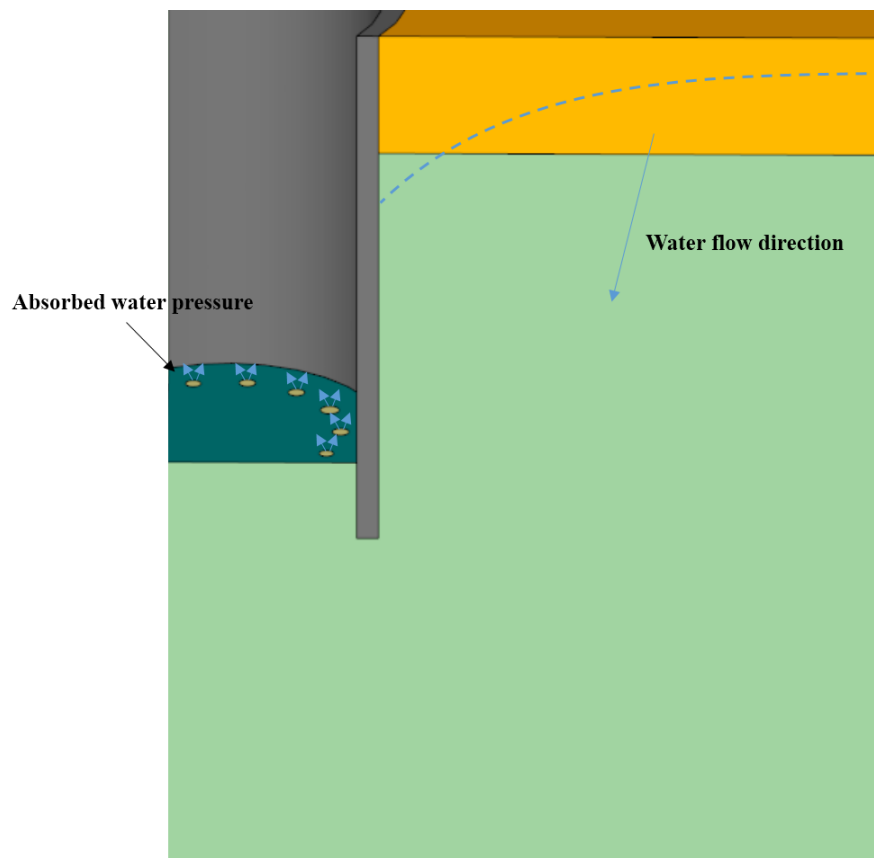
Figure 4.9 System sketch for the construction pit with relief boreholes

In addition to the relaxation of the groundwater within the less permeable marl, the overlying Quaternary soils and backfills can also be drained via the relaxation boreholes.

The mathematical modelling of the groundwater flow resulting from the excavation of the soil and simultaneous drainage via the retaining wall and the bottom of the construction pit is based on Darcy's law. The effective stress was calculated in the form of a coupled analysis, i.e. the distribution of the pore water pressure determined in a calculation of flow and used as the initial condition for the subsequent stress calculation. The groundwater flow calculated in the respective excavation state and the calculated flow pressure describes the steady-state.

Before the calculation starts, a point of the mesh is chosen to know its displacements. This point, as it was said before, is the one located in the middle of the excavation. When the calculation is finished there are many possible results that can be examined but the ones which are more pertinent to this study are the Deformed mesh, and the Total Displacements, to know how the soil behaves in the moment just before its failure (figure 4.10). As it was said before, that the

most sensitive part of the model is the tip of the plate, and this constructive element, because it is fixed, effectively does not move.
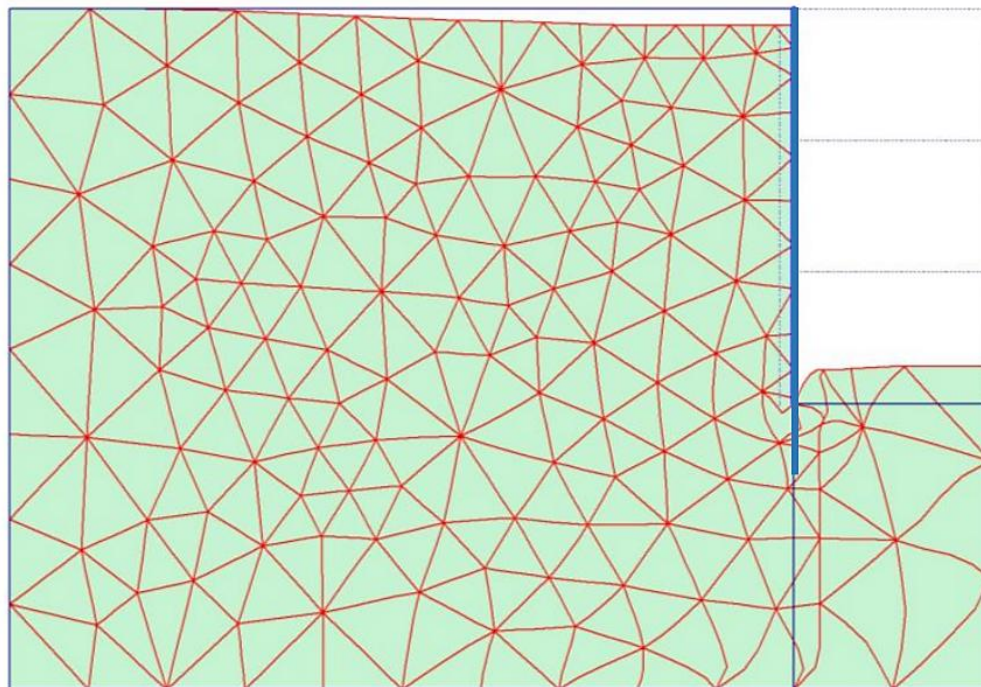
Figure 4.10 The Deformed mesh

Another figure that needs to be analysed carefully is the Total displacements. Eventually these arrows seem to be not so linear in that location, which could mean that t he interface has a more important role than the one mentioned in Faheem (2003)"s paper in terms of obtaining the safety factor.

4.2.4. Results and Discussion

4.2.4.1. Overall stability without countermeasures

The following investigation deals with the verification against excavation bottom instability. The first part of this research work consists of evaluating the maximum excavation depth that can be reached without applying any countermeasures.

After calculating the initial stress state by initialising the stresses in the model with the coefficient K_0 of lateral pressure of the earth at rest $K_0 = 1- \sin\varphi$, the excavation states were displayed in 1 m excavation steps and here the calculation of the strain state under stress was coupled to the calculation of the groundwater flow.

The performed calculations indicate that the excavation process is safe enough without any countermeasures reaching down to a depth of 25 m from the ground surface. For a deeper excavation process, the situation would be exposed to the collapse of the excavation base. Here, the drainage system (sand columns) must be installed. In order to demonstrate the failure mechanism, the drilling process was attended up to 26m, where the bottom of the excavation at that depth was affected by hydraulic failure.

Figure 4.11 shows the path of the groundwater within the soil of the studied case at the critical moment where the excavation base is exposed to collapse. The water located in the upper layer goes in a horizontal direction and accumulates at the wall front, then fast-flowing down creates an intensive upward seepage force at the downstream side. The reason for this is that the low permeability of the lower layer (marl) creates isolation at the soil interface leading to preventing water from passing down on the ground.

At the moment where the situation exposed to the collapse of the excavation base, Figure 4.12 shows the mechanism of failure. The soil at the base of the excavation lifted completely owing to the intensive upward seepage forces resulting from the ground stratification and their different soil permeability. It appears as general heave, and the prism of failure does not give a specific region.
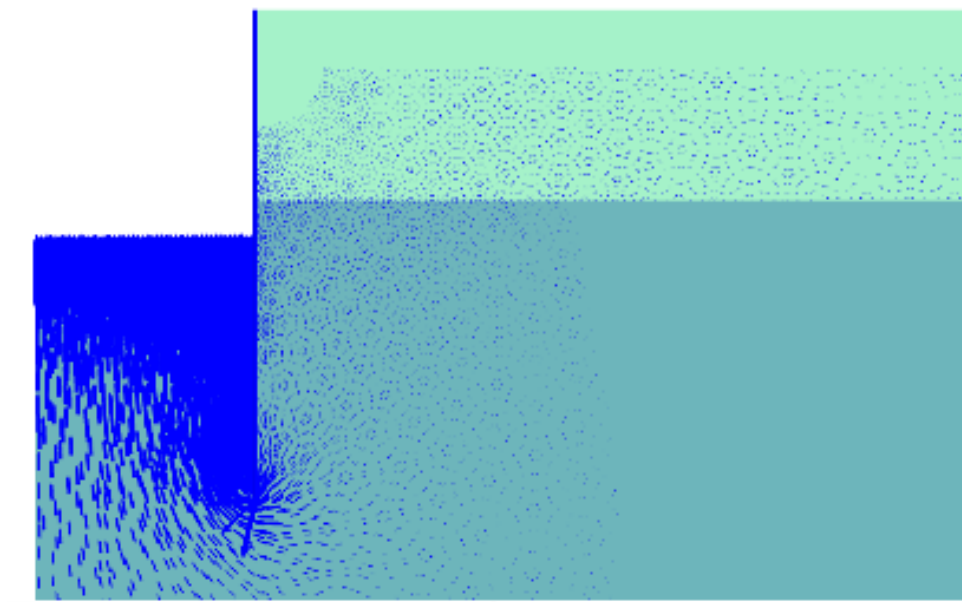
Figure 4.11. The path of the groundwater flow through the soil

Comparing the obtained failure mechanism from this study to those accomplished by Benmebarek & al (2006)- Koltuk & al (2019) in which three types of failure have been presented (triangular, rectangular prisms and boiling) and the rectangular failure body with width D/2 represented by Terzaghi (1943), shows clearly that they are not in good agreement. Therefore, it becomes clear that for real cases, where horizontal stratification exists between the excavation base and the wall tip and for specific soil characteristics, the mechanism of failure cannot be generalised to all situations, and its diagnosis varies from case to case.
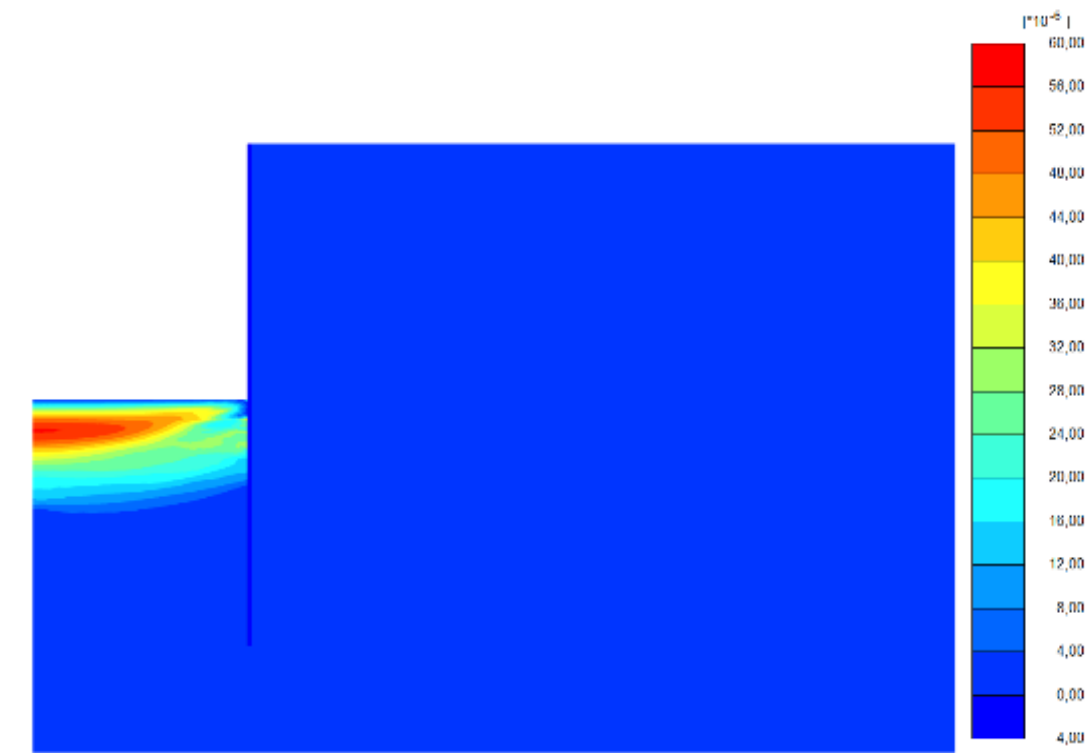
Figure 4.12. The capture of failure mechanisms before applying the countermeasures

The most recent research in which is similar to our problematic was done by ZHAO and al (2020) by analysing the failure mechanism of an excavation faced the hydraulic heave without introducing any countermeasure. Here, the only parameter can be compared is the mechanism of failure which is insufficient to our goal of this research work.

By comparing our results with those gained by ZHAO and al (2020), we can note that the failure mechanism was similar for the excavation depth of -3.2m correspond to ZHAO and al (2020),

see figure 4.13. Except that the failure location changes its position taking the place near the wall when the excavation depth gets -3.6m not like the result obtained from this work where the failure mechanism keep in the same shape.

a   b
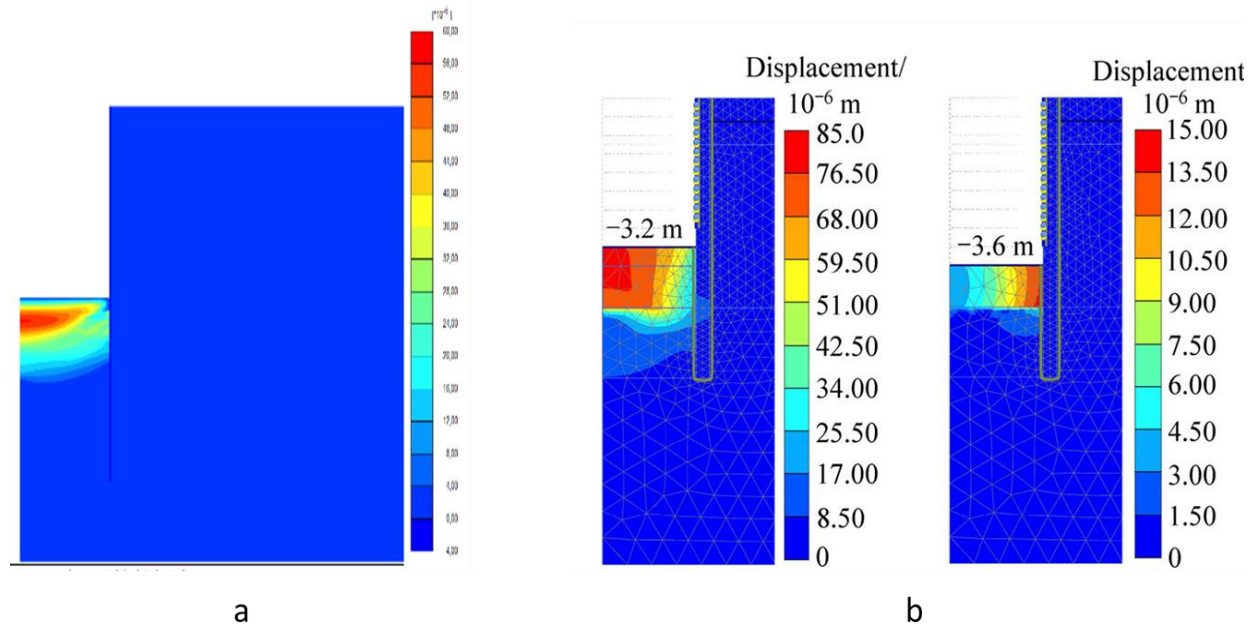
Figure 4.13. Comparison the mechanisms of failure: (a) our result, (b) ZHAO and al (2020).

4.2.4.2. Overall stability with the implemented countermeasures

As countermeasures, the second part of this research is related to applying the drainage system and testing its effectivity against the failure of the excavation base due to the water seepage forces. For this project, the implemented drainage system consists of 39 columns of sand with a high coefficient of permeability reaching down 90 m from the ground surface. As the material of the drainage system consists of sand, the 39 clean sand columns can easily be excavated with the surrounding soil.

The results indicate that, for all the excavation states, the situations have the required safety to achieve the targeted depth of 45 m deep. However, it is not clear which failure mechanism becomes relevant in the case of excavations with a drainage system in the subsoil. It does not seem to be admissible to transfer the classical failure mechanisms to these situations.

In aiming to give the present case study more precise design values in economic terms, and taking into consideration safety as the first criterion, varied depths and positions of the drainage system have been analysed.

4.2.4.3. Optimisation of the penetration depth

In order to study the effect of the drainage system penetration beneath the subsoil, the length of the columns, *te,* is reduced from the designed value, 90 m, while keeping the same characteristics of the soils until the occurrence of collapse at the base of the excavation. The results presented in Figure 4.14 indicate that the situation expose to collapse for an excavation process more than 25 m in depth before applying the drainage system. By inserting the sand columns, the safety factor rises with an average of 30% and attained the maximum value at 83 m in penetration depth of sand columns.

For a penetration depth of 76 m of the drainage system beneath the subsoil, the geo-hydraulic situation is safe enough against the failure of the excavation base. At a further reduction in the penetration depth of the drainage system (less than 76 m), the situation falls, and collapse occurs. however, it remained stable from 86.5 m to 90 m. That slight increase of *Fs* value may be considered non-economic because, at a depth of penetration of 76 m, all the excavation states have the required safety. The reason for this could be that the flow path from upstream was limited by global driving contours, whereas the point of intersection for the lower limit of this with the drainage system was located at -76 m from the ground's surface. The other deepest flow path can be considered non-influential on the behaviour of the phenomenon.

Also, the permeability of the drainage material has been reduced in order to test its effect on the stability of the excavation base. The results indicate that for permeability of less than $k<10^3$, the seepage problem cannot be resolved no matter how deep the drainage system is.
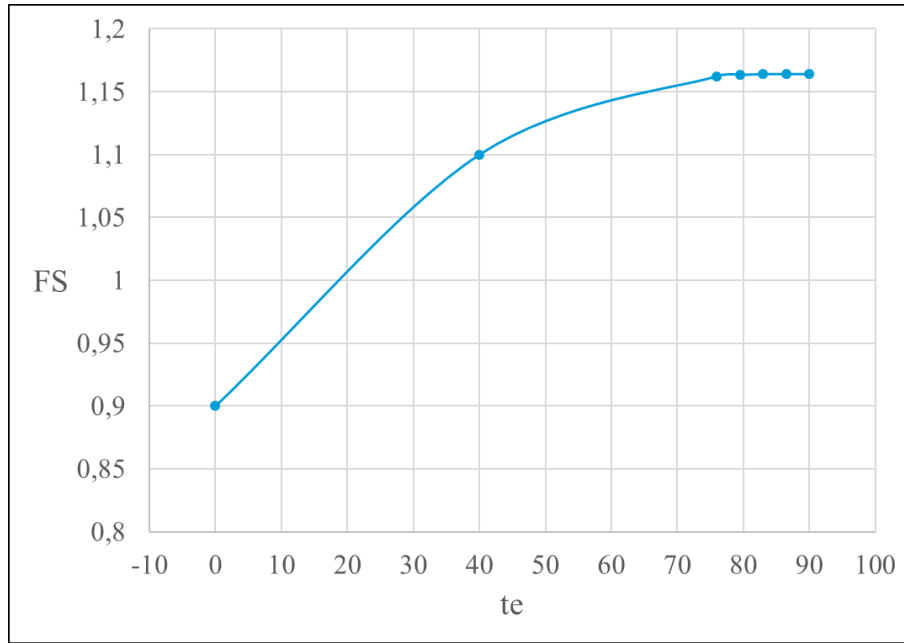
Figure 4.14. Effect of drainage system penetration

4.2.4.4. Optimisation of the position

In this part, the drainage system moved from the wall going to the centre of the pit with a distance *de* by a step of 0.5 m. The first position was attached to the wall with a distance of 0.25 m, as it is the nearest possible position to the wall. In each step, the factor of safety has to be gained for each position ending at the optimal position.

Figure 4.15 shows that from position D/2 of the drainage system closer to the wall, the safety factor is increased by an average of 16% and reaches the maximum value near the wall. In other words, from the other side with the position D/2 of the drainage system heading towards the middle of the pit, the process of the excavations fails before achieving the required depth (45 m deep) and the drainage system cannot solve the situation even if reaches very deep. Here, it could be noted that, for the analysis of the basal heave of excavations, the upward seepage flow from the upstream side is limited by the diving contours with a distance *D*/2 from the wall.

Comparing what was mentioned in the literature by Terzaghi (1943), where the relevant zone suggested for seepage failure is a rectangular prism adjacent to the wall with *D*/2 in width (Figure 4.16), with the acceptable limit of drain positions developed from this study, they are obviously in good agreement.
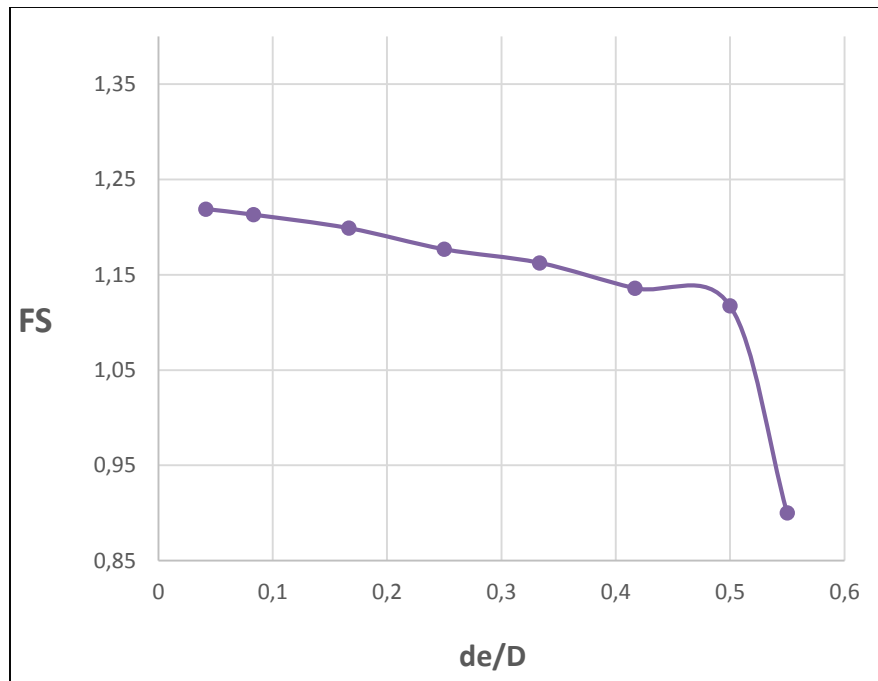
Figure 4.15. Effect of drainage system position
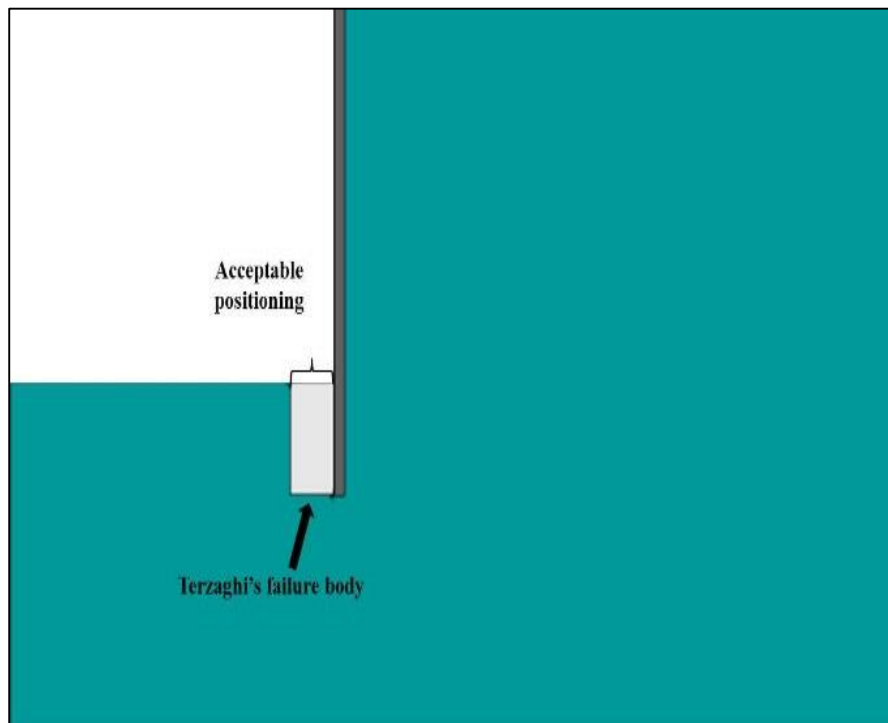
Figure 4.16. The acceptable positioning of the drainage system

Lastly, through the obtained results, it could be supposed that for the stability of the excavation base against seepage flow, the mechanism of failure is not related to the vulnerable region.

4.3. Stone Columns Method

The ground improvement techniques applied are tools used by the geotechnical engineer for "fixing" the problems of poor ground, when a poor ground exists at the project site (Ghanti & Kashliwal, 2008).

Ground improvement in simple words can be defined as "the process of enhancing the quality of soil." Stone columns are a common improvement technique for foundation of embankments or structures on soft soils. The gravel columns have a higher strength, stiffness and permeability than the natural soft soil. Therefore, they improve the bearing capacity and the stability of embankments and natural slopes, reduces the total and the differential settlements, accelerates the soil consolidation and reduces the liquefaction potential. Besides, column installation also modifies the properties of the surrounding natural soft soil.

In our case of study seems that using the stone columns technic is out of field to improve the stability at excavation base against seepage phenomenon. Here, the idea of choosing the stone columns is to test the column installation effect on the improvement of excavation base stability where the columns installation technics modifies the properties of the surrounding natural soil in which can give a good result for our problematic.

4.3.1. Numerical Model

In aim to test the effect of stone columns installation on enhancing the surrounding soil, a numerical analysis using 2D finite element tool (Plaxis 2D, v2012) was chosen.

Using the numerical method advantages, an axisymmetric model is used where the FE mesh consists of 15-nodes of triangular elements. The size of the calculation model was chosen so that the boundaries do not influence the deformation behaviour of the model. Theoretically, the tensile stresses that can be absorbed by the ground are cut-off.

Figure 4.17 presents the model where the case study was chosen for this part of study. It shows a circular excavation with an inside diameter B=20 m. The surrounding soil is retained by

an impermeable wall of 2 m in thickness and 50m in depth. The drainage system (stone columns) is assumed to be inserted by 3m beneath the toe of the retaining wall.

In order to simulate the excavation stages and applying the stones columns technic, the calculation was divided into several groups based on the actual excavation planning. The parameters, such as the permeability, the modulus and so on, for the soil of the used model and the stone columns are determined with the Hardening Soil Model used for all situations, table 4.2
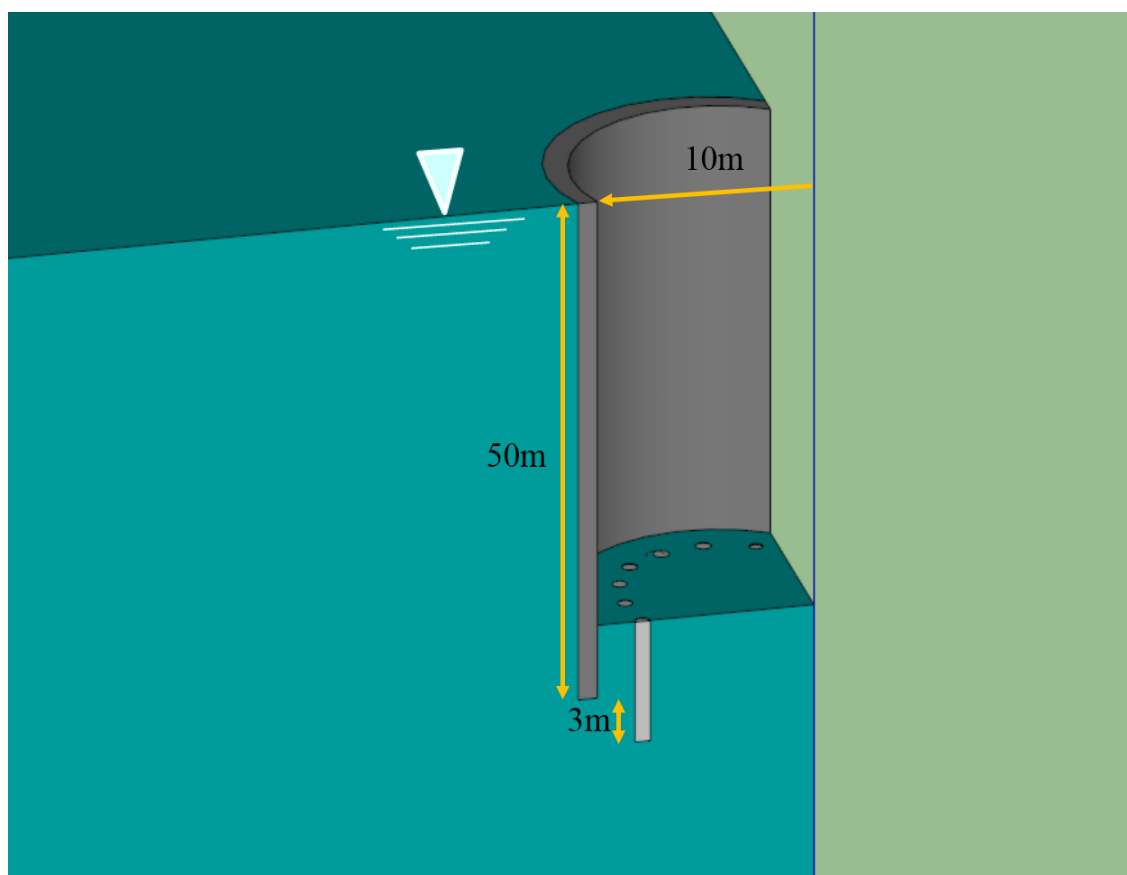
Figure 4.17: a 3D general view of the model

The next step is to define the plate. In this analysis, the plate was considered rigid, so its stiffness has a great value to make sure it does not deform itself, since this is not being studied in this work. In addition, the plate is fixed, so the option Total fixities were applied, to make sure that the sheet-pile does not move at all. To the whole model Standard fixities were

applied too, which means that in the bottom of the model horizontal and vertical fixities were applied, and in the sides only vertical fixities. Another feature that had to be taken in consideration was the application of the interfaces in both sides of the plate. For this part of study, we will identify two cases and compare their results. For both cases, the drainage system positioned at 1.8m from the wall and have 0.6m in diameter.

The first part, is by introducing a simple tranche of stone columns as draining system without applying any lateral pressure on it and analyse the stability the excavation base against seepage phenomenon. Figure 4.18 showed the presented geometric of the model by inserting non-pressurized stone columns.

Table 4.2. Main hydraulic and mechanical properties of soft clay material and stones

Parameter	Soft Clay	Stone
Unsaturated unit weight γ_{unsat} (kN/m³)	16.5	19
Saturated unit weight γ_{sat} (kN/m³)	16.5	19
Friction angle (°)	34	45
Cohesion (kN /m²)	1	1
Dilation angle (°)	0	15
Wall-friction and -adhesion R	0.2	-
Permeability (m/s)	0.116×10^{-7}	0.197×10^{-4}
E_{50}^{ref} (kN /m²)	4350	80000
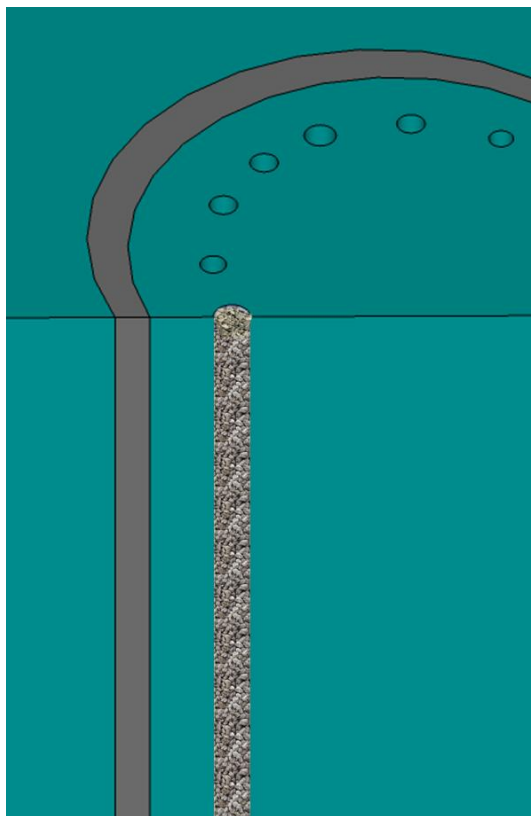
Figure 4.18: General view of the model with a non-pressurized stone columns

For the second part, The main concept of the stone column numerical modelling is based on the method of installation and its effect on the soil surrounding the columns. Figure 4.19 showed the presented geometric of the model by inserting pressurized stone columns. That is, the creation of the borehole using a vibroflot. This column was then expanded to model a displacement stone column (Figure 4.19); that is, the compaction of the stone to create the installation effect.

To insure the large area effected by stone columns installation, Al Ammari, K., & Clarke, B. G. (2018) showed that an increase in displacement by applying the cavity expansion increases the confining stress acting on the stone column and the increase extends to at least six times the column diameter, which exceeds the distance between adjacent columns. Thus, the stresses within the soil between two columns will be affected by both columns.
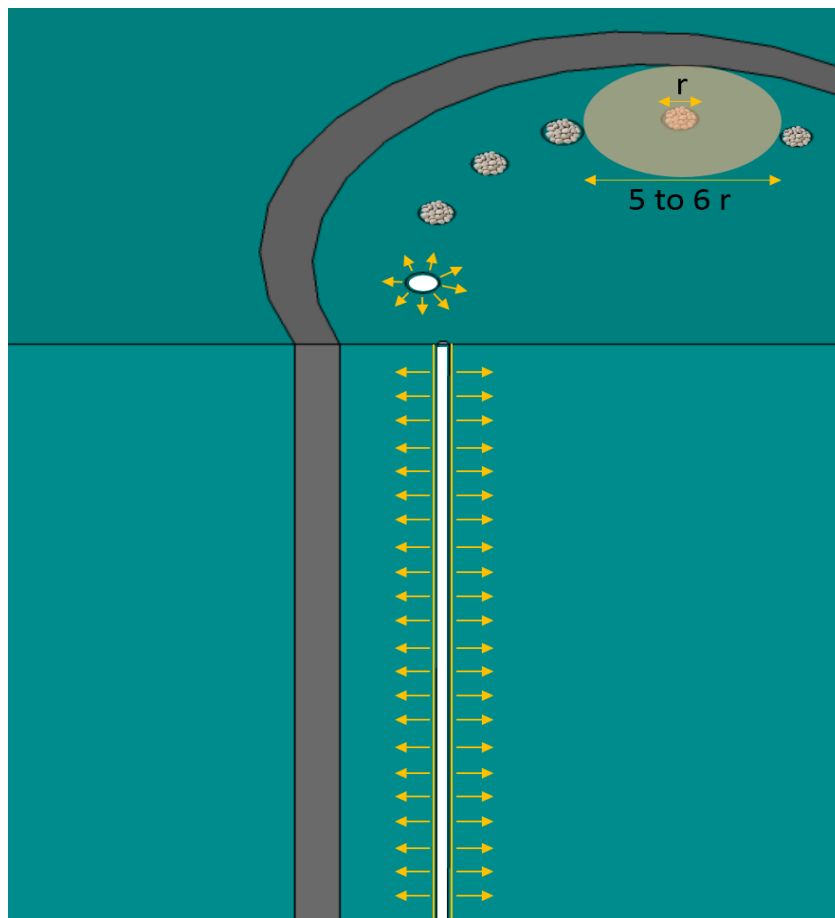
Figure 4.19: General view of the model using cavity expansion method

4.3.2. Numerical Analysis and Results

- **Case one**

For the first case, a simple tranche of stone columns as draining system without applying any lateral pressure inserted and the following investigation deals with the verification against excavation bottom instability.

After calculating the initial stress state by initialising the stresses in the model with the coefficient K_0 of lateral pressure of the earth at rest $K_0 = 1 - \sin\varphi$, the plate must be activated and by inserting a simple tranche of stone columns as draining system without applying any lateral pressure to it, the excavation states were displayed in 1 m excavation steps and here the calculation of the strain state under stress was coupled to the calculation of the groundwater flow. After reaching deep in excavation process where inside of the hole must be dry, thus leading to change

in contour line of ground water level making a slight down curve (Figure 4.20). We found that the ground water level near the retaining wall is lower than in boundary location, this can obviously clarify why the hydraulic gradient at the wall region take the highest value.
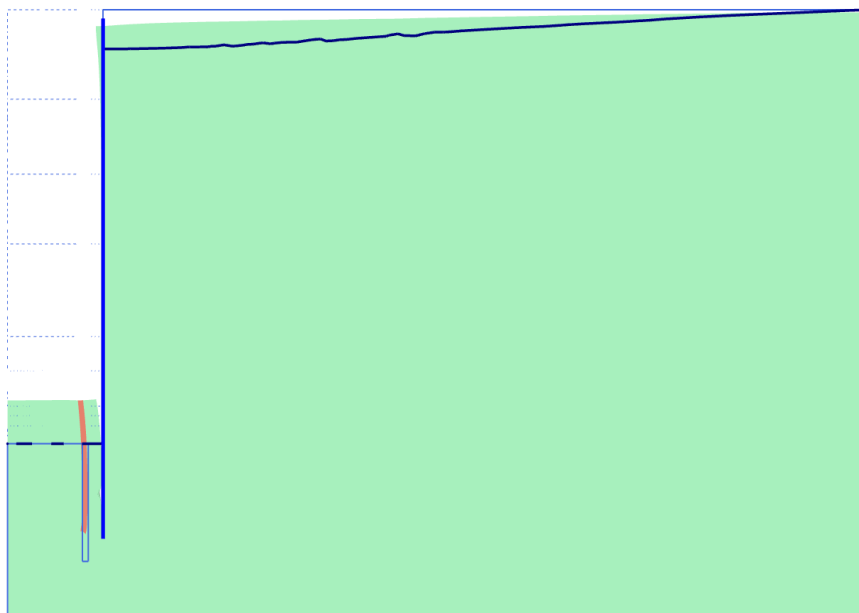
Figure 4.20: change in contour line of ground water level after excavating

The performed calculations indicate that the excavation process is safe reaching down to a depth of 40 m from the ground surface. For a deeper excavation process, the situation would be exposed to the collapse of the excavation base.

At the moment where the situation exposed to the collapse of the excavation base, Figure 4.21 shows the mechanism of failure. The soil at the base of the excavation lifted completely and appears as general heave. The prism of failure does not give a specific region.
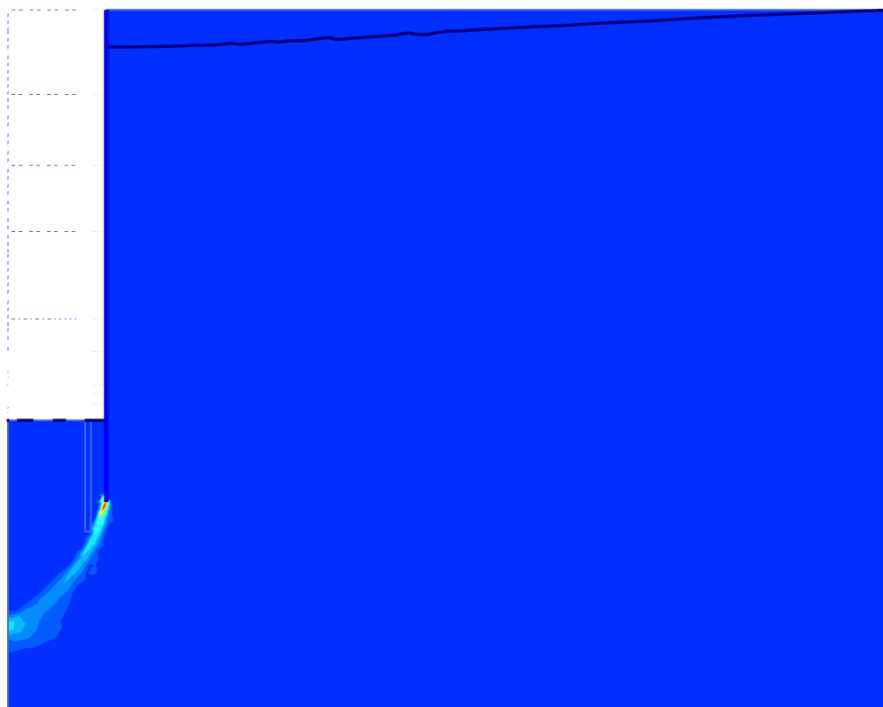
Figure 4.21: The capture of failure mechanisms for case one

- **Case Two**

For the second case, the aim is to test the effect of stone column installation on the soil surrounding the columns. the following investigation deals with the verification against excavation bottom instability.

To rightfully model the column installation, each step of the column construction needs to be represented by the numerical procedure. The vibro-replacement method consists of the following steps (Hurley & al (2015)):

(1) insertion of the vibrating probe down to the required depth,

(2) stone pushing through the end of the probe that is lifted up and

down to compact the stone and expand the diameter until the required length is obtained

(3) repeating the process until the full column is built.

The numerical modelling tries to recreate accordingly the construction processes with certain simplifications. In terms of soil behaviour, these processes can be seen as follows:

(1) Cavity expansion of the soil, from a nil radius to a radius equal to the probe diameter (Vesic 1972);

(2) Gradual lateral loading of the surrounding soil caused by the insertion of stone and the expansion of the stone column into the soil;

(3) creating a group effect of columns representing the meshing geometry.

After reaching deep in excavation process where inside of the hole must be dry, the performed calculations indicate that the excavation process is safe reaching down to a depth of 44.5m from the ground surface. For a deeper excavation process, the situation would be exposed to the collapse of the excavation base.

From the obtained results we found that, after applying the principle of cavity expansion, the excavation process can reach down 4.5m more than using the simple tranche of stone columns.

At the moment where the situation exposed to the collapse of the excavation base, Figure 4.21 shows the mechanism of failure.

We found that stone columns installation not only effect the amount of excavation depth as it gives extra deep in excavation but also, from figure 4.22 (b), the surrounding soil of stone columns affected by the process of installation did not subject to failure where the mechanism of failure starts after the region affect by the installation method. Instead having the ordinary shape of failure which take place at the whole excavation base, we found it here goes to the center of the excavation.

(a)
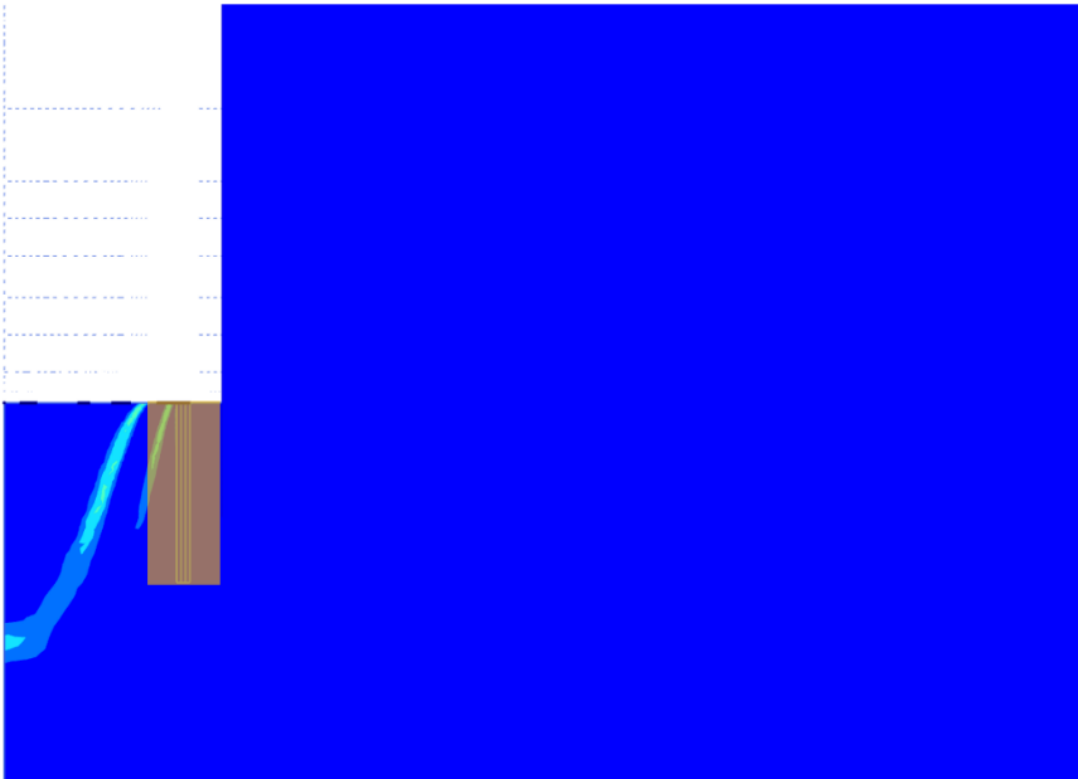
(b)

Figure 4.22: the capture of failure mechanisms for case two

This last, present a very interesting contribution. By comparing the trees failure mechanisms presented in figure 4.23; (a) sand columns, (b) stone columns without cavity expansion and (c) stone columns with cavity expansion, we go with a conclusion that using a technic of cavity expansion for stone columns installation is the most appropriate for excavations basal stability against seepage phenomenon. This conclusion based on two advantages, the first one is that technic of cavity expansion for stone columns installation provide an extra excavation deep, also by using the cavity expansion method, the reinforced soil surrounding the retaining wall keep stable in which insure an extra range of safety to the wall against failure.

The result presented in figure 4.24 showed that the region affected by the cavity expansion method is 6 time the column diameter, in which is in good agreement with Al Ammari, K., & Clarke, B. G. (2018)

<div align="center">(c)   (b)   (a)</div>
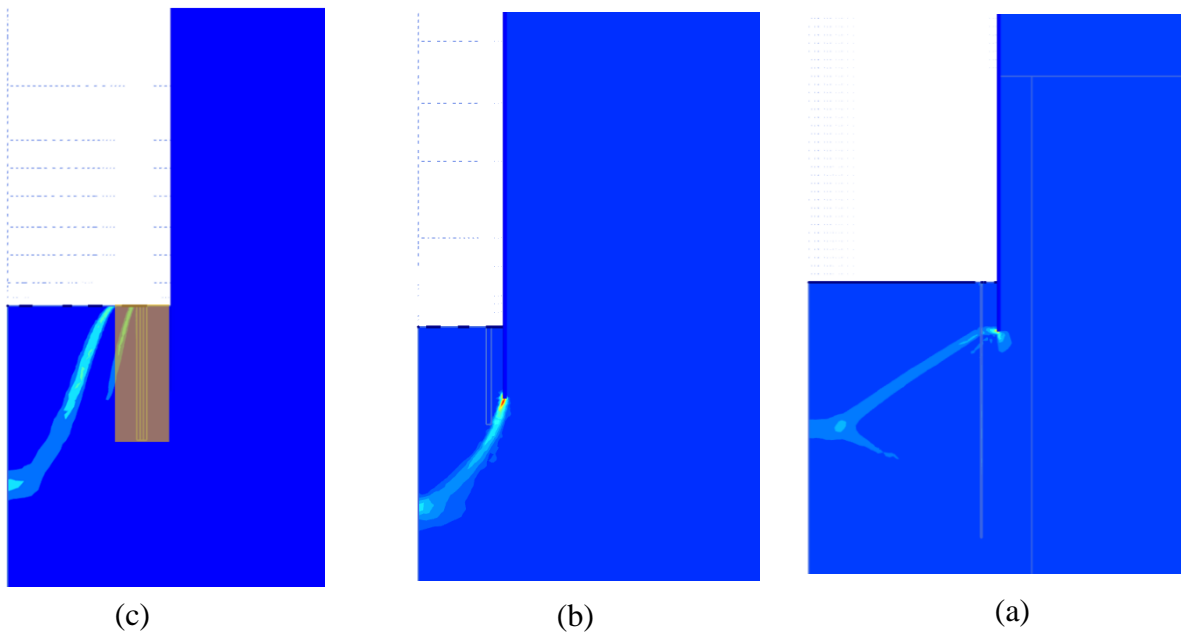
Figure 4.23: The capture of failure mechanisms: (a) sand columns, (b) stone columns without cavity expansion, (c) stone columns with cavity expansion
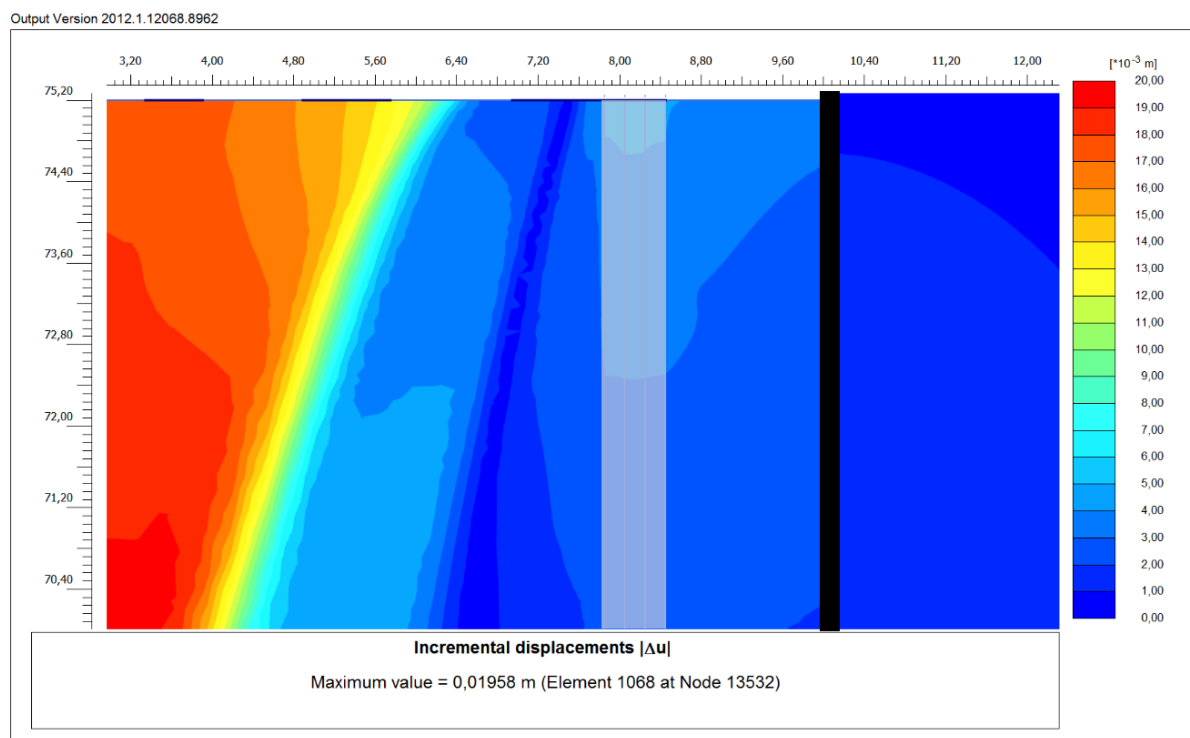
Figure 4.24: effect of cavity expansion method on failure location

4.4. Conclusions

Safety against water flow in deep excavations represents a crucial aspect of design. In many cases, both the design and the overall cost of the excavation system are dictated by this problem of hydraulic failure. In this research, a real project of deep-braced excavation located in the Ruhrgebiet, Germany, subjected to seepage flow, was established using the elastic–plastic FEM to predict the failure mechanism caused by groundwater flow and to perceive the factor of safety values against the failure of the excavation base. A drainage system, consisting of clean sand with high permeability, was adopted and implemented for this case study to relax the excess porewater pressure. This has been numerically tested for its effectivity. To underscore the scientific value of this research work, the optimised length of the drainage system and its effective position from the wall have been analysed with regard to the economic aspect, bearing in mind safety as the first criterion. The results that have been mentioned in the literature were compared with those obtained by numerical simulations in this work. The conclusions are as follows:

- Before applying any countermeasures, the soil at the base of the excavation lifted completely owing to the intensive upward seepage forces resulting from the ground stratification and their different soil permeability. In that situation, the achieved excavation depth was slightly more than half of the required depth. The mechanism of failure appears as general heave, and the prism of failure does not give a specific region. Therefore, it becomes clear that for real cases, where horizontal stratification exists between the excavation base and the wall tip and for specific soil characteristics, the mechanisms of failure cannot be generalised to all situations, and their diagnosis varies from case to case.

- To achieve the required excavation depth, the adopted drainage system has been implemented. Results showed that the drainage system was quite an effective countermeasure against the failure of the excavation base.

- By analysing the effect of the drainage system penetration beneath the subsoil, results indicated that with 76 m in penetration depth, the drainage system could sufficiently support the geo-hydraulic situation against the failure of the excavation base. A slight increase in the safety factor when the drainage system reached down 90 m, however, may be considered a non-economic decision.

- From the position D/2 of the drainage system going closer to the wall, all excavation processes were safe enough until reaching the required depth and the factor of safety was raised and achieved the maximum value near the wall. Otherwise, the drainage system could not resolve the situation even if they reached very deep, and the process of the excavation failed before achieving the required depth.

- For similar projects subjected to hydraulic heave, the obtained results can be provided as a reference to use for stability evaluation with regards to the applicability of the adopted system and its efficacy of safety and economy.

- In the case using simple tranche of stone columns without any lateral expansion of stones, the failure mechanism was the same when using sand columns.

- We found that stone columns installation not only effect the amount of excavation depth by giving extra deep in excavation, but also, the surrounding soil of stone columns affected by the process of installation did not subject to failure where the mechanism of failure starts

after the region affect by the installation method. Instead having the ordinary shape of failure which take place at the whole excavation base, we found it took place at the center of the excavation.

4.5. Future aspects of the research

As the problematic treated in this research work considered one of sensitive topics in geotechnical engineering, therefore, more research must be carried out in order to determine the possible effective countermeasures against a basal failure of excavation.

General conclusion

In this thesis we have presented two parts. The first contains four chapters relating a bibliographic synthesis in line with the field studied. And the second has two chapters relating to numerical modelling, the behavioural models used, and compare the review of the state of the art (in close connection with the cases studied) to the analysis done in this scientific work.

First of all, the bibliographical synthesis carried out enabled the following conclusions to be drawn:

- Groundwater is still a source of major difficulties in carrying out works. It is an important and decisive factor in most geotechnical problems.

- The flow of water can therefore fundamentally modify the reaction of the ground to the digging of excavations, in particular by considerably increasing the risks of short-term instability.

- The results obtained should not be assessed on the basis of the precision of the resolution method (largely sufficient), but on the basis of the often very large uncertainty linked to soil parameters and boundary conditions;

- The choice of retaining systems is not only linked to the requirements of the land, but also to the concern for the protection of the personnel working on the site;

- The retaining systems must be defined with sufficient precision to guarantee their effectiveness. And special attention must be paid to the following:

- Ability to adapt to the shape of the excavation;

- Continuity of supports, junction between elements (sheet piles, diaphragm walls etc ...) put in place during successive phases;

- Contact support-ground, possibility of maintaining a support of regular shape well placed on the ground despite the irregularities of the excavation;

- Possibility of rapid reinforcement of the support;

General conclusion

- Very particular attention must also be paid to the problems related to the presence of water and its movements in the ground.

- Semi-flexible and flexible retaining walls have a much more complex behaviour than rigid walls.

- Conventional calculation methods (at limit states) remain well suited for the sizing of the vast majority of sheet pile walls. They give superabundant results. With these methods, the deformation of the screen is not involved in the calculation.

- Numerical modelling allows the understanding, prediction and knowledge of the phenomena studied by starting from a design of a problem on the basis of the assumptions and models adopted (geometric-mechanical-statistics). And to test the influence of certain parameters using different numerical techniques;

Secondly, we have analysed the stability of excavations in the presence of water flow around retaining wall. This through, on the one hand, the numerical evaluation (numerical simulation) using the Plaxis 2D finite element code) of the maximum achieved depth of the excavation and the failure mechanism before applying the drainage system, also, the affectivity of the adopted drainage system inside the excavation pit to relax the pore water pressure in order to achieve the required excavation depth. The retaining structures studied are supposed to be embedded at an horizontal, semi-infinite terrain, and made up of soil from real case. Here, taking into account the characteristics of the soil, those of the soil / wall interface and the permeability isotropy of the medium.

The numerical results enabled us to note out that the use of numerical modelling to understand the structures and their environment is becoming essential where it is necessary to define a goal for modelling, to clarify it and translate it into a language understood by all those who are interested in the targeted modelling.

However, the FEM offers the possibility of determining the groundwater flow and the associated pore water pressure distribution with very good accuracy, especially in complex spatial systems. In a stress and deformation calculation based on this water pressure distribution, the reduction in the effective soil stress and the associated reduction in the shear strength can be taken

into account. Here, the assumption of a rectangular failure body for the verification against heave by conventional calculation methods is not generally correct.

- The use of sand columns for draining system as relief boreholes to improve the geo-hydraulic situation beneath the bottom of an excavation becomes a very helpful tool where they should be reached below the toe of the retaining wall taking in consideration that from the position *D/2* of the drainage system going closer to the wall, all excavation processes were safe enough until reaching the required depth and the factor of safety took the maximum value near the wall. Otherwise positions, the drainage system could not resolve the situation even if they reached very deep.

- Using a technic of cavity expansion for stone columns installation is the most appropriate for excavations basal stability against seepage phenomenon. This conclusion based on two advantages, the first one is that technic of cavity expansion for stone columns installation provide an extra excavation deep, also by using the cavity expansion method, the reinforced soil surrounding the retaining wall keep stable in which insure the safety of the wall against failure.

References

Al Ammari, K., & Clarke, B. G. (2018). Effect of vibro stone-column installation on the performance of reinforced soil. *Journal of Geotechnical and Geoenvironmental Engineering*, *144*(9), 04018056.

Banerjee, P. K., & Butterfield, R. (1981). *Boundary element methods in engineering science* (Vol. 17, p. 578). London: McGraw-Hill.

Baumgart W. S. und Davidenkoff R. (1929). Upon Design of Substuctures on Pemeable Grounds (in russischer Sprache).

Bazant Z. (1940). Grundbruch unter der Spundwand, Die Bautechnik, Nr. 52, pp. 595-602.

Bazant, Z. (1953). Stability of a non-cohesive soil under elliptic upward seepage. In *Proceedings of Third International Conference on Soil Mechanics and Foundation Engineeing, Zürich/Switzerland*.

Bazant, Z. (1963). Ergebnisse der Berechnung der Stabilitat gegen Hydraulischen Grundbruch mit Hilfe der Elektronen-Rechenan-lage. In *Proc. of the Int. Conf. on Soil. Mech. and Found, Eng., Budapest* (pp. 215-223).

Benmebarek, N., Benmebarek, S., & Kastner, R. (2005). Numerical studies of seepage failure of sand within a cofferdam. *Computers and Geotechnics*, *32*(4), 264-273.

Benmebarek, N., Benmebarek, S., Kastner, R., & Soubra, A. H. (2006). Passive and active earth pressures in the presence of groundwater flow. *Geotechnique*, *56*(3), 149-158.

Boley C. und Schober P. (2013), „Hydraulisch verursachtes Versagen von Baugrubensohlen - hydromechanische Grundlagen und Bemessung," 20. Darmstädter GeotechnikKollquium: Jubiläumsquolloquium.

Butler, F.G. (1975). Heavily over-consolidated clays. Review paper: Session III. Conf. on Settlement of Structures, Pentech Press, London.

Clayton, C. R., Woods, R. I., Bond, A. J., & Mililitsky, J. (2014). *Earth pressure and earth-retaining structures*. CRC press.

Craig, R. F. (2004). *Craig's soil mechanics*. CRC press.

Cundall, P. A. (1976). Explicit finite differnce method in geomechanics. In *Second Int. Conf. Numerical Methods in Geomechanics, Blacksburg, 1976* (Vol. 1, pp. 132-150).

Das, B. M. (2007). Fundamentals of Geotechnical Engineering. 3rd ed. London : Taylor and Francis.

References

David, M., & Zdravkovic, L. (1999). *Finite element analysis in geotechnical engineering: theory*. Thomas Telford.

Davidenkoff, R. (1970). *Unterläufigkeit von Stauwerken*. Werner.

Eurocode 7. Geotechnical Design (n.d.). doi:10.3403/03181153u.

Faheem, H., Cai, F., Ugai, K., & Hagiwara, T. (2003). Two-dimensional base stability of excavations in soft soils using FEM. *Computers and Geotechnics*, *30*(2), 141-163.

Gere, J. M., & Timoshenko, S. P. (1991). Stresses in beams. In *Mechanics of Materials* (pp. 250-377). Springer US.

Harza, L. F. (1935). Uplift and seepage under dams on sand. *Trans. of ASCE*, *100*, 1352-1406.

Hill, R. (1950). The mathematical theory of plasticity, Clarendon. *Oxford*, *613*, 614.

Hirose, T., Tanaka, T., Inoue, K., & Sakaida, T. (2006, January). Decrease in the Safety Factor for Seepage Failure of Subsoil due to Bridge Abutment Construction within a Cofferdam. In *The Sixteenth International Offshore and Polar Engineering Conference*. International Society of Offshore and Polar Engineers.

Hurley, O., Nuth, M., & Karray, M. (2015). Finite element modelling of stone column installation: Review of modelling practices and case study with Plaxis 2D.

https://worldbuilding.stackexchange.com/questions/152572/how-quickly-could-a-country-build-a-tall-concrete-wall-around-a-city/152620

Knaupe, W. (1968). *Hydraulischer Grundbuch an Baugrubenumschließung*

Koltuk, S., Song, J., Iyisan, R., & Azzam, R. (2019). Seepage failure by heave in sheeted excavation pits constructed in stratified cohesionless soils. *Frontiers of Structural and Civil Engineering*, *13*(6), 1415-1431.

Lee, J. S., & Pande, G. N. (1998). Analysis of stone-column reinforced foundations. *International Journal for Numerical and Analytical Methods in Geomechanics*, *22*(12), 1001-1020.

Love, A.E.H. (1927). A Treatise on the Mathematical Theory of Elasticity. 4th edn. Cambridge University Press.

Marsland, A. R. T. H. U. R. (1953). Model experiments to study the influence of seepage on the stability of a sheeted excavation in sand. *Geotechnique*, *3*(6), 223-241.

Mc Geever, J. (2012). Soil Mechanics Lecture Notes, DK_ECIVL_7_Y2: Soil Mechanics. Dundalk Institute of Technology, Department of Infrastructure and Environmental Engineering: unpublished.

References

Muskat, M. (1938). The flow of homogeneous fluids through porous media. *Soil Science*, *46*(2), 169.

Ou, C. Y. (2014). *Deep excavation: theory and practice*. Crc Press.

Pane, V., Bellavita, D., Cecconi, M., & Vecchietti, A. (2017). Hydraulic failure of diaphragm walls: a possible methodology for safety improvement. *Geotechnical and Geological Engineering*, *35*(2), 765-780.

PK, 2015. Plaxis Knowledgebase. [Online]. Available at: http://kb.plaxis.nl/tips-and-tricks/safety-analysis-and-displacements .[Accessed 05 05 2015].

PMMM, 2015. Plaxis Material Model Manual. [Online]. Available at: http://www.plaxis.nl/files/files/2D-3-Material-Models.pdf. [Accessed 19 03 2015].

Potts, D. M., Zdravković, L., Addenbrooke, T. I., Higgins, K. G., & Kovačević, N. (2001). *Finite element analysis in geotechnical engineering: application* (Vol. 2). London: Thomas Telford.

Powers, J. P., Corwin, A. B., Schmall, P. C., & Kaeck, W. E. (2007). *Construction dewatering and groundwater control: new methods and applications*. John Wiley & Sons.

Prandtl, L. (1921). Uber die eindringungsfestigkeit plastischer baustoffe und die festigkeit von schneiden, zeitschrift fur angewandte. *Math. Mech.*, *1*(1), 15-20.

PRM, 2015. Plaxis Reference Manual. [Online]. Available at: http://www.plaxis.nl/files/files/2DAnniversaryEdition-2-Reference.pdf [Accessed 02 03 2015].

PSM, 2015. Plaxis Scientific Manual. [Online]. Available at: http://www.plaxis.nl/files/files/2D-4-Scientific.pdf. [Accessed 19 03 2015].

Rankine, W. J. M. (1857). II. On the stability of loose earth. *Philosophical transactions of the Royal Society of London*, (147), 9-27.

Rudrabir, G., & Kashliwal, A. (2008). Ground Improvement Techniques–with a Focused Study on Stone Column. *Dept. of Civil Engineering, VIT University*.

Sentko, M. (1961). *Der zeitliche Ablauf des Schwimmsandaufbruches und der Einfluß der geometrischen Anordnung der Baugrubenumschließungen auf das kritische Gefälle* (Vol. 7). Inst. für Bodenmechanik und Felsmechanik.

Steinbrenner, W. (1934). Tafeln zur Setzungsberechnung, Die Strasse, v. 1, 121–124. also see. In *Proc. 1st ICSMFE* (pp. 142-143).

Taube.G & Martin, P.E., P.G.2002, Stone Columns for Industrial Fills, Nicholson Construction Company, Cuddy, Pennsylvania.

Terzaghi, K. (1925). Erdbaumechanik auf bodenphysikalischerGrundlage, Leipzig/Wien: Franz Deuticker.

References

Terzaghi K. und Jelinek R. (1954). Theoretische Bodenmechanik, Berlin/Göttingen/Heidelberg: Springer-Verlag.

Terzaghi K. und Peck R. (1961). Die Bodenmechanik in der Baupraxis, Berlin/Göttingen/Heidelberg: Springer Verlag.

Terzaghi, K., Peck, R. B., & Mesri, G. (1996). *Soil mechanics in engineering practice*. John Wiley & Sons.

Tanaka, T., & Verruijt, A. (1999). Seepage Failure of Sand Behind Sheet Piles—The Mechanism and Practical Approach to Analyze—. *Soils and foundations*, *39*(3), 27-35.

Tanaka, T., Toyokuni, E., & Ozaki, E. (1996). Prismatic failure-A new method of calculating stability against boiling of sand within a cofferdam. In *Geotechnical aspects of underground construction in soft ground* (pp. 219-224).

Timoshenko, S. P., & Woinowsky-Krieger, S. (1959). *Theory of plates and shells*. McGraw-hill.

Vesic, A. S. (1972). Expansion of cavities in infinite soil mass. *Journal of Soil Mechanics & Foundations Div*, *98*(sm3).

Zhao, G. Q., Yang, Y. Y., & Meng, S. Y. (2020). Failure of circular shaft subjected to hydraulic uplift: Field and numerical investigation. *Journal of Central South University*, *27*(1), 256-266.